2010

The Fabrication Of Polymer-derived Sicn/sibcn Ceramic Nanostructures And Investigation Of Their Structure-property Relationship

Sourangsu Sarkar
University of Central Florida

THE FABRICATION OF POLYMER-DERIVED SiCN/SiBCN CERAMIC NANOSTRUCTURES AND INVESTIGATION OF THEIR STRUCTURE-PROPERTY RELATIONSHIP

by

SOURANGSU SARKAR
B.Tech. University of Calcutta, 2003

A dissertation submitted in partial fulfillment of the requirements
for the degree of Doctor of Philosophy
in the Department of Chemistry
in the College of Sciences
at the University of Central Florida
Orlando, Florida

Fall Term
2010

Major Professor: Lei Zhai

ABSTRACT

Polymer-derived Ceramics (PDCs) represent a unique class of high-temperature stable materials synthesized directly by the thermal decomposition of polymers. This research first focuses on the fabrication of high temperature stable siliconcarbonitride (SiCN) fibers by electrospinning for ceramic matrix composite (CMC) applications. Ceraset™ VL20, a commercially available liquid cyclosilazane, was functionalized with aluminum sec-butoxide in order to be electrospinnable. The surface morphology of the electrospun fibers was investigated using the fibers produced from solvents. The electrospun fibers produced from the chloroform/*N,N*-dimethylformamide solutions had hierarchical structures that led to superhydrophobic surfaces. A "dry skin" model was proposed to explain the formation of micro/- and nanostructures. The second objective of the research is to align the multiwalled carbon nanotubes (MWCNTs) in PDC fibers. For this purpose, a non-invasive approach to disperse carbon nanotubes in polyaluminasilazane chloroform solutions was developed using a conjugated block copolymer synthesized by ATRP. The effect of the polymer and CNT concentration on the fiber structure and morphology was also examined. Detailed characterization using SEM and TEM was performed to demonstrate the orientation of CNTs inside the ceramic fibers. Additionally, the electrical properties of the ceramic fibers were investigated.

Finally, the structural evolution of polymer-derived amorphous siliconborocarbonitride (SiBCN) ceramics with pyrolysis temperatures was studied by solid-state NMR, Raman and EPR spectroscopy. Results suggested the presence of three major components: (i) hexagonal boron nitride (*h*-BN), (ii) turbostratic boron nitride (*t*-BN), and (iii) BN_2C groups in the final ceramic.

The pyrolysis at higher temperature generated boron nitride (BN_3) with a simultaneous decomposition of BN_2C groups. A thermodynamic model was proposed to quantitatively explain the conversion of BN_2C groups into BN_3 and "free" carbon. Such structure evolution is believed to be the reason that the crystallization of $Si_{4.0}B_{1.0}$ ceramics starts at 1500 $^{\circ}$C, whereas $Si_{2.0}B_{1.0}$ ceramics is stable upto 1600 $^{\circ}$C.

ACKNOWLEDGMENTS

First and foremost I would like to thank God for giving me life and the guidance in the path of righteousness. I would like to express my deep and sincere gratitude to my advisor Professor Lei Zhai for his enormous support and encouragement. Working with him has been one of my best and memorable experiences, not only in science but also in life. I am grateful to him for his valuable time, new ideas and financial support over the years for my research, and also for giving me personal and caring guidance to be a better and successful human being. I would always look upto him as a successful scientist, advisor, professor and above all a good human being.

I am also grateful to my committee members, Dr. Andre Gesquiere, Dr. Diego Diaz, Dr. Yi Liao, Dr. Qun Huo, Dr. Linan An, Dr. Florencio Hernandez, and Dr. Andres Campiglia for their valuable and constructive criticism in my research and proposal. My gratitude goes to Dr. Linan An who has always been a great help for his constructive and important advice, support and encouragement. My special thanks go to Dr. Hernandez, Dr. Campiglia, and Dr. Yi Liao not only being a member of my committee but also as great teachers in my graduate classes. I warmly thank Dr. Diaz as my first teacher in UCF in Analytical Chemistry, the area I was completely unaware of and learnt a lot from his guidance. My sincere thanks go to Dr. Gesquiere who has been the mentor in my seminar presentation and for his proper guidance in acquiring knowledge in organic solar cells. I would also like to thank Dr. Huo for allowing me to use her lab facilities over all these years which have been a great help throughout my research.

I would like to thank my research group members, Dr. Jianhua Zou, Dr. Jianhua Liu, Dr. Anindarupa Chunder, Qiang Li, Binh Tran, and Kennneth Etcheverry for invaluable suggestions,

help and congenial ambience to conduct my research. Fruitful discussions with Dr. Liu, research or non-research related, has helped me a lot in broadening my knowledge. The camaraderie I shared with Ken will always be one I will cherish for my life. I also appreciate the help and support from the group members of Dr. Linan An, especially Dr. Tao Jiang, Yaohan Chen and Cheng Li. My thanks go to all my colleagues at NSTC and Department of Chemistry. I also thank my friends, Sanjiban, Sanchita, Anirban, Shurba, Debasis, Soumitra, Satarupa, and especially Poulami Joshi, Cristine DCruz, and Ricky for the time they spent with me which make me feel home away from home.

I am thankful to Kirk Scammon, Mikhail Klimov, and Dr. Qi Zhang for their immense help in operating instruments including SEM, TEM, XRD, and XPS. I also thank Dr. Hans van Tol, Dr. Andrew Ozarowski and Dr. Zhehong Gan for EPR and NMR analysis at National High Field Magentic Lab at Florida State University.

My wife, Ranita, deserves my special thanks. I would not have been able to do anything without her continuous sacrificial love and support during the hard time of my PhD. The time and effort she has spent so that I can concentrate on my research go beyond words. Words will fall short if I continue to describe her sacrifice. So my deepest and heartiest gratitude and love go to my wife.

I cannot complete this acknowledgement without mentioning about my parents, my father and mother, my grandmother and my parent-in-laws back home in India for their unconditional love and encouragement throughout my research. Their continuous inspiration makes me feel their

presence and motivated me in my research. I sincerely thank all my friends and relatives back home, especially Swagata and Somenath for their continuous support and love.

Finally, last but definitely not the least, I would like to thank NSTC and the Department of Chemistry for providing me the financial support to conduct my research and graduate studies in UCF. My sincere gratitude goes to UCF for providing me the platform and opportunity to obtain the most respected highest degree in any field, the DOCTORAL DEGREE.

I am almost certain that I have overlooked many others who have a direct or indirect influence in my research and life. If you are among them, please forgive me this oversight.

TABLE OF CONTENTS

LIST OF FIGURES

CHAPTER 1 INTRODUCTION

1.1 Overview of Polymer-Derived Ceramics

Preceramic polymers were reported about 40 years ago as the precursor materials to fabricate silicon-based (Si) ceramics, commonly known as polymer-derived ceramics (PDCs). This direct polymer to ceramic synthesis led to major achievements in the field of ceramic science and engineering, such as the development of coatings, fibers, microcomponents, or ultrahigh temperature stable (up to 2200 $^{\circ}$C) materials with respect to their crystallization, decomposition, phase separation, oxidation, and creep resistance properties. Recently, many important advancements such as the multifunctionality associated with the PDCs have been achieved. In addition to that, novel insights into the nanostructures have significantly contributed to the basic understanding of the unique high temperature properties of PDCs, such as chemical, oxidation and creep resistance or even their semiconducting behavior. PDCs have been structurally manipulated to fabricate ordered mesoporous structures, tested to join ceramic components, and have also been processed to make bulk ceramic components. As a result, a variety of applications of PDCs including high temperature resistant materials for energy, automotive, and aerospace applications, materials for catalyst support or functional materials in microelectronics have been explored by the materials scientists and engineers throughout the world. The micro-/nanoscience and technology of PDCs is a highly interdisciplinary field of research in true sense, with the expertise from chemists, physicist, materials scientists and engineers providing significant contributions to the growth of PDCs in real-life applications. Moreover, structural components

made from PDCs have already been commercialized by several industries with a dramatic increase in the production and availability of preceramic precursors over the last few years.

1.2 Background

PDCs are a unique class of additive-free ceramic materials possessing excellent high temperature oxidation and corrosion resistance. Ainger and Herbert,[1] Cheantrell and Popper,[2] first reported the fabrication of non-oxide base ceramics synthesized from molecular precursors in early 1960s. Ten years later, in 1970s, Verbeek et. al.[3-5] first reported the fabrication of Si_3N_4/SiC ceramic fibers for high temperature applications by the direct transformation of polysilazanes, polysiloxanes and polycarbosilanes into ceramics. Since then significant achievements have been made in PDCs with the development of several classes of PDCs including binary systems (Si_3N_4, SiC, BN, AlN), ternary systems (SiCN, SiCO, BCN), and as well as quarternery systems (SiBCN, SiAlCN, SiCNO) from preceramic polymers. The polymer precursors used in the synthesis of PDCs are inorganic/organometallic systems which provide final ceramics with a tunable chemical composition and well defined nanostructures by controlled thermal annealing (curing and pyrolysis) under suitable atmosphere. This direct polymer-to-ceramic conversion route is an emerging technology as evidenced by the ever increasing commercial development of preceramic polymers to produce near-bulk shape materials in a way not known for other techniques.[6] Moreover, unlike conventional ceramics obtained by sintering corresponding powders, which requires the presence of sintering aids and significantly constrains technical applications, this unique direct polymer-to-ceramic conversion route of PDCs makes them suitable for the fabrication of unconventionally shaped ceramic components and devices such as

fibers, coatings, or composite materials.[7-10] Another advantage of PDCs lies in their relative low synthesis temperature of 1100-1300 °C, which means lower energy consumption compared to conventional ceramic processing, which requires 1700-2000 °C to obtain Si_3N_4- and Si-based ceramics by sintering powders.

Polymer-derived ceramics, in general, manifests improved thermo-mechanical properties related to their crystallization and decomposition, creep and oxidation resistance, or phase separation at higher temperatures of 1500 °C or higher. For example, polymer-derived siliconcarbonitride (SiCN) ceramics exhibit excellent oxidation and creep resistance at annealing temperatures as high as 1500 °C.[11,12] However, in the presence of excess carbon in the SiCN ceramics, the solid-state reaction of Si_3N_4 with carbon generates SiC and nitrogen at temperatures greater than 1450 °C and the material crystallizes.[13] Recent studies have shown that in boron containing polymer-derived siliconborocarbonitride (SiBCN)ceramics, the high temperature stability with respect to decomposition have dramatically increased to 2200 °C. These polymer-derived SiBCN ceramics have higher thermal, mechanical, and chemical stability than boron free SiCN ceramics. This extraordinary thermal stability of SiBCN ceramics is believed to be due to the structural disorder leading to the increase in the activation energies of both solid state reaction of silicon nitride and carbon and the crystallization.[14] The detailed structural evolution of SiBCN ceramics is discussed in the forthcoming chapters.

1.3 Preceramic Polymer Precursor Synthesis

The design and synthesis of preceramic polymer precursors is one of the key aspects of PDCs because the molecular structure can not only influence the composition of the final ceramics but also the micro-/ nanophase and the phase distribution in the final ceramic matrix. Thus, the macroscopic physical and chemical properties of the PDCs can be significantly altered with the design of the starting polymer precursor.

An organosilicon polymer can be simply represented as in Figure 1.1, where the group X determines the classes of Si-based polymers (Figure 1.2) such as X= Si for poly(organosilanes), X = CH_2 for poly(organocarosilanes), X = O for poly(organosiloxanes), X= NH poly(organosilazanes), poly (organoborosilazanes) with X= B and the substituent groups R^1 and R^2 can be either hydrogen or aliphatic or aromatic side groups. The solubility, viscosity and thermal stability of the polymer, which are important with respect to their processibility, are controlled by the R groups. It is worthwhile to mention that the R group in fact controls the total carbon content in the final ceramic composition.

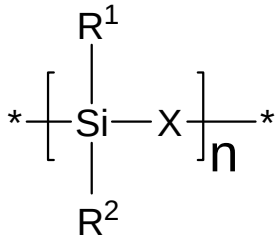

Figure 1.1 Structural representation of the molecular structure of the preceramic polymer.

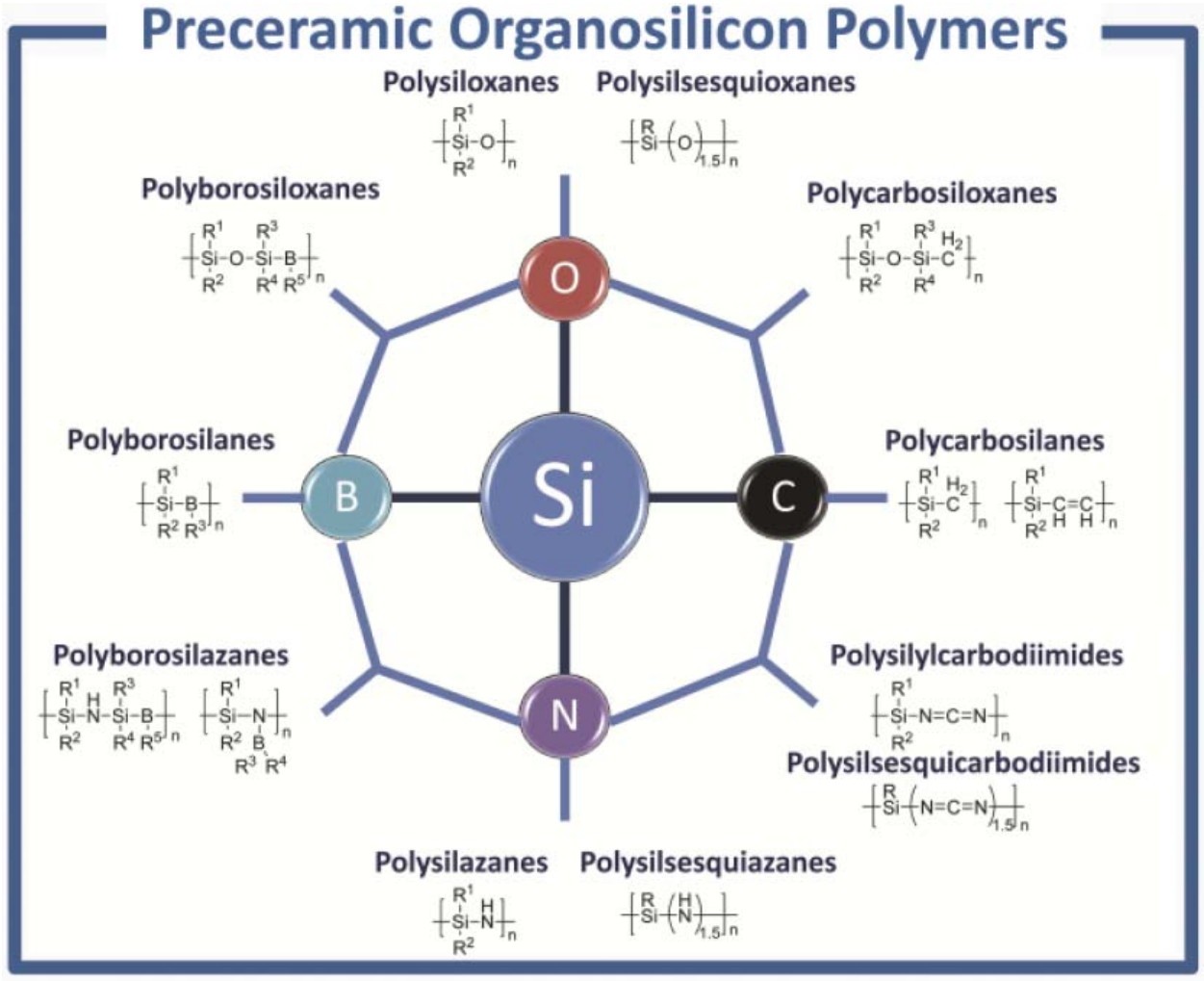

Figure 1.2 Main classes of preceramic polymer precursors for the fabrication of Si-based PDCs (Reprinted from [15] with permission from Wiley-VCH).

There are some important prerequisites for a preceramic polymer to be effective during the thermal treatment.[16] The polymer should have sufficiently high molecular weight in order to avoid the volatilization of low molecular weight oligomers. They should have suitable rheology or viscoelasticity and solubility to be suitable for shaping process. They should have the functional groups (latent reactivity) in order to obtain appropriate curing properties. They also

should have the polymeric structure with cages or rings to reduce the volatization of the fragments due to the backbone cleavage.

One of the important characteristics of PDCs is their ability to incorporate carbon in their ceramic composition, which is controlled by the side group (R) functionalization. It is generally believed that the presence of excess carbon is detrimental for the high temperature properties such as resistance to crystallization and mechanical properties of PDCs. However, recent studies have demonstrated that in certain cases, SiCO ceramics containing high carbon exhibit excellent resistance towards crystallization and decomposition.[17,18] The following discussion focuses on the synthesis of poly(organosilazanes) and poly(organoborosilazanes) for the research purpose.

1.3.1 Synthesis of Poly(organosilazanes)

Polysilazanes can be synthesized by the reaction of chlorosilanes with ammonia (ammonolysis) or with primary amines (aminolysis). Both of the synthetic methods suffer from the disadvantage of the elimination of the polymer from the solid byproducts, NH_4Cl or H_3NRCl respectively (Figure 1.3a).[19] Several other synthetic approaches have been reported so far starting from the novel polymerization method reported by Seyferth et. al.[20] in which low molecular weight oligomers containing Si-H groups adjacent to an N-H group, i.e., -$[RSiHNH]_x$-, reacts with catalytic amounts of alkali metal base such as KH to give planar structure poly(organosilazane). Later Laine et. al. reported transition-metal-catalyzed ring-opening polymerization of silazane monomers to form polysilazanes.[21] Also, the silazane monomers have been modified with urea or isocyanate to obtain silazane oligomers with improved chemical and physical properties.

Schwark et. al. reacted methylvinylsilazane cyclic silazane oligomers with isocyanates and synthesized poly(ureamethylvinyl)silazanes (PUMVS).[22] Depending on the amount of isocyanates, the products varied in their rheological properties such as viscosity. Nowadays, a series of polysilazanes are commercially available, most of them are produced by KiON® Speciality Polymers, a Clariant Business specialized in silazane technology. Their products include the following commercial derivatives: Ceraset™ Polysilazane 20, Ceraset™ Polyureasilazane and HTT 1800 Polysilazane/Heat-Curable High Temperature Resin (VL 20). For research purpose, Ceraset™ VL 20 (Figure 1.3b) is used as the precursor for the fabrication of SiCN ceramics.

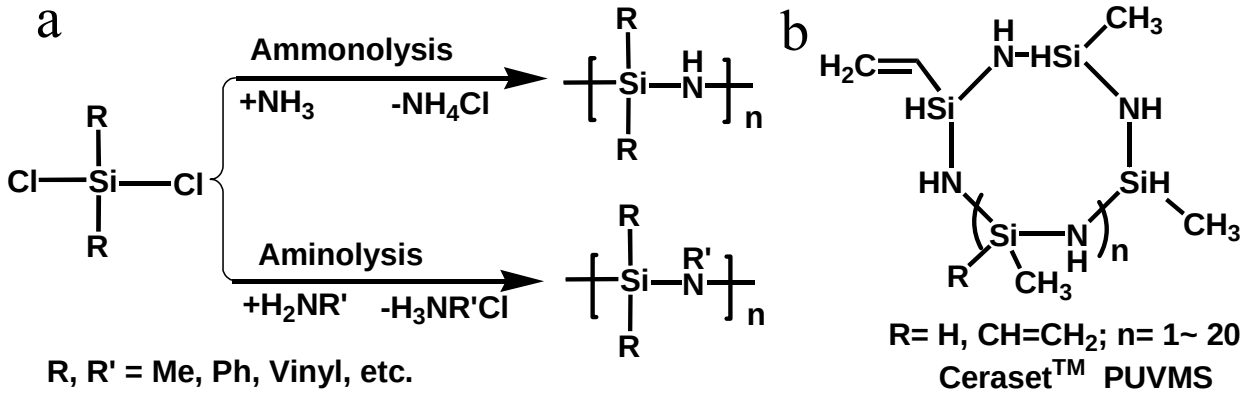

Figure 1.3 (a) Fabrication of poly(organosilazane) from chlorosilanes, and (b) chemical structure of Ceraset™ VL20.

1.3.2 Synthesis of Poly(organoborosilazane)

Several research groups reported the synthesis of poly(organoborosilazane) precursors starting from Si-based monomers or oligomers. In 1990, research groups from MIT (Seyferth and

colleagues)[23] reported the synthesis of borosilazane preceramic polymers by the reaction of borane, $BH_3 \bullet Me_2S$ with cyclic oligomers, such as $(CH_3SiHNH)_n$ obtained by the ammonolysis of methyldichlorosilane (CH_3SiHCl_2), which resulted in hydrogen (H_2) gas evolution and the formation of a crosslinked product containing boron atoms connected to three nitrogen atoms. The first step involved the formation of cyclosilazane-BH_3 complex followed by the evolution of H_2 and formation of a borazane ring, where the cyclosilazane rings maintained their structure. Finally, the borazine rings were formed by the ring opening reaction of the cyclosilazane ring (Figure 1.4). The product, when pyrolyzed in the presence of argon, gave a ceramic yield as high as 90%. Since then substantial progress have been made with the synthesis of the various polyborosilazane precursors including the choice of the starting Si-based material, synthesis route and also the silicon to boron ratio (Si:B).

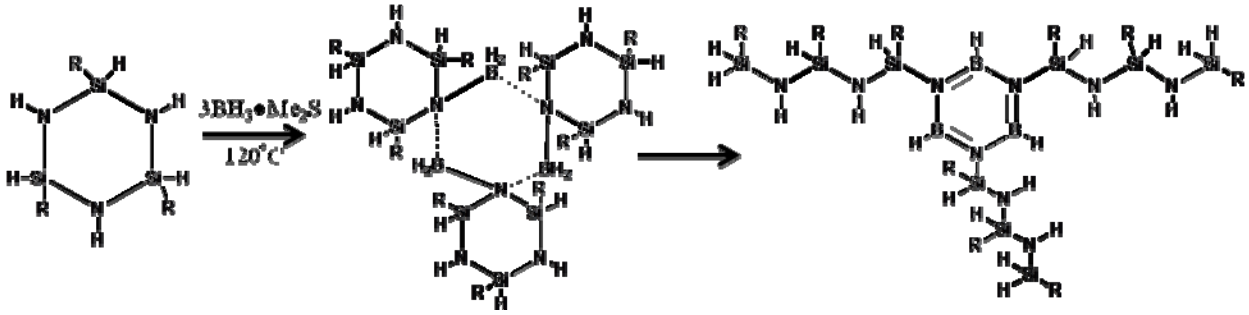

Figure 1.4 Synthesis of poly(organoborosilazane) by Seyferth et. al.

One of the classical approaches involves the utilization of vinyl groups to attach boron in the silazane backbone. Riedel et. al.[24] reported a classical hydroboration reaction to the dichloromethylvinylsilane to obtain tris(methyldichlorosilylethyl)borane. This was then followed by the ammonolysis yielding the boron modified polysilazane (Figure 1.5a). This method is

referred to as monomer route since the polymer precursor is obtained from an already boron modified monomer. Replacement of Si-CH_3 groups by Si-Ph groups produces poly(borosilazane) prepolymer (Figure 1.5b), which gives a ceramic thermally stable upto 2200 $^{\circ}$C and resists crystallization upto 1700 $^{\circ}$C. It is believed that the introduction of phenyl (Ph) group in place of CH_3 group results into a reduced crosslinking state to provide enhanced disorder in the resulting amorphous SiBCN ceramic network. This additional disorder increased the free activation energies for crystallization.[14] More into the structures of SiBCN ceramics is discussed in the following chapters. In an another effort, Bernard and colleagues synthesized preceramic polymers by the reaction of tris(dichloromethylsilylethyl)borane with methylamine (Figure 1.5c).[25] This novel polyborosilazane functionalized with Si- and N-bonded methyl groups inhibited extensive crosslinking to yield a tractable polymer which was successfully processed into polymer green fibers by melt-spinning process. In polymer route, the prepolymer is achieved by the functionalization of the polymeric precursor, for example, the hydroboration of polymethylvinylsilazane (Figure 1.6). The polymer route offers a very high output and also the reaction is inexpensive, rapid and free from salt separation (sometimes called salt-free method).[26]

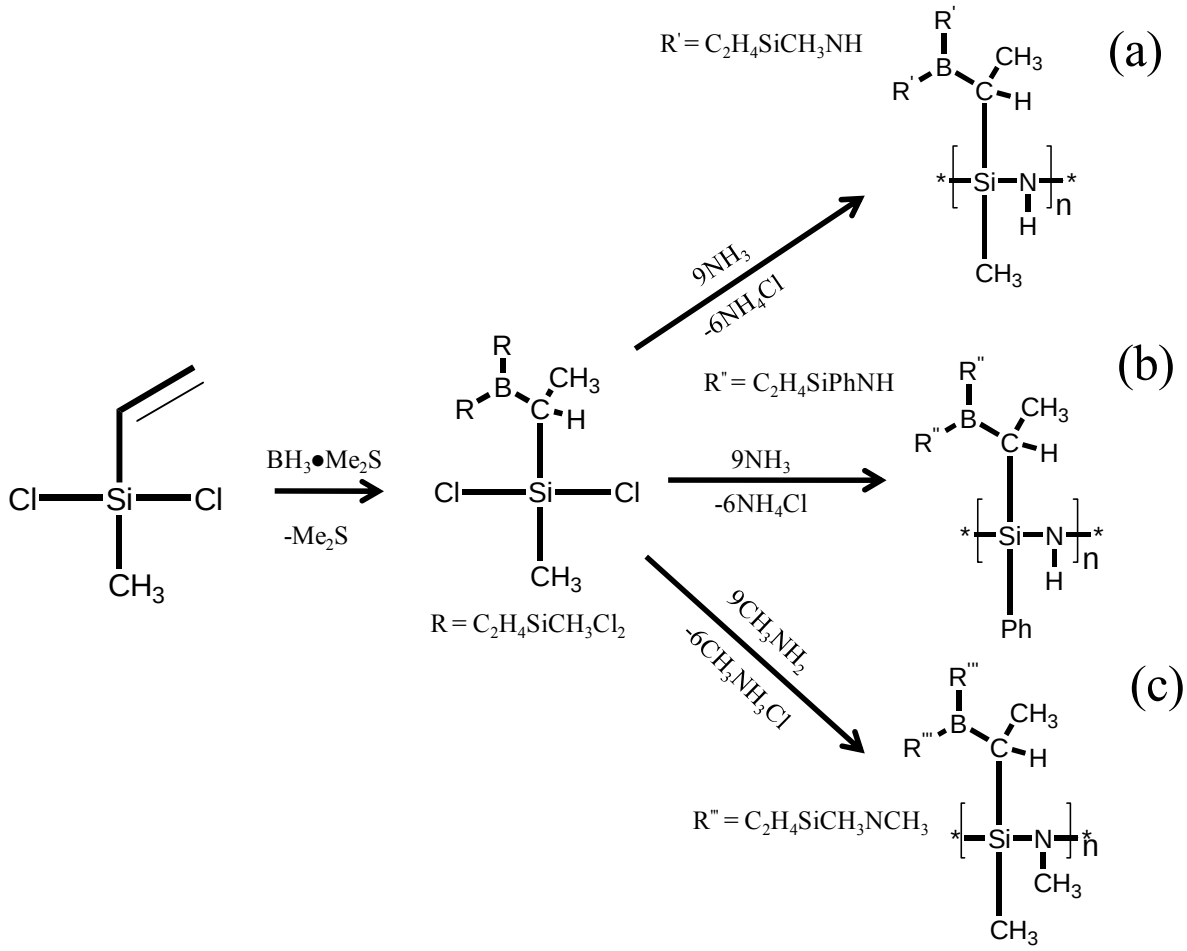

Figure 1.5 Synthesis of poly(organoborosilazane) by monomer route.

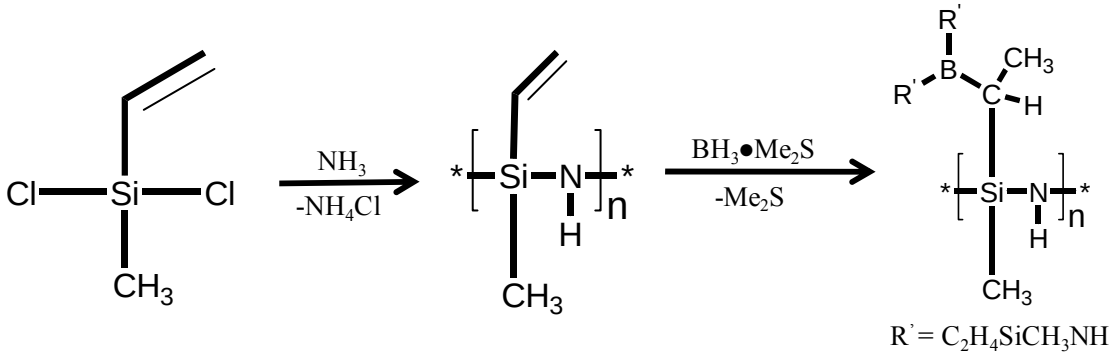

Figure 1.6 Synthesis of poly(organoborosilazane) by polymer route.

1.4 Processing of the Ceramic Polymer Precursors

1.4.1 Shaping and Crosslinking

Polymer-derived ceramics technique can be used to fabricate unconventional shaped components which cannot be achieved with conventional powder processing by sintering the corresponding powders. The main characteristic of PDC precursors is that they are polymeric in nature at the temperature at which they are shaped into various components. Therefore, they can be easily subjected to different shaping methods, which are far more easily exploited with the polymers than ceramic powders. PDCs also have the advantage over conventional sol-gel process with respect to the processing parameters. For example, PDCs, in general, do not require long processing times such as for gelation and drying. Typically the preceramic polymer can be a crosslinkable liquid, or a meltable and curable solid, or an unmeltable but solvent-soluble solid. The preliminary requirement to fabricate components using liquid polymers is that, after the shaping step, the parts need to be crosslinked so that they retain their shape during pyrolysis. In general, the presence of functionalities such as vinyl (Si-CH=CH_2) or silyl (Si-H) groups enable the formation of thermally crosslinked products via vinyl group polymerization or hydrosilylation (reaction between Si-H and Si-CH=CH_2) that occur, typically, below 200°C.[27] It is generally believed that hydrosilation dominates the crosslinking reactions at lower temperatures due to the high reactivity of Si-H and Si-CH=CH_2.[28] The polymers cal also be chemically crosslinked using a photoinitiator, such as 2,2-dimethoxyl-2-phenyl acetophenone.[29] Photopolymerization is a cost-effective, well controlled soft approach, where solidification can be achieved by the exposure of the polymer to the UV radiation rather than by the heat treatment.

Since these preceramic polymers can be given a shape that is maintained during pyrolysis, therefore these polymers offer the opportunity to create low dimensional components such as micro- and nanofibers in comparison to powder processing technique. Several forming techniques have been explored in the field of PDCs including coating, self-assembly, photolithography, melt-spinning, and electrospinning. For the research purpose, the fabrication of non-oxide polymer derived ceramic fibers by spinning technologies is emphasized.

1.4.2 Polymer-to-Ceramic Conversion (Pyrolysis)

The final step to the fabrication of ceramics is the conversion of the shaped polymer (and crosslinked if required) to the ceramic at high temperatures by a process called pyrolysis. During polymer to ceramic transformation organic groups such as methyl, phenyl, vinyl and Si-H, Si-OH, or Si-NH get decomposed or eliminated. Typically this transformation involves two important features: one is the weight loss, typically known as ceramic yield, and the other is the compositional change accompanied by the pyrolysis. To quantitatively monitor the weight loss during polymer to ceramic conversion thermogravimetric analysis (TGA) is the method of choice. The weight loss is predominantly caused by the evolution of oligomers at lower temperatures followed by the release of by-product gases at higher temperatures. For example, for polysilazanes, a three-stage weight loss was observed by Choong et.al.[28] First, a weight loss occurs at about 400 $^{\circ}$C due to the evolution of low molecular weight oligomers. The second weight loss occurs in the temperature range of 400 to 700 $^{\circ}$C due to the loss of hydrocarbons, such as CH_4, C_2H_6 and others, and the third and final weight loss was due to the loss of hydrogen evolution. Thus TGA was found to be an efficient tool to investigate and also to optimize the

polymer-to-ceramic transformation during the thermal treatment. The other aspect of pyrolysis is the change in the chemical composition from polymer to ceramic, which depends on number of factors, such as the starting polymer precursor, pyrolysis atmosphere and also the degree of crosslinking. The final amorphous ceramic composition, for example, in case of polysilazanes is the stable ternary phases of silicon nitride (Si_3N_4), silicon carbide (SiC) and the carbon (C). The final ceramic composition can therefore be expresses as SiC. $n$$Si_3N_4$. xC, where n is the measure of the relative amounts of Si-C and Si-N bonds in the amorphous structure and the x measures the free carbon bonded interatomically.

1.4.2.1 Polymer-Derived Non-oxide Ceramic Fibers

Non-oxide ceramic fibers have been widely used as the skeletal structures in ceramic matrix composites (CMCs) for high temperature applications where the metallic materials suffer serious corrosion and mechanical property deterioration.[30] The drastic condition in turbine engines, rocket nozzles and furnace requires superior mechanical and chemical properties from the ceramic fibers. Generating non-oxide ceramic fibers from their polymer precursors allows the control of the ceramic fiber composition and structures to provide the required properties. PDCs provide the platform for such process that includes three basic steps: (i) synthesizing/modifying preceramic polymers, (ii) spinning (melt spinning or electrospining), and solidifying polymer fibers, and (iii) pyrolyzing the polymer fibers into ceramic fibers. The direct polymer-to-ceramic processing route of PDCs not only provides the processable materials for the fabrication of ceramic fibers, but also allows the control over the polymer precursor composition which contributes significantly to the final ceramic fiber properties. Green polymer fibers are fabricated

through either a melt-spinning or an electrospinning process. Both melt spinning and electrospinning are highlighted in the following discussion with strong emphasis on electrospining for the purpose of research.

1.4.2.1.1 Melt Spinning

Melt spinning is a traditional technique to manufacture polymer fibers without the use of flammable solvents, where the melt polymer is pumped through a spinnert with lots of small holes. Appropriate viscosity is required for the melt polymers to be spinnable. The soft polymer fibers cool down and solidify after passing through the holes, and are collected on a take-up wheel (Figure 1.7a). The size of the polymer fibers, ranging from several micrometers to tens of micrometers, is controlled by the spinnert hole diameter and spin rate. The polymer structures can be altered by stretching extruded polymer fibers when solidifying. Such process orients polymer chains along the fiber axis, creating a stronger fiber and leading to more ordered crystalline ceramic structures.

1.4.2.1.2 Electrospinning

Electrospinning is a simple and versatile technique to generate continuous ultrathin fibers in nanometers and micrometers from various polymeric materials. The first patent that depicted the electrospinning appeared in 1934, when Formhals invented an apparatus to produce ultrathin polymer fibers using the electrostatic repulsion between surface charges.[31] It was until 1993, the process was known to be electrostatic spraying and received little attention. Reneker group at the

University of Akron revived interest in this technique to fabricate ultrathin fibers from polymers.[32,33] Since then significant progress have been achieved with the electrospinning, both experimental and the theortical.[34-37]

In a typical design, the electrospinning setup consists of four basic components: a high voltage power supply, a syringe pump, a spinnert, and an electrically conductive collector. For most of the electrospinning purposes, an ordinary hypodermic needle and an aluminum foil or silicon (Si) wafer is used as the spinnert and collector electrode respectively (Figure 1.7b). The polymer solution is fed into a plastic syringe connected to the metallic needle. The syringe pump is used to control the flow rate of the polymer solution during electrospinning. The basic working principle is primarily based on electrostatic interactions. When a high electrical voltage is applied between the spinnert and the collector plate, the pendent droplet becomes highly charged and takes the shape of a cone-like meniscus, often referred to as Taylor cone, as a result of electrostatic repulsions between the surface charges and also the electrostatic attractions from the oppositely charged collector electrode, which is grounded. When the voltage or the electrical field strength surpasses a critical or threshold value to overcome the surface tension, a jet is emitted and moves towards the collector electrode. The electrified jet then continuously experiences a rapid bending and whipping process in which the jet is continuously stretched and elongated by the electrostatic forces, the solvent evaporates, leading to the formation of non-woven fabric mat on the collecting electrode.[38-40]

Electrospinning requires that polymers have good solubility in solvents with decent spinnability. It provides good control over the fiber size and morphology by tuning the polymer solution

properties (i.e. polymer concentration and the choice of solvents) and operating parameters (i.e. voltage, solution feeding rate and electrode distance).

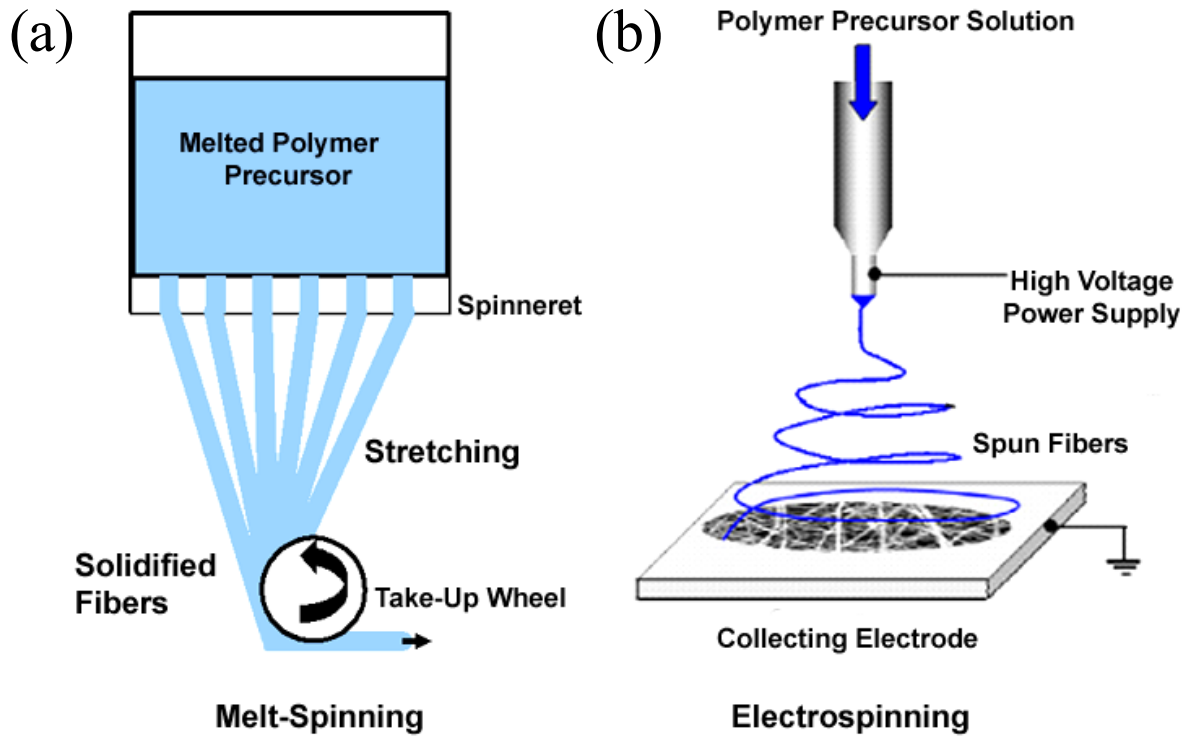

Figure 1.7 Illustration of melt-spinning and electrospinning process.

1.4.2.1.2.1 Fiber Morphology Control in Electrospinning

Electrospinning generally generates fibers with well controlled diameter and smooth surface morphology. But for a number of applications, such as tissue engineering, filtration, catalysis, nanofiber reinforcement, it could be advantageous to switch from smooth surface to a porous surface, which would increase significantly increase the surface area to the benefit of such applications. One of the approaches involves the selective removal of one of the component

polymer from the nanocomposite fiber made from a mixture of polymers. Wendroff and coworkers investigated the structural changes that an electrospun polylactide (PLA)/poly(vinylpyrrilidone) (PVP) nanocomposite fiber from dichloromethane solutions undergo when one of the two components was selectively removed.[41] It was found that highly porous nanostructured fibers were formed from a 1:1 composition of the polymer blends. If one of the polymers was much higher concentration than the other polymer, smooth fibers were generated. This behavior was believed to be due to the rapid phase separation induced by solvent evaporation and solidification during electrospinning. It was also found by the same group that the porous morphology of the electrospun fibers of PLA and polycarbonate (PC) could be controlled upon judicial selection of the electrospinning parameters and the solvent systems (Figure 1.8).[42] Rabolt et. al. also studied the electrospinning of polymers such as PC, polystyrene (PS), poly(methylmethacrylate) (PMMA) and found out that the solvent vapor pressure and level of humidity has an influence on the formation of porous fibers.[43,44] It was suggested that along with the phase separation induced by solvent evaporation, cooling effect caused by the volatilization of solvents during electrospining might induce moisture condensation onto fiber surface and promotes the pore formation. Apart from the porous structures, electrospinning could also be used to generate hierarchical structures as demonstrated by Rutledge and colleagues.[45] Electrospun poly(caprolactone) (PCL) fibers, consisting of nanoscale roughness and micrometer-scale beads, generated the hierarchical roughness and then coated with a thin conformal coating of a low surface energy material, poly(tetrafluoroalkyl ethyl methacrylate) by chemical vapor

deposition. The combination of these two effects led to the formation of super-water repellent, commonly known as superhydrophobic, electrospun fiber mat.

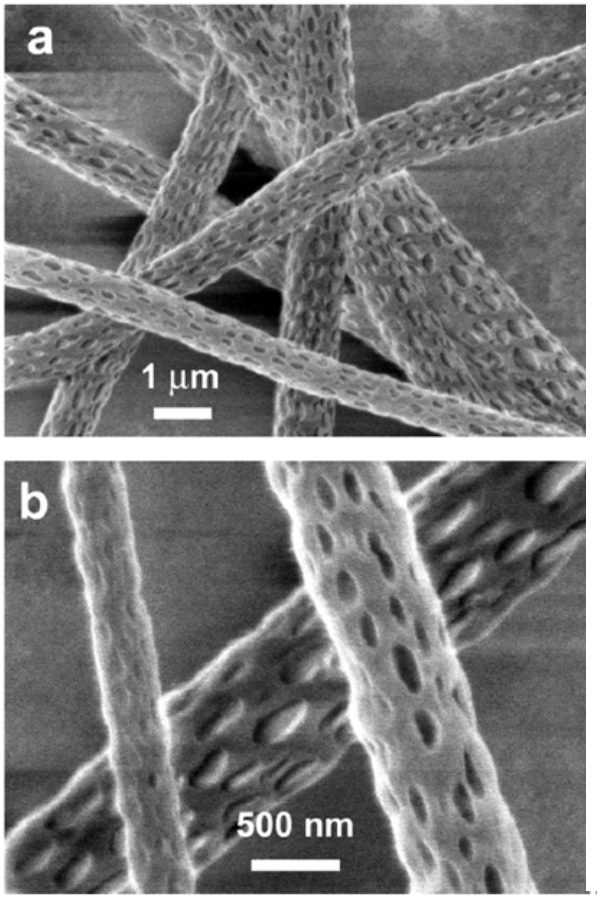

Figure 1.8 Representative example of porous electrospun PLA fibers from dichloromethane (Reprinted from [42] with permission from Wiley-VCH).

1.4.2.1.2.2 Encapsulation of Functional Materials

Electrospinning offers the advantage of direct introduction of wide range of functional materials such as nanoparticles, nanotubes, to obtain nanofibers with well-defined compositions and functionalities. Nanoparticles have been incorporated into nanofibers by the addition of

appropriate precursor to the solution prior to electrospinning, followed by post-treatment to obtain polymer fibers incorporated with nanoparticles. For example, Greiner et. al. added palladium diacetate to a PLA solution to increase the conductivity of the polymer solution in order to achieve thinner fibers.[46] Annealing the electrospun fibers at elevated temperatures led the formation of Pd nanoparticle-doped electrospun polymer fiber. Later on, Reneker and coworkers reported the introduction of iron (Fe) nanoparticles into electrospun carbon fibers by adding an iron salt, Fe (acetylacetonate)$_3$, to a polyacrylonitrile (PAN) solution in DMF. When properly heat treated at suitable atmosphere, carbon fibers with Fe nanoparticles were produced. These Fe nanoparticles were further used as a catalyst to grow carbon nanotubes (CNTs) onto the carbon nanofibers to generate hierarchical structures.[47]

Similar to nanoparticles, CNTs have also been incorporated into electrospun polymer nanofibers to improve the mechanical and the electrical properties of the composite fibers. Ko and coworkers[48] showed that the orientation of the CNTs in the electrospun fibers was dependent on the polymer and most importantly, how well the CNTs were dispersed in the solution. For example, single-walled CNTs could be well dispersed in the N,N-dimethylformamide (DMF) solution of polyacrylonitrile (PAN) and when electrospun, the nanotubes maintained their longitudinal morphology and orient parallel to the axial direction of the electrospun fiber. In contrast, when CNTs were added into poly(lactic acid) solution, the CNTs were distributed inhomogeneously in the fiber matrix to form highly entangled agglomeration of carbon nanotubes. Mechanical property measurement showed the reinforcement effect of the carbon nanotubes at less than 3 wt% of SWCNTs due to the stiffening of the polymer as a result of the

interaction of the polymer with the nanotubes. Several other research groups, such as Gorga et. al. reported the morphological, electrical, and mechanical characterization of the electrospun nanofiber mats from poly(ethylene oxide) (PEO) containing multiwalled carbon nanotubes (MWCNTs) to form electrically conducting porous nanocomposite fibers.[49] Above a percolation threshold of 0.35 wt% in PEO, the conductance increased by a factor of 10^{12} and then became stabilized with further increase in the MWCNT concentration. Mechanical testing also showed an improvement in the Young's modulus when compared a 1 wt% MWCNT loading to the pure electrospun PEO. Thus, provided CNTs are well dispersed into the polymer solution, CNTs play an important reinforcing encapsulation material in electrospun polymer fibers.

In order to obtain ceramic fiber with desired properties, the structure of the polymer precursors needs to be carefully designed to meet several requirements. Polymer composition should be controlled to generate specific ceramic fiber such as SiC, SiCN, ideally, with selected nanostructures after pyrolysis. Suitable rheology in melt state and in solution is necessary for melt spinning and electrospinning. The green polymer fibers must be infusible after post-spun treatment to maintain the fiber integrity upon pyrolysis. The amount of extraneous small groups in polymer precursors should be minimized to increase the ceramic yield and the density, as well as avoid the formation of pores/voids.

1.4.2.1.3 Fabricating Non-Oxide Amorphous Ceramic Fibers

The objective of fabricating non-oxide ceramic fibers was to replace carbon fibers in CMCs for high temperature applications. Although being widely used in composite reinforcement, carbon

fibers suffer from a low oxidation onset temperature around 450 °C in air, which limits their application at high temperatures in an oxidative environment.[50] Therefore, the target ceramic fibers are required to maintain good mechanical properties and oxidation resistance at high temperature. The design concept for non-oxide ceramic fibers is to build a structure by the combination of Si and B with N or C where the diffusion coefficients of Si or B in the compounds are extremely low. The strong covalent bonds would show negligible contributions to the enthalpy of formation from long-range bonding interactions that drive crystallization. Such amorphous structure could meet the requirements of durability while resisting crystallization.

SiC (silicon carbide) based ceramic fibers were first reported by Yajima, through an alkali metal promoted dehalocoupling of chlorosilanes followed by a Kumada rearrangement (Figure 1.9).[51] The resultant polymers, with a molecular weight around 1500 Da, were melt-spun into green fibers (~20 μm) in N_2 gas. The curing of the green fibers were performed by either thermal oxidation in air at temperature of 100-200 °C or by electron beam (EB) irradiation by He gas followed by a thermal treatment in an inert gas. In thermal oxidation, green fibers became infusible by the cross-linkage via Si-O-Si and Si-O-C bonds with 7% increase of oxygen in the fibers.[52-54] In comparison, EB crosslinked the Si-H, -CH_2- or -CH_3 groups that introduced less than 1 % oxygen in the fibers.[55,56] Green fibers cured by both methods were pyrolyzed at 1200 °C in Ar or N_2, which led to high tensile strength SiCO (about 10 % oxygen) and SiC (less than 1 % oxygen). The characterization of these ceramic fibers revealed that SiCO fibers contained β-SiC nanocrystals, free carbon and an amorphous silicon oxycarbide (SiC_xO_y), while the microstructures of SiC fibers is a mixture of β-SiC crystals with large amount of glassy carbon

and a very small amount of SiC_xO_y. This technology was later used by Nippon Carbon Co., Ltd. (NCK) to produce continuous SiC based ceramic fibers under the trade name Nicalon NL-200™ (thermal treated, $Si_{0.566}C_{0.317}O_{0.117}$) and Hi-Nicalon™ (irradiation treated, $Si_{0.624}C_{0.371}O_{0.0.005}$). The Hi-Nicalon™ has similar tensile strength and tensile modulus as Nicalon NL-200™ at room temperature, but demonstrates better stability at high temperature. After a high temperature treatment, the size of β-SiC crystallite in Hi-Nicalon™ is smaller than that of β-SiC crystallite in Nicalon NL-200™. The inhibition of the β-SiC crystal growth is due to the presence of large amount of free carbon in Hi-Nicalon™. In contrast, Nicalon™ prepared by oxidation curing loses carbon and oxygen as CO by a carbothermal reduction. The remaining SiC material tends to grow into larger crystals at high temperature.[57] When the SiC based ceramic fibers are heated above 1200 °C, the grain coarsening and the crystal growth as well as the release of gases cause the loss of structural integrity.[58,59]

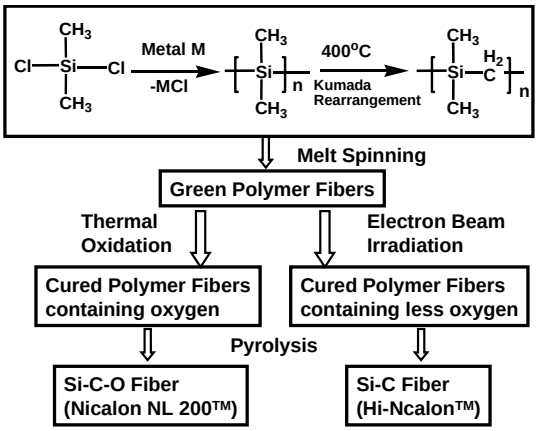

Figure 1.9 Fabrication scheme of SiCO and SiC fibers.

Improvement of the thermal stability and oxidation resistance of non-oxide ceramic fibers has been achieved by polycarbosilazane-derived SiCN fibers and SiBCN fibers. The rigid nanostructures from the covalent bonds in these multinary ceramic fibers lead to a very low diffusive mobility of the molecular species at high temperature, preventing the grain coarsening and crystal growth. SiCN fibers that can retain structural integrity upto 1400 $^{\circ}$C have been fabricated from poly(organosilazanes) obtained through ammonolysis or aminolysis reactions with chlorosilanes (Figure 1.3), as well as from commercially available precursors such as Ceraset™ (PUMVS).[60] Ceraset™ are oligosilazanes with average molecular weight of 400. These oligomers are not suitable for melt-spinning due to low viscosity. Further polymerization to increase the molecular weight produces a three-dimensional crosslinked unspinnable product due to the crosslinking of the vinyl groups. Raj and coworkers used zirconium alkoxides to control the polymerization of PUMVS. The procedure produced a viscous spinnable polymer which was melt-spun into ~10-60 μm fibers. These fibers were crosslinked at room temperature for overnight (probably through hydrolysis) and pyrolyzed at 1000 $^{\circ}$C to obtain ceramic fibers with the composition $SiZr_{0.13}C_{0.46}N_{0.785}O_{0.69}$. The tensile strength (2.2-2.8 GPa) and Young's Modulus (160-190 GPa) of the fibers are comparable with Hi-Nicalon™ fibers. The systematic investigation of oxidation behavior of SiCN based and SiC based ceramic fibers demonstrates that the oxidation rates (parabolic rate) of the SiCN fibers are lower than those of the SiC fibers. The oxidation resistance of Si based ceramic fibers is due to the formation of a thin layer of silicon dioxide (SiO_2) on the fiber surface that can greatly reduce the oxygen permeability. The dependence of the oxidation rate on the fraction of Si-C and Si-N bonds in SiCN systems

suggests that the possible formation of silicon oxynitride (SiON) or silicon oxycarbonitride (SiCON) sub-layers further reduces the oxygen permeability. The SiCNZr ceramic fibers from zirconium alkoxide treated Ceraset™ have the lowest parabolic rate due to their low carbon content.[61-64]

As mentioned earlier, incorporation of boron into SiCN ceramic matrices resulted into SiBCN bulk ceramics which retain their amorphous structures usually at 1600 °C and even upto 2200 °C, attributed to the presence of boron in the ceramic to retard the crystallization process.[65] Although the polymer precursors synthesized to date can generate high performance ceramics, their poor solubility and high degree of crosslinking prevents the fabrication of ceramic fibers. The modification of the polymer synthesis route aimed at reducing the degree of crosslinking to make polymer spinnable. Sneddon and coworkers used monofunctional boranes such as pinacolborane (PIN), 1,3-dimethyl-1,3-diaza-2-boracyclopentane (BCP) and 2,4-diethylborazine (DEB)[66] to replace multifunctional borazine[67] in the reaction with hydridopolysilazane (HPZ, by Dow Corning) to develop melt-spinnable boron-based polymer precursors (Figure 1.9). Uniform fibers were fabricated from the melt polymers via melt-spinning. PIN-HPZ polymer green fibers (30 to 40 μm) were cured with $HSiCl_3$ followed by an exposure to humid air. The subsequent pyrolysis at 1200 °C in argon (Ar) produced SiBCN ceramic fibers that remained amorphous at 1600 °C.

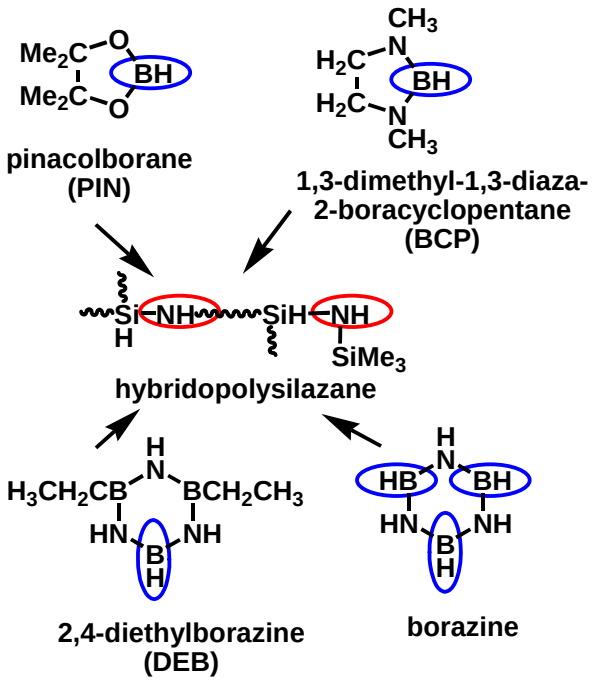

Figure 1.10 Monofunctional boranes replaced borazine to react with HPZ for spinnable polymers.

Miele et.al. took another route to fabricate SiBCN ceramic fibers by using tris(dichloromethylsilylethylborane) developed by Riedel and coworkers to synthesize the preceramic polymer.[25] In contrast to Riedel's route[24] (Figure 1.5a) where ammonia was used, using less reactive methylamine to slow down the crosslinking temperature leads to a meltable polymer with suitable rheology for melt-spinning (Figure 1.5c). Uniform green fibers with an average diameter of 18 μm were obtained from melt-spinning. The curing of the green fibers was performed by a slow heating to 200 °C in an ammonia atmosphere, which crosslinked the polymer backbone. The pyrolysis of the green fibers in nitrogen at 1400 °C produced 8-10 μm $Si_{3.0}B_{1.0}C_{5.0}N_{2.4}$ ceramic fibers with 1.5 GPa tensile strength at room temperature and 1.3 GPa tensile strength at 1600 °C. The high temperature stability and oxidation resistance of the SiBCN

ceramic fibers was investigated in nitrogen and air, respectively. As shown in Figure 1.11, the glassy-like texture of the SiBCN fibers retains at 1500 and 1650 °C, while granular texture appears at 1750 °C due to an amorphous to crystalline transition. The oxidation studies showed only a slight weight increase (2.9 %) during the oxidation treatment from 1100 °C to 1500 °C, suggesting that the SiBCN fibers had good oxidation resistance.[25] High quality SiBCN ceramic fibers have also been fabricated by the pyrolysis of a preceramic N-methylpolyborosilazane made from trichlorosilylaminodichlorobornae ($Cl_3Si\text{-}NH\text{-}BCl_2$)[68] and polysilazane made from one-step condensation of silane, BCl_3 and silazane.[69]

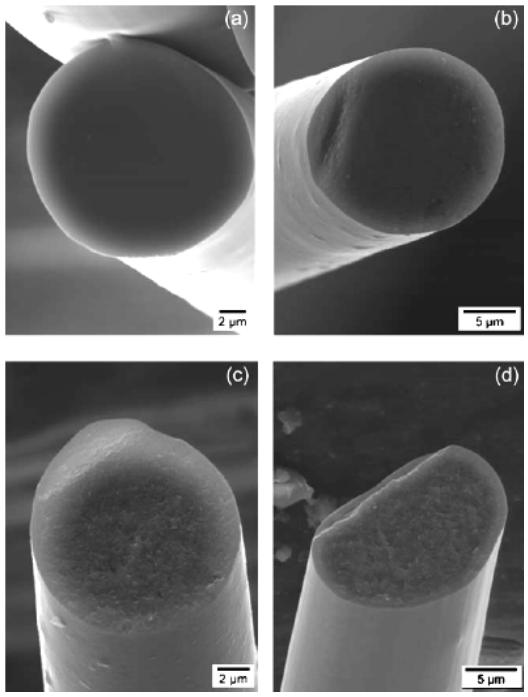

Figure 1.11 SEM images of the cross-sections of the $Si_{3.0}B_{1.0}C_{5.0}N_{2.4}$ ceramic fibers annealed at (a) 1500 °C, (b) 1650 °C, (c) 1750 °C, and (d) 1900 °C (Reproduced from [25] by permission of The Royal Society of Chemistry).

It is worth mentioning out that although most of the works on Si based non-oxide SiC, SiCN and SiBCN ceramics reported till date are based on melt-spinning, electrospinning has also been employed to fabricate Si based ceramics since electrospinning can generate polymer fibers in nanometers with good control of fiber size and morphology. Larsen et. al.[70] reported the fabrication of SiC ceramic fibers by electrospinning a sol solution of Novolac resin and tetraethylorthosilicate (TEOS), followed by conversion of these fibers into SiC ceramics by high-temperature pyrolysis. Sneddon et. al. reported the fabrication of nanoscale freestanding, porous boron carbide/carbon ceramic fibers through electrospinning of a single source polymer precursor, poly(norbornenlyldecaborane) (PND), followed by pyrolysis to convert into ceramic fibers.[71] The electrospinning of PND in tetrahydrofuran (THF) solutions of different concentrations generated microsize fibers (20 %), nanosize fibers (13 %) and nanoscale fibers with beads (10 %). Boron carbide fibers were produced through the pyrolysis of the green fibers at 1000-1300 $^{\circ}$C. SiC fibers were produced by Youngblood et. al. through the electrospinning of preceramic poly(carbomethylsilane) (PCmS). Polystyrene (PS) was added to low molecular weight PCmS (3500 Da) solutions to improve the spinnability. The amount of PS was kept low to prevent the void formation in the fibers during the pyrolysis. The electrospun fibers were crosslinked by a UV radiation and pyrolyzed at 1200 $^{\circ}$C. This process produced SiC/silica core-shell nanofibers with a 30 nm thick silica shell.[72] Recently Salles et. al.[73] reported the fabrication of novel boron nitride (BN) submicron diameter fibers by thermal conversion of electrospun fibers from a blend of polyacrylonitrile (PAN) and poly[(B-(methylamino)borazine] blend solutions. Twelve-percent PAN was added to the low molecular weight (900 Da) to the poly[(B-

(methylamino)borazine] solution in *N,N*-dimethylformamide (DMF) solutions, which otherwise cannot be electrospun and forms droplets due to inappropriate solution viscosity. The as-formed mat was composed of a network of polymer fibers of 500 nm diameter characterized by smooth cylindrical surface, without beads, and a reduced diameter distribution. The polymer fibers were first pyrolyzed at 1000 $^{\circ}$C in ammonia (NH_3) atmosphere and then again pyrolyzed at 1800 $^{\circ}$C to generate BN fibers.

1.5 Microstructure of Polymer-Derived Ceramics (PDCs)

PDCs, when pyrolyzed at high temperatures greater than 1000 $^{\circ}$C, undergo profound microstructural changes. Their unique properties such as resistance to crystallization and thermal decomposition, electrical, optical and mechanical properties strongly depend on the amorphous phase microstructures of the ceramics. One of the characteristics features of PDCs is that they always contain nanodomains in the microstructures that persist up to very high temperatures. Recent studies by Mera et. al.[74] showed the composition and structures of these nanodomains by small-angle X-ray scattering technique (SAXS). The fact that PDCs can remain amorphous in the temperature range 1000 $^{\circ}$C to 1800 $^{\circ}$C mainly depends on their molecular level structure and composition of the polymer precursor. For example, the introduction of boron (B), for example, into the preceramic polymers can significantly enhance their high temperature stability, the feature that is directly related to their nanostructures of the ceramics. Regarding microstructural evolution of the PDCs at higher temperatures leading to crystalline state from the amorphous state, the initial amorphous network undergoes phase separation, including separation of a “free” carbon phase, defined as the stoichiometric amount of carbon not bonded to silicon in the

ceramic, which is subjected to graphitization. Finally with increasing temperatures, local nucleation and growth of nanocrystals occurs. To investigate the structural evolution of the PDCs, currently there are several techniques in place such as Magic Angle Spinning Nuclear Magnetic Resonance (MAS-NMR), Fourier Transform Infrared Spectroscopy (FTIR), X-ray Diffraction (XRD), Raman spectroscopy, and Electron Paramagnetic Resonance (EPR), which can provide detailed information about the structural evolution of these ceramics from amorphous to the crystalline state. The following segments emphasize on these characterization techniques and their effectiveness in examining the structures of PDCs.

1.5.1 Raman Spectroscopy

One unique structural characteristic of PDCs is that they always some amount of "free" carbon of graphitic nature formed during pyrolysis.[75] Raman spectroscopy can determine the existence of graphene sheets with some degree of long-range order.[76] However, Raman spectroscopy is a "local" characterization method since the laser beam is focused on only few micrometers (< 1 μm in diameter) of the samples, resulting in an average signal over the specimen volume. Nevertheless, Raman spectroscopy has been employed as a non-destructive tool for the investigation of structural evolution of "free" carbon phase in PDCs.[77] The major features of "free" carbon in the Raman spectra of PDCs are the so-called disordered-induced D-band approximately at 1350 cm^{-1} and the G-band at 1600 cm^{-1} due to the in-plane stretching of the sp^2 carbon. Furthermore, the nanoscaled "free" carbon clusters play an important role in tailoring the properties, such as resistance to crystallization and decomposition. Therefore, a detailed

structural investigation of the "free" carbon phase by Raman spectroscopy could provide a significant direction towards the structure-property relationship of the PDCs.

1.5.2 Multinuclear MAS-NMR

Multinuclear MAS-NMR is one of the most accurate average techniques to investigate the coordination environment of NMR sensitive elements in amorphous and crystalline PDCs. For example, ^{29}Si MAS-NMR measurements of the Si-C-N based PDCs obtained from polysilazanes and polyorganosilylcarbodiimides have completely different architectures: The polysilazane-derived Si-C-N ceramics consisted of single phase SiC_xN_y ($x + y = 4$), where Si is attached to C and N, while polysilylcarbodiimide-derived Si-C-N ceramics were composed of Si_3N_4 units interconnected with amorphous carbon (C). The formation of these particular structures resists crystallization and phase separation which lead to the thermodynamically stable Si_3N_4 and SiC phases. Studies have shown that incorporation of boron in the preceramic polymer backbone can significantly improve the high-temperature stability of PDCs. Solid-state ^{11}B NMR of the SiBCN ceramics thermally annealed at 1000 $^{\circ}$C revealed a mixture of BN_2C and BN_3 sites independent of the ratio of silicon to boron (Si/B). Further investigation into the ^{13}C NMR suggests the dissociation of B-C bonds with the evolution of methane and ethane and simultaneous migration of nitrogen at bonded to silicon atoms to form BN_3 sites. Also studies show that boron in homogeneously distributed into the silicon carbonitride matrix supporting the high temperature stability of SiBCN ceramics.[78]

1.5.3 Electron Paramagnetic Resonance (EPR)

1.5.3.1 What is Electron Paramagnetic Resonance

Electron paramagnetic resonance (EPR) is a resonant absorption spectrum that arises from the transition of an electron in paramagnetic species from one energy level to another in the presence of a strong magnetic field. It is a technique to study chemical species containing one or more unpaired electrons like organic or inorganic free radicals or inorganic transition metal complexes. The basic concept of EPR is analogous to Nuclear Magnetic Resonance (NMR), but it is the electron spins that are excited instead of atomic nuclei spins. Since most stable molecular species have all their electrons paired, EPR is a less widely used technique compared to NMR. However, this limitation to paramagnetic species makes EPR highly specific technique in nature.

Every electron has a magnetic moment and a spin quantum number s = ½, with its magnetic components m_s = + ½ and - ½. In the presence of an external magnetic field of strength B_o, the electron's magnetic moment can align in only two directions, i.e., two spin states, either parallel (m_s = - ½) or anti-parallel (m_s = + ½) to the field. Each alignment corresponds to a specific energy level, parallel alignment corresponds to the lower energy level and anti-parallel corresponds to the higher energy level. This phenomenon is known as Zeeman Effect. At resonance, when an incident electromagnetic radiation of frequency v corresponds to this energy gap (ΔE), the electron can move between these two energy states and an EPR absorption spectrum is generated.

The fundamental equation of EPR spectroscopy for this energy level transition of an unpaired electron at resonance condition can be represented as in Equation 1.1

$$\Delta E = h\nu = g_e \mu_B B_0 \ldots\ldots\ldots \qquad \textit{Equation 1.1}$$

where,

ΔE = The energy difference between the two energy states

h = Planck's Constant

ν = Frequency of the electromagnetic radiation

g_e = g-factor of free electron = 2.0023[79]

μ_B = Bohr Magneton (the value of Bohr Magneton is $9.274 * 10^{-28}$ J/G (10,000 G = 1 T)

B_0 = External magnetic field strength

In principle, EPR spectra can be obtained either by varying the incident photon frequency at constant magnetic field, or by varying the magnetic field at constant photon frequency. Generally, the photon frequency is kept constant. A collection of paramagnetic center, free radicals for example, is exposed to a fixed microwave frequency. Increasing the external magnetic field, the energy gap between the two energy states is increased until the gap corresponds to the microwave energy. Since typically there are more electrons in the lower energy state due to the Maxwell-Boltzmann distribution, there is a net absorption of energy. This absorption is then amplified, converted and represented as a first or second order derivative of

the absorption in EPR spectra. EPR absorption spectra are characterized by their *g*-factor, line width and the spin intensity.

1.5.3.1.1 g-factor

The value of the *g*-factor can provide information about the electronic structure of the paramagnetic structure. An unpaired electron responds not only to the applied magnetic field B_0, but also to any local magnetic fields of neighboring atoms or molecules. The effective field B_{eff} is thus written as

$$B_{eff} = B_0(1-\sigma)\ldots\ldots\ldots \qquad \textit{Equation 1.2}$$

where σ includes the effects of local fields (σ can be positive or negative). Therefore at resonance condition Equation 1.1 can be written as

$$h\nu = g_e\mu_B B_{eff} = g_e\mu_B B_0(1-\sigma)\ldots\ldots\ldots \qquad \textit{Equation 1.3}$$

The quantity $g_e(1-\sigma)$ is denoted as g and known as *g*-factor, so that the final equation at resonance condition becomes

$$h\nu = g_e\mu_B B_{eff} = g\mu_B B_0\ldots\ldots\ldots \qquad \textit{Equation 1.4}$$

The fact the value of g is not equal to g_e implies that the ratio of unpaired electrons spin magnetic moment to its angular magnetic moment differs from the value of free electron. Since the spin magnetic moment of an unpaired electron is constant (approximately the Bohr Magneton), then the unpaired electron must have gained or lost angular momentum through spin-orbit coupling.

The different *g* values provide information about the nature of the atomic or molecular species possessing the free electron, by which materials with different structure can be identified. For example, carbon with different structures such as graphite, planar graphite, turbostratic carbon, and multiwall carbon nanotubes have different *g* values of 2.0027, 2.018, 2.02, and 2.012, respectively.[80]

1.5.3.1.2 Line Width

EPR line width reflects the interactions of the spins with their environment. It is defined as the half-width at half-maximum, i.e., the distance measured from the line's center to the point at which the absorption value is half of the maximum absorption value in the centre of the resonance line and expressed in terms of magnetic induction *B*, and its corresponding units.

1.5.3.1.3 Spin Intensity

Spin intensity can be used to estimate unpaired electrons or sometimes called dangling bonds in case of PDCs, for example, which is related to the conduction of materials, especially for amorphous semiconductors. Spin intensity can be calculated from the integrated area of the EPR spectrum and can be quantified with respect to a reference material of known spin concentration.

1.5.3.2 Structure Characterization of PDCs by EPR

Electron paramagnetic resonance (EPR) has been employed as an important tool to study the structural evolution of PDCs. As mentioned earlier, silazane-derived polymer derived SiCN[77,80]

and SiBCN[81] ceramics always contain "free" carbon in their matrix. As for the presence of the free carbon phase, it is formed in the bulk SiCN ceramics during the pyrolysis as the temperature increases to 600 $^{\circ}$C, when CH_3 groups of the polymer chains are decomposed and unpaired bonds are bonded together, forming "free" carbon nanoparticles in the final state of the ceramic matrix.[82] Molecular-dynamic calculations suggest that carbon radicals are bonded aromatically and characterized by graphene network structure in SiCN ceramics.[83] As for the presence of "free" carbon, it significantly affects both electrical and the mechanical properties of the PDCs. Now, the presence of the "free" carbon phase in the ceramic matrix should originate pronounced EPR signal since the formation of "free" carbon involves unpaired electrons. Therefore, EPR could prove to be instrumental in detailed investigation of structure evolution of PDCs. Mishra et. al.[80] , for example, observed two EPR spectral lines due to the carbon related sp^2 dangling bonds: (1) on the surface of the free-carbon phase with the *g*-value of 2.0027 and (2) in the bulk of the SiCN ceramic matrix with *g*-factor 2.0032. Similarly, SiBCN ceramics also been investigated for the presence of carbon-related dangling bonds by EPR spectroscopic technique.[84]

1.6 Outlook

1.6.1 Applications of PDCs

Due to their physical and chemical properties and their ability of being shaped, PDCs have attracted enormous attention in industrial applications such as information technology, energy, biomedical components and microelectromechanical systems (MEMS). Polymer-derived ceramic

fibers are one of the successful applications of preceramic polymers enabling components for ceramic matrix composites (CMC). For example, incorporation of 1 wt% multiwall carbon nanotubes (MWCNTs) led to an increase in the tensile strength of green SiCN fibers by 100 %.[85] Preceramic polymers have been extensively used in manufacturing CMCs. One such example is as high performance brake components with potential applications in automobiles, and airplanes. These brakes have less wear and tear and better coefficient of friction compared to metal brakes. Another interesting example of PDCs is their ability to fabricate features below 1 μm in size using lithographic methods, however special attention needs to be taken to minimize shrinkage during pyrolysis. The ability to be fabricated as miniature components coupled with their excellent thermomechanical properties, PDCs allow MEMS such as photonic and fluidic devices, actuators, glow plug find potential applications under harsh oxidizing conditions at high temperatures. SiCN has also attracted lots of attention as anode materials in lithium (Li) ion batteries due to their chemical stability in corrosive environments.[86] This could protect graphite from exfoliation during charging and discharging. Results showed that in terms of intercalation/deintercalation, SiCN was an active phase because it contained disordered carbon which acted as percolation path for both lithium and electrons. Therefore, SiCN acted as both the binder phase for graphite and also as conductive additive phase. Exciting opportunities lay ahead with the possibility of applying preceramic polymer-based mixture in polymeric state, which subsequently undergoes *in situ* ceramization during service. This has the application as a repair material for small cracks that can develop from damage to the reinforced carbon-carbon composite of the Space Shuttle's wing leading edge. These preceramic polymers can adhere to

the substrate and upon reentry to the earth; these materials undergo ceramization at high temperatures generated due the friction with earth atmosphere, without shrinkage, crack or melting. Overall, enormous flexibility in terms of their synthesis, processing and forming preceramic polymers into shaped ceramic articles have endowed PDCs to play a major role in variety of applications.

1.6.2 Theme of Research

- Unlike conventional ceramics obtained by sintering of corresponding powders, PDCs are synthesized directly from polymer to ceramic transformation. This direct polymer to ceramic route makes PDCs suitable to fabricate unconventionally shaped components. For example, polymer-derived ceramic fibers find potential applications in aerospace industry which is in high demand for new generation thermo-structural composite materials for aeronautic propulsion concepts and hypersonic applications. Electrospinning is a widely used technique to fabricate micro- and nanofibers from polymer solutions with a control in their structure and morphology. However, Ceraset™ VL20, a commercially available preceramic polymer for SiCN-based ceramics, is a liquid oligosilazane and cannot be directly used for electrospinning. Therefore, Ceraset™ VL20 required functionalization in order to be suitable for electrospinning of preceramic polymer fiber.

- Ceraset™ VL20 was functionalized with aluminum sec-butoxide in order to synthesize a solid polyaluminasilazane suitable for electrospinning from common organic solvents

such as chloroform, *N,N*-dimethylformamide. The effect of mixed solvent, a mixture of a high boiling solvent and a low boiling solvent, on the fiber structure and morphology was studied. Studies revealed that electrospinning from a mixture of solvents could generate hierarchical structures, i.e. micro- and nanostructures which retain their morphology upon pyrolysis. The dual structures led to the fabrication of superhydrophobic ceramic fibers via a chemical vapor deposition of low surface energy material, perfluorosilane, onto the rough fibers. These superhydrophobic fibers possessed good chemical and thermal stability and could find potential applications as fabric materials for military's toxicological agents' protective suit.

- Electrospinning of polyaluminasilazane solutions with well-dispersed MWCNTs followed by pyrolysis was used to fabricate polymer-derived ceramic fibers with aligned multiwalled carbon nanotubes (MWCNTs). A novel non-invasive approach using conjugated block copolymer, Poly(3-hexylthiophene)-*b*-poly (poly (ethylene glycol) methyl ether acrylate) (P3HT-*b*-PPEGA), was developed to disperse MWCNTs in polyaluminasilazane chloroform solutions. The first objective of this study was to achieve a homogeneous and stable dispersion of MWCNTs into the preceramic polymer solution. Secondly, the major focus was to investigate the effect of polymer and CNT concentration on the fiber structure and morphology. A significant effort was put into the characterization of the alignment of MWCNTs in the ceramic fibers. Focused ion beam (FIB) and high resolution transmission electron microscopy (HRTEM) was employed to study the orientation of the nanotubes inside the fibers. The research also shed light on

measurement of electrical conductivity of individual ceramic fibers. 1.2 % aligned MWCNTs was measured to be 1.58×10^{-6} S/cm that is more than 500 times higher than that of bulk ceramics (3.43×10^{-9} S/cm).

- Finally, the structural evolution of polymer-derived siliconborocarbonitride (SiBCN) ceramics from their amorphous to crystallization state was studied. Because SiBCN ceramics are known for their high temperature stability and resistance to thermal degradation, it is worth investigating their structural features that undergo changes during the thermal annealing. The primary objective of the investigation focused on the boron (B) related structural changes when pyrolyzed at successively higher temperatures using solid-state NMR spectroscopy. The study revolved around the microstructure evolution from a thermodynamic modeling approach and to correlate the thermal stability with structures associated with boron and "free" carbon. Raman spectroscopy was employed to semiquantitatively analyze the role of "free" carbon in stabilizing the ceramics at high temperatures. Finally electron paramagnetic resonance (EPR) was utilized to investigate the presence of any characteristics dangling bonds that might be a contributing factor in the electrical properties of SiBCN ceramics.

- In summary, the novelty of this research was, first of all, the functionalization of a commercially available preceramic polymer to make it suitable for electrospinning. Once the polymer was electrospinnable, window of opportunities open to engineer functionalized ceramic fibers starting from creating hierarchical structures onto the fiber surfaces to incorporating carbon nanotubes into the fibers. Secondly, investigation of

structural evolution of SiBCN ceramics with pyrolysis temperature was predominantly focused on the amorphous intermediates and quantitatively analyzed to obtain valuable information on the influence of boron and "free" carbon related structures on the thermal stability of SiBCN ceramics.

1.7 List of References

1. F. W. Ainger and J. M. Herbert, "The Preparation of Phosphorous-Nitrogen Compounds as Non-porous Solids"; pp. 168-82 in *Special Ceramics*, Edited by P. Popper. Academic Press, New York, 1960.

2. P. G. Chantrell and P. Popper, "Inorganic Polymers and Ceramics"; pp. 87-103 in *Special Ceramics*, Edited by P. Popper. Academic Press, New York, 1965.

3. W. Verbeek, "Production of Shaped Articles from Homogeneous Mixtures of Silicon Carbide and Nitride"; *Ger. Offen.*, 2218960 (Bayer AG), November 8, U. S. Patent No. 383567, 1973.

4. W. Verbeek and G. Winter, "Formkoerper aus Silicumcarbid und Verfanren zu Ihrer Herstellung"; *Ger. Offen*., 2236078, 1974.

5. G. Winter, W. Verbeek and M. Mansmann, "Formkoerper aus Homogenen Mischungen von Silicumnitrid und Verfanren zu Ihrer Herstellung"; *Ger. Offen*., 2243527, 1974.

6. S. Bernard, K. Fiaty, D, Cornu, P. Miele, and P. Laurent, "Kinetic Modeling of the Polymer-Derived Ceramics Route: Investigation of the Thermal Decomposition Kinetics of Poly[*B*-(methylaminoborazine] Precursors into Boron Nitride," *J. Phys. Chem. B*, **110** [18] 9048-60 (2006).

7. S. Yajima, Y. Hasegawa, K. Okamura, T. Matsuzawa, "Development of High Tensile Strength Silicon Carbide Fiber Using an Organosilicon Polymer Precursor," *Nature*, **273** [5663] 525-7 (1978).

8. L. An, W. Xu, S. Rajagopalan, C. Wang, H. Wang, J. Kapat, L. Chow, Y. Fan, L. Zhang, D. Jiang, B. Guo, J. Liang, R. Vaidyanathan, "Carbon-Nanotube-Reinforced Polymer-Derived Ceramic Composites," *Adv. Mater*., **16** [22] 2036-40 (2004).

9. L. Liew, W. Zhang, L. An, S. Shah, R. Lou, Y. Liu, T. Cross, K. Anseth, V. Bright, and R. Raj, "Ceramic MEMS: New Materials, Innovative Processing and Future Applications," *Am. Ceram. Soc. Bull*., **80** [5] 25-30 (2001).

10. W. Yang, H. Miao, Z. Xie, L. Zhang, and L. An, "Synthesis of Silicon Carbide Nanorods by Catalyst-Assisted Pyrolysis of Polymeric Precursor," *Chem. Phys. Lett*., **383**[5,6] 441-4 (2004).

11. G. Mera and R. Riedel, "Organosilicon –Based Polymers as Precursors for Ceramics"; pp. 51-89 in *Polymer-Derived Ceramics: From Nanostructures to Applications*, Edited by P. Colombo, R. Riedel, G. D. Sorarù, and H. –J. Kleebe. DEStech Publications Inc., Lancaster, PA, USA, 2009.

12. R. Riedel, G. Mera, R. Hauser, and A. Klonczynski, "Silicon-Based Polymer-Derived Ceramics: Synthesis, Properties and Applications- A Review," *J. Ceram. Soc. Jpn.*, **114**, 425-44 (2006).

13. R. Riedel, G. Passing, H. Schönfelder, and R. J. Brook, "Synthesis of Dense Silicon-Based Ceramics at Low Temperatures," *Nature*, **355** [6362] 714-7 (1992).

14. Z.-C. Wang, F. Aldinger, and R. Riedel, "Novel Silicon-Boron-Carbon-Nitrogen Materials Themally Stable up to 2200°C," *J. Am. Ceram. Soc.*, **84** [10] 2179-83 (2001).

15. P. Colombo, G. Mera, R. Riedel, and G. D. Sorarù, "Polymer-Derived Ceramics: 40 years of Research and Innovation in Advanced Ceramics," *J. Am. Ceram. Soc.*, **93** [7] 1805-37 (2010).

16. M. Birot, J. P. Pilliot,a nd J. Dunogues, "Comprehensive Chemistry of Polycarbosilanes, Polysilazanes, and Polycarbosilazanes as Precursors to Ceramics," *Chem. Rev.*, **95** [5], 1443-77 (1995).

17. Y. D. Blum, D. B. MacQueen, and H. –J. Kleebe, "Synthesis and Characterization of Carbon-Enriched Silicon Oxycarbides, *J. Eur. Ceram. Soc.*, **25** [2-3], 143-9 (2005).

18. H. –J. Kleebe, and Y. D. Blum, "SiCO Ceramics with High Excess Free Carbon," *J. Eur. Ceram. Soc.*, **28** [5], 1037-42 (2008).

19. M. Hörz, A. Zern, F. Berger, J. Haug, K. Müller, F. Aldinger, and M. Weinmann, " Novel Polysilazanes as Precursors for Silicon Nitride/Silicon Carbide Composites Without "Free" Carbon," *J. Eur. Ceram. Soc.*, **25** [2-3], 99-110 (2005).

20. D. Seyferth, and G. H. Wiseman, "High-Yield Synthesis of Si_3N_4/SiC Ceramic Materials by Pyrolysis of a Novel Polyorganosilazane." *Comm. Am. Ceram. Soc.*, **67** [7] C-132-3 (1984).

21. Y. D. Blum, and R. M. Laine, "Catalytic methods for the Synthesis of Oligosilazanes," *Organometallics*, **5** [10] 2081-6 (1986).

22. J. M. Schwark, "Isocyanate-Modified Polysilazane Ceramic Precursors," *Polym. Prepr.*, **32**, 567-8 (1991).

23. D. Seyferth, and H. Plenio, "Boasilazane Polymeric Precursors for Borosilicon Nitride," *J. A. Ceram. Soc.*, **73** [7] 2131-3 (1990).

24. R. Riedel, A. Kienzle, W. Dressler, L. Ruwlsch, J. Bill, and F. Aldinger, "A Silicoboron Carbonitride Ceramic Stable to 2,000 °C," *Nature*, **382** [6594] 796-8 (1996).

25. S. Bernard, M. Weinmann, P. Gerstel, P. Miele, and F. Aldinger, "Boron-Modified Polysilazane as a Novel Single Source Precursor for SiBCN Ceramic Fibers: Synthesis, Melt-Spinning, Curing and Ceramic Conversion," *J. Mater. Chem.*, **15** [2] 289-99 (2005).

26. F. Aldinger, M. Weinmann, and J. Bill, "Precursor-derived Si-B-C-N Ceramics," *Pure & Appl. Chem.*, **70** [2] 439-48 (1998).

27. Y-L, Li, E. Kroke, R. Riedel, C. Fasel, C. Gervais, and F. Babonneau, "Thermal Cross-Linking and Pyrolytic Conversion of Poly(ureamethylvinyl)silazanes to Silicon-Based Ceramics," *Appl. Organomet. Chem.*, **15** [10] 820-32 (2001).

28. N. S. Choong Kwet Yive, R. J. P. Corriru, D. Leclercq, P. H. Mutin, and A. Vioux, "Silicon Carbonitride from Polymeric Precursors: Thermal Cross-linking and Pyrolysis of Oligosilazane Model Compounds," *Chem. Mater.*, **4** [1] 141-6 (1992).

29. L.-A. Liew, Y. Liu, R. Luo, T. Cross, L, An, V. M. Bright, M. Dunn, J. W daily, and R. Raj, "Fabrication of SiCN MEMS by Photopolymerization of Preceramic Polymer," *Sens. Act. A.*, **95** [2-3] 120-34 (2002).

30. H. Schneider, R. Naslain, W. Krenkel, "High Temperature Ceramic Matrix Composites," *John Wiley & Sons Inc., New York,* 2006.

31. A. Formhals, *US Patent 1975 504,* 1934.

32. J. Doshi, and D. H. Reneker, "Electrospinning Process and Applications of Electrospun Fibers," *J. Electrost.*, **35** [2-3] 151-60 (1995).

33. D. H. Reneker, and I. Chun, "Nanometer Diamter Fibers of Polymer, Produced by Electrospinning," *Nanotechnology*, **7** [3] 216-23 (1996).

34. Z. -M. Huang, Y. -Z. Zhang, M. Kotaki, and S. Ramakrishna, "A Review on Polymer Nanofibers by Electrospinning and their Applications in Nanocomposites," *Compos. Sci. Technol.*, **63** [15] 2223-53 (2003).

35. D. Li, and Y. Xia, "Electrospinning of Nanofibers: Reinventing the Wheel," *Adv. Mater.*, **16** [14] 1151-70 (2004).

36. A. Greiner, and J. H. Wendorff, "Electrospinning: A Fascinating Method for the Preparation of Ultrathin Fibers," *Angew. Chem. Int. Ed.*, **46** [30] 5670-703 (2007).

37. D. H. Reneker, and A. L. Yarin, "Electrospinning Jets and Polymer Nanofibers," *Polymer*, **49** [10] 2387-425 (2008).

38. Y. M. Shin, M. M. Hohman, M. P. Brenner, and G. C. Rutledge, "Electrospinning: A Whipping Fluid Jet Generates Submicron Polymer Fibers," *Appl. Phys. Lett.*, **78** [8] 1149-51 (2001).

39. A. L. Yarin, S. Koombongse, and D. H. Reneker, "Bending Instability in Electrospinning of Nanofibers," *J. Appl. Phys.*, **89** [5] 3018-26 (2001).

40. Y. M. Shin, M. M. Hohman, M. P. Brenner, and G. C. Rutledge, "Experimental Characterization of Electrospinning: The Electrically Forced jet and Instabilities," *Polymer*, **42** [25] 9955-67 (2001).

41. M. Bognitzki, T. Frese, M. Steinhart, A. Greiner, J. H. Wendorff, A. Schaper, and M. Hellwig, "Preparation of Fibers with Nanoscale Morphologies: Electrospinning of Polymer Blends," *Polym. Eng. Sci.*, **41** [6] 982-9 (2001).

42. M. Bognitzki, W. Czado, T. Frese, A. Schaper, M. Hellwig, M. Steinhart, A. Greiner, J. H. Wendorff, "Nanostructred Fibers Via Electrospinning," *Adv. Mater.*, **13** [1] 70-2 (2001).

43. S. Megelski, J. S. Stephens, D. B. Chase, and J. F. Rabolt, "Micro-and Nanostructured Surface Morphology on Electrospun Polymer Fibers," *Macromolecules*, **35** [22] 8456-66 (2002).

44. C. L. Casper, J. S. Stephens, N. G. Tassi, D. B. Chase, and J. F. Rabolt, "Controlling Surface Morphology of Electrospun Polystyrene Fibers: Effect of Humidity and Molecular Weight on the Electropsinning Process," *Macromolecules*, **37** [2] 573-8 (2004).

45. M. Ma, Y. Mao, M. Gupta, K. K. Gleason, and G. C. Rutledge, "Superhydrophobic Fabrics Produced by Electrospinning and Chemical Vapor Deposition," *Macromolecules*, **38** [23] 9742-8 (2005).

46. H. Hou, Z. Jun, A. Reuning, A. Schaper, J. H. Wendorff, and A. Greiner, "Poly(p-xylene) Nanotubes by Coating and Removal of Ultrathin Polymer Template Fibers," *Macromolecules*, **35** [7] 2429-31 (2002).

47. H. Hou, and Reneker, "Carbon Nanotubes on Carbon Nanofibers: A Novel Structure Based on Elecrospun Polymer Nanofibers," *Adv. Mater.*, **16** [1] 69-73 (2004).

48. F. Ko, Y. Gogotsi, A. Ali, N. Naguib, H. Ye, G. Yang, C. Li, and P. Willis, "Electrospinning of Continuous Carbon Nanotube-Filled Nanofiber Yarns," *Adv. Mater.*, **15** [14] 1161-5 (2003).

49. S. D. McCullen, D. R. Stevens, W. A. Roberts, S. S. Ojha, L. I. Clarke, and R.E. Gorga, "Morphological, Electrical, and Mechanical Characterization of Electrospun Nanofiber Mats Containing Multiwalled Carbon Nanotubes," *Macromolecules*, **40** [4] 997-1003 (2007).

50. E. Fitzer, and M. Heine, in *Fiber Reinforcements for Composite Materials*, *ed. A. R. Bunsell, Elesevier, New York*, 79-148 (1988).

51. S. Yajima, Y. Hasegawa, K. Okamura, and T. matsuzawa, "Development of High Tensile Strength Silicon Carbide fiber using an Organosilicon Polymer Precursor," *Nature*, **273** [5663] 525-7 (1978).

52. Y. Hasegawa, M. Imura, and S. Yajima, "Synthesis of Continuous Silicon Carbide Fibers," *J. Mater. Sci.*, **15** [3] 520-8 (1980).

53. H. Ichikawa, F. Machino, S. Mitsuno, T, Ishikawa, K. Okamura, and Y. Hasegawa, "Synthesis of Continuous Silicon Carbide Fiber Part 5 Factors Affecting Stability of Polycarosilane to Oxidation," *J. Mater. Sci.*, **21** [12] 4352-8 (1986).

54. T. Taki, S. Maeda, K. Okamura, M. Sato, and T. Matuszawa, "Oxidation Curing Mechanism of Polycarbosilane Fibers by Solid-State ^{29}Si High-Resolution NMR," *J. Mater. Sci. Lett.*, **6** [7] 826-8 (1987).

55. T. Taki, K. Okamura, M. Sato, T. Seguchi, and S. Kawanishi, "A Study on the Electron Irradiation Curing Mechanism of Polycarbosilane Fibers by Solid-State ^{29}Si Nuclear Magnetic Resonance Spectroscopy," *J. Mater. Sci. Lett.*, **7** [3] 209-11 (1988).

56. M. Sugimoto, T. Shimoo, K. Okamura, and T. Seguchi, "Reaction Mechanisms of Silicon Carbide Fiber Synthesis by Heat Treatment of Polycarbosilane Fibers cured by Radiation:I, Evolved Gas Analysis," *J. Am. Ceram. Soc.*, **78** [4] 1013-7 (1995).

57. M. Takeda, J. Sakamoto, Y. Imai, and H. Ichikawa, "Thermal Stability of Low-Oxygen-Content Silicon Carbide Fiber, HiNicalon™," *Compos. Sci. & Technol.*, **59** [6] 813-9 (1999).

58. S. M. Johnson, R. D. Brittain, R. H. Lamoreaux, and D. J. Rowcliffe, "Degradation Mechanisms of Silicon Carbide Fibers," *J. Am. Ceram. Soc.*, **71** [3] C-132-C-135 (1988).

59. T. Mah, N. L. Hechtht, D. H. McCullum, J. R. Hoenigman, H. M. Kim, A. P. Katz, and H. A. Lipsitt, "Thermal Stability of SiC Fibers (Nicalon®)," *J. Mater. Sci.*, **19** [4] 1191-1201 (1984).

60. A. Saha, S. R. Shah, and R. Raj, "Amorphous Silicon Carbonitride Fibers Drawn from Alkoxide Modified Cearset," *J. Am. Ceram. Soc.*, **86** [8] 1443-5(2003).

61. G. Chollon, R. Pailler, R. Naslain, F. Lannani, M. Monthioux, and P. Olry, "Thermal Stability of a PCS-Derived SiC Fiber With a Low Oxygen Content (Hi-Nicalon)," *J. Mater. Sci.*, **32** [2] 327-47 (1997).

62. G. Chollon, M. Czerniak, R. Pailler, X. Bourrat, R. Naslain, J. P. Pillot, and R. Cannet, "A Model SiC-Based Fiber With a Low Oxygen Content Prepared from a Polycarbosilane Precursor," *J Mater. Sci.*, **32** [4] 893-911 (1997).

63. G. Chollon, "Oxidation Behavior of Ceramic Fibers from Si-C-N-O Systems and Related Sub-Systems," *J. Eur. Ceram. Soc.*, **20** [12] 1959-74 (2000).

64. A. Saha, S. R. Shah, and R. Raj, "Oxidation Behavior of SiCN-ZrO_2 Fiber Prepared From Alkoxide-Modified Silazane," *J. Am. Ceram. Soc.*, **87** [8] 1556-8 (2004).

65. M. A. Schiavon, G. D. Sorarù, and I. V. P. Yoshida, "Poly(borosilazanes) as precursors for Si-B-C-N glasses: Synthesis and High Temperature Properties," *J. Non-Cryst. Solids*, **348** , 156-61 (2004).

66. T. Wideman, E. Cortez, E. E. Remsen, G. A. Zank, R. J. Carrol, and L. G. Sneddon, "Reactions of Monofunctional Boranes with Hydridopolysilzanes: Synthesis, Characterization, and Ceramic Conversion Reactions of New Processible Precursors to SiNCB Ceramic Materials," *Chem. Mater.*, **9** [10] 2218-30 (1997).

67. K. Su, E. E. Remsen, G. A. Zank, and L. G. Sneddon, "Synthesis, Characterization, and Ceramic Conversion Reactions of Borazine-modified Hydridopolysilzanes: New Polymeric Precursors to SiNCB Ceramic Composites," *Chem. Mater.*, **5** [4] 547-56 (1993).

68. P Baldus, M. Jansen, and D. Sporn, "Ceramic Fibers for Matrix Composites in High – Temperature Engine Applications," *Science*, **285** [5428] 699-703 (1999).

69. Y. Tang, J. Wang, X. –D. Li, H. Wang, W. –H. Li, and X. –Z. Wang, "Preceramic Polymer for Si-B-C-N Fiber Via One-Step Condensation of Silane, BCl_3, and Silazane," *J. Appl. Poly. Sci.*, **110** [2] 921-8 (2008).

70. G. Larsen, R. Velarde-Ortiz, K. Minchow, A. Barrero, and I. G. Loscertales, "A Method for Making Inorganic and Hybrid (Organic/Inorganic) Fibers and Vesicles with Diameters in the Submicrometer and Micrometer Range Via Sol-Gel Chemistry and Electrically Forced Liquid Jets," *J. Am. Chem. Soc.*, **125** [5] 1154-5 (2003).

71. D. T. Welna, J. D. Bender, X. Wei, L. G. Sneddon, and H. R. Allcock, "Preparation of Boron-Carbide/Carbon Nanofibers from a Poly(norbornenyldecaborane) Single-Source Precursor Via Electrostatic Spinning," *Adv. Mater.*, **17** [7] 859-62 (2005).

72. B. M. Eick, and J. P. Youngblood, "SiC Nanofibers by Pyrolysis of Electrospun Preceramic Polymers," *J. Mater. Sci.*, **44** [1] 160-5 (2009).

73. V. Salles, S. Bernerd, A. Brioude, D. Cornu, and P. Miele, "A New Class of Boron Nitride Fibers with Tunable Properties by Combining an Electrospinning Process and the Polymer-Derived Ceramics Route," *Nanoscale*, **2** [2] 215-7 (2009).

74. G. Mera, A. Tamayo, H. Nguyen, S. Sen, and R. Riedel, "Nanodomain Structure of Carbon-Rich SiCN Polymer-Derived Ceramics," *J. Am. Ceram. Soc.*, **93** [4] 1169-75 (2010).

75. R. Raj, R. Riedel, and G. D. Sorarù, "An Introduction to the Special Topical Issue on Ultrahigh-Temperature Polymer-Derived Ceramics," *J. Am. Ceram. Soc.*, **84** [10] 2158-2159 (2001).

76. F. Tunistra, and J. L. Koenig, "Raman Spectrum of Graphite," J. Chem. Phys., 53 [2] 1126-1130 (1970).

77. S. Trassl, G. Motz, E. Rossler, and G. Ziegler, "Characterization of the Free-Carbon Phase in Precursor-Derived SiCN Ceramics," J. Non-Cryst. Solids, 293-295, 261-262 (2001).

78. C. Gervais, F. Babonneau, L. Ruwisch, R. Hauser, and R. Riedel,, "Solid-State NMR Investigations of the Polymer Route to SiBCN Ceramics," *Can. J. Chem.*, **81** [11] 1359-69 (2003).

79. B. Odom, D. Hanneke, B. D'Urso, and G. Gabrielse, "New Measurement of the Electron Magnetic Moment Using a One-Electron Quantum Cyclotron," *Phys. Rev. Lett.*, **97** [3] 030801-4 (2006).

80. S. I. Andronenko, I. Stiharu, and S. K. Mishra, "Synthesis and Characterization of Polyureasilazane Derived SiCN Ceramics," *J. Appl. Phys.*, **99** [11] 113907-11 (2006).

81. K. Yamamoto, N. Tsuganezawa, S. Makimura, D. Sawa, S. Nakahigashi, and K. Kozima, "Local Structure and Defects in Ultra-High Temperature Materials of Borosilicon Carbonitride," *J. Mater. Res.*, **23** [6] 1642-1646 (2008).

82. S. Trassel, H-J. Kleebe, H. Störmer, G. Motz, E. Rössler, and G. Ziegler, "Characterization of The Free Carbon Phase in Si-C-N Ceramics: Part II, Comparison of Different Polysilazane Precursors," *J. Am. Ceram. Soc.*, **85** [5] 1268-74 (2002).

83. N. Resta, C. Kohler, and H-R. Trebin, "Molecular Dyanmics Simulations of Amorphous Si-C-N Ceramics: Composition Dependence of The Atomic Structure," *J. Am. Ceram. Soc.*, **86** [8] 1409-14 (2003)

84. F. Berger, A. Muller, F. Aldinger, and K. Muller, "Solid-State NMR Investigations on the Si-B-C-N Ceramics Derived From Boron-Modified Poly(allylmethylsilazane)," *Z. Anorg. Allg. Chem.*, **631** [2-3] 355-363 (2005).

85. S. Kakott, L. Heymann, and G. Motz, "Rheology and Processability of Multi-walled Carbon Nanotubes – ABSE Polycabosilazane Composites," *J. Eur. \Ceram. Soc.*, **28** [5] 1015-21 (2008).

86. R. Kolb, C. Fasel, V. L-. Kunzmann, and R. Riedel, "SiCN/C-Ceramic Composite as Anode Material for Lithium Ion Batteries," *J. Eur. Ceram. Soc.*, **26** [16] 3903-8 (2006).

CHAPTER 2 SUPERHYDROPHOBIC MATS OF POLYMER-DERIVED CERAMIC FIBERS

2.1 Abstract

Solid preceramic polyaluminasilazane was synthesized through the reaction between liquid cyclosilazane and aluminum tri-sec-butoxide at 160 °C. Electrospinning of polyaluminasilazane/polyethylene oxide (1/0.0001 mass ratio) in chloroform solutions generated smooth fibers while the electrospun fibers from the chloroform/*N,N*-dimethylformamide solutions had submicron structures on the fiber surfaces. Smooth and rough SiCNO ceramic fibers were obtained by the pyrolysis of the green fibers with 80 % yield. Superhydrophobic mats of ceramic fibers were fabricated via a chemical vapor deposition of perfluorosilane onto the rough fibers. These superhydrophobic mats possess good chemical and thermal stability.

2.2 Introduction

Superhydrophobic surfaces, which exhibit extraordinarily high water contact angle (> 150°) and low contact angle hysteresis (the difference between advancing and receding contact angles < 5-10°), have attracted extensive attention for their applications in water repellence and self-cleaning.[1-3] Studies on insects and plants revealed that superhydrophobicity requires not only a low surface energy but also a hierarchical surface roughness composed of at least two different, micrometer and nanometer, length scales.[4-5] The most classic example among the natural surfaces is the lotus leaf. The key feature in the lotus leaf is the presence of a low surface energy hydrophobic surface coating (epicuticular wax crystalloids) on a microscopic rough structure.[5] Inspired by nature, numerous synthetic superhydrophobic surfaces have been produced by

creating nanometer scale features on micrometer scale roughened surfaces.[6-9] Typically, a certain degree of micro-/nanopattern is first created and the patterned rough surface is passivated using a low surface energy coating to lower the surface energy, reducing the affinity of the water droplets to the surface. These previous studies primarily focused on polymeric and silicon-based materials due to the availability of micro-/nano-fabrication technologies of these materials. On the other hand, ceramic materials are potentially important for those applications where requirements such as mechanical strength, stiffness and resistance to corrosion prevent the use of other materials. However, up-to-date ceramic-based superhydrophobic surfaces have received little attention. This could be due to the fact that creating a dual-feature-scale surface structure presents a significant challenge for the conventional ceramics which are synthesized using powder metallurgy-based processing techniques. In this chapter, a unique simple technique to synthesize ceramic superhydrophobic, non-woven mats using the polymer-derived ceramics (PDCs) technique is described. Unlike conventional ceramics obtained by sintering corresponding powders, PDCs are synthesized by direct thermal decomposition of polymeric precursors.[10,11] The unique direct polymer-to-ceramic route of PDCs makes them suitable for fabricating various unconventionally shaped ceramic components and devices.[12-15] By taking advantage of the PDC processing, ceramic fibers with dual micro- and nanostructures are generated in this study by electrospinning preceramic polymeric precursors, followed by pyrolysis. Electrospun fibers themselves naturally provide one level of roughness (micro-scale) because of the small fiber size.[16-24] The submicron-scaled features in my studies, in contrast with reported methods where the nanostructures were introduced either by the formation of beads-on-

fiber structure[18,20] or by subsequent deposition of nanoparticles on the fibers[24], are introduced onto the surfaces of the fibers in the spinning process by tailoring the evaporation rates of the solvents. The dual length scale structures are maintained in the subsequent pyrolysis and provide a suitable template for fabricating superhydrophobic surfaces.

2.3 Experimental

2.3.1 Materials

Ceraset™ VL20 was purchased from Kion Corporation, USA. Aluminum tri-sec-butoxide, poly(ethylene oxide) (PEO, M_n = 1,000,000), chloroform ($CHCl_3$) and *N,N*-dimethylformamide (DMF) was purchased from Sigma-Aldrich Chemical Co., USA and was used without any further purifications.

2.3.2 Modification of Oligosilazane

In a typical procedure, 40.100 g of Ceraset™ VL20 was mixed with 8.010 g of aluminum tri-sec-butoxide in a 100 mL conical flask under magnetic stirring. Then the dissolved mixture was heated at 160 $^{\circ}$C under Argon atmosphere under magnetic stirring. The reaction was allowed to proceed overnight during which the solid polymer was produced.

2.3.3 Electrospinning of polyaluminasilazane

A 45.0 wt% polysilazane stock solution in DMF was prepared by dissolving 2.253 g of polysilazane in 2.752 g of DMF. To make a 20 wt% polysilazane solution in 1:1 DMF/chloroform, 0.307 g of 1 wt% solution of polyethylene oxide (PEO) in chloroform was

added to 0.998 g of 45.0 wt% solution. 0.305 g chloroform and 0.651 g DMF were added to this mixture. In a typical electrospinning procedure, the polymer solution was loaded into a disposable 5 mL syringe equipped with a stainless steel needle. The needle was connected to a high-voltage power supply purchased from Glassman High Voltage Inc., High Bridge, NJ. The solution was then fed at a rate of 0.3 mL/h using a syringe pump supplied by New Era Pump Systems Inc., Wantagh, NY. The solution was electrospun at 10.0 kV and the electrospun fiber was collected on a metal electrode at a needle collector distance of 24.0 cm. The pyrolysis of the polymer fibers was performed in a tube furnace by heating the fibers to 1000 $^{\circ}$C in argon, with a temperature increasing rate of 5 $^{\circ}$C/min.

2.3.4 Deposition of perfluorosilane

A ceramic mat was placed in a vacuum chamber together with (tridecafluoro-1,1,2,2-tetrahydrooctyl)-1-trichlorosilane. The chemical vapor deposition (CVD) was performed by applying a 1 Torr vacuum to the chamber at room temperature for 2 h. Then, the samples were placed in an oven and heated at 180 $^{\circ}$C for 2 h.

2.3.5 Analysis

Solid polysilazanes were characterized using a PerkinElmer Fourier transform infrared (FTIR) spectrometer (PerkinElmer Inc., Waltham, MA) and a JASCO Gel Permeation Chromatography system (JASCO Inc., Easton, MD) with ultraviolet, refractive index, and static light scattering detectors. The morphology of the fibers was examined using a JEOL 6400 scanning electron microscope (JEOL Ltd., Tokyo, Japan).

The thermogravimetric analysis (TGA) was performed on a Q5000 Thermogravimetric Analyzer (Texas Instruments, Dallas, TX), with the temperature-increasing rate of 5 $^{\circ}$C/min to 1000 $^{\circ}$C. The surface element composition was examined using an X-ray Photoelectron Spectrometer (XPS) (Physical Electronics 5400 ESCA, Physical Electronics, Inc., Chanhassen, MN). Contact angle measurement was performed on a Rame-Hart Standard Goniometer (Rame-Hart Instrument, Co., Netcong, NJ). The elemental analysis was performed by the M&P Lab (Schenectady, NY) and Midwest Microlab, LLC (Indianapolis, IN).

2.4 Results and Discussion

A commercially available cyclosilazane (Ceraset™ VL20, Si:C:N = 1:1.4:1) has been used as the precursor for SiCN-based ceramics.[25] However, Ceraset™ VL20 is a low molecular weight liquid cyclosilazane with average molecular weight around 300,[26] and cannot be directly used for electrospinning fibers. In this study, a solid polyaluminasilazane was synthesized by treating VL20 with aluminum tri-sec-butoxide. The elemental analysis of the product showed that the molar ratio of Si:C:N:H:Al was 1:1.7:0.5:3.4:0.07. The chemical structures of VL20 and the polyaluminasilazane were examined using a FTIR spectrometer (Figure. 2.1). The FTIR spectra showed that the spectrum of the polyaluminasilazane is similar to that of VL20. However, the intensity change of absorption of N-H, Si-N and Si-O is observed. The absorption bands attributed to Si-N stretching vibration (859 cm^{-1}) decrease, while the absorption band attributed to Si-O stretching vibration (1030 cm^{-1}) increase. Such changes might be caused by the breaking of Si-N bonds and the formation of Si-O bonds in the reaction. In addition, the intensity of N-H stretching vibration (3370 cm^{-1}) and N-H deformation vibration (1150 cm^{-1}) decreases in the

reaction probably due to the coupling between Al and N in the reaction. The mechanism of the reaction is discussed in the following chapter.

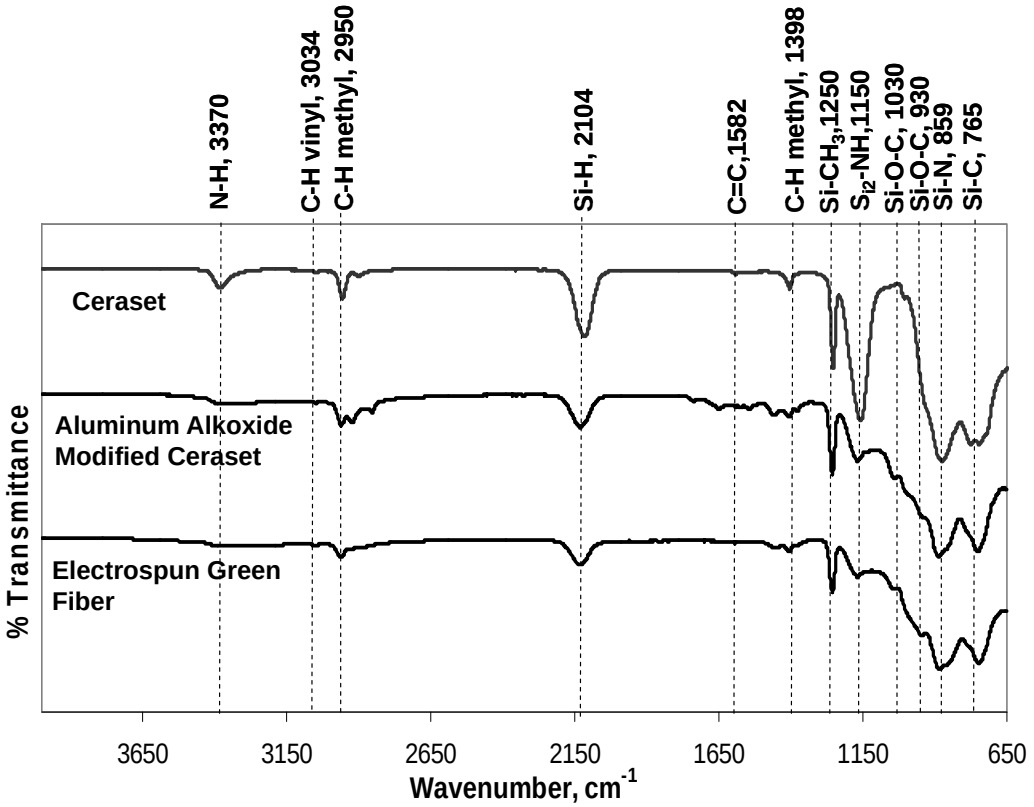

Figure 2.1 FTIR spectra of Ceraset™ VL 20, aluminum tri-sec-butoxide-treated Ceraset™ VL 20 and electrospun green fibers of aluminum tri-sec-butoxide treated Ceraset™ VL 20.

The solid polyaluminasilazane is soluble in common solvents such as chloroform ($CHCl_3$), tetrahydrofuran (THF), *N,N*-dimethylformamide (DMF) and acetone, and thus suitable for electrospinning. However, polyaluminasilazanes are short polymers with rigid back bones. Electrospinning of all polyaluminasilazane solutions resulted in the formation of polymer droplets due to insufficient chain overlap between the chains.[27] In order to improve the fiber

formation capability of the precursor, a small amount of PEO (M_n = 1,000,000) was also added into the solutions.[28] It is believed that PEO interacts with polyaluminasilazane through hydrogen bonding and increases the chain overlap of the polymers. Figure 2.2 shows scanning electron microscopy (SEM) images of polymer fibers produced by electrospinning a 20 % polyaluminasilazane chloroform solution. The fibers electrospun from the pure chloroform solution have smooth surfaces, and are lacking the nano-scaled structures necessary to be superhydrophobic surfaces.

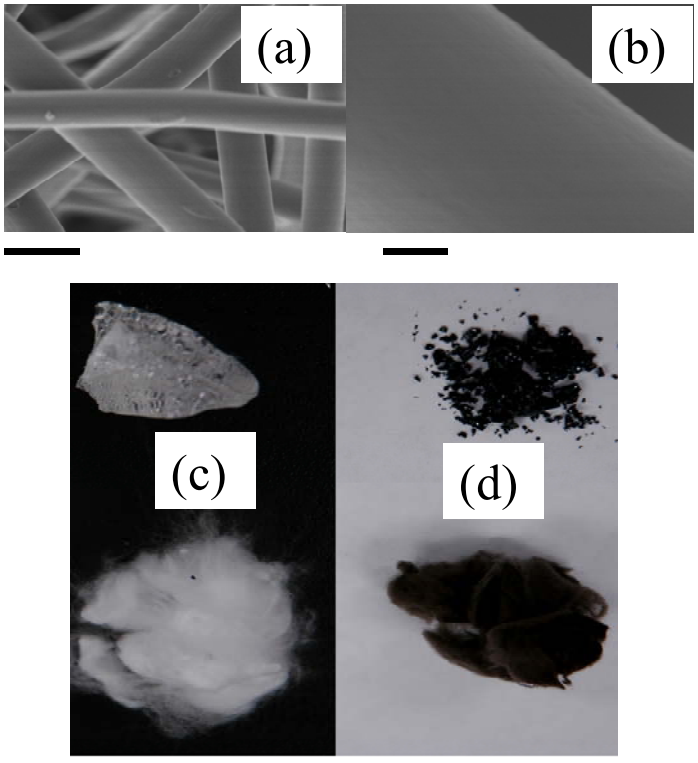

Figure 2.2 (a,b) Scanning electron images of polysilazane fibers electrospun from a 20% chloroform solution (The scale bar for a and b is 10 μm and 1 μm, respectively.), (c) pictures of aluminum alkoxide modified Ceraset™ VL 20 and electrospun fibers from its chloroform solutions, and (d) ceramic powders and fibers after pyrolysis.

Previous studies[29-33] suggested that it is possible to generate nanostructures on electrospun fiber surfaces by using a mixture of solvents with different evaporation rates to induce a phase separation. In this study, mixtures of chloroform (T_b = 61.2 °C) and the less volatile *N,N*-dimethylformamide (DMF, T_b = 153.0 °C) were used as the solvents. Fig. 2.3 shows the effect of the ratio of chloroform-to-DMF on the size and surface morphology of the electrospun polymer fibers. It is seen that the fibers obtained from the mixed solutions with the chloroform-to-DMF ratio of 0.5 and 1, possess nano-scaled domains on their surfaces (Fig. 2.3a-d). The roughness of the fiber surfaces decreases with an increase in chloroform-to-DMF ratio (or an increase of evaporation rate). The result is in good agreement with the previous study reporting that the surface roughness is probably caused by a rapid phase separation induced by differential solvent evaporation rates, and increases with increasing boiling point of the mixture of solvents.[29] Another possible mechanism of the formation of such puckered surfaces can be explained by the "dry skin" model.[31] In the process of electrospinning, the solvent evaporates faster on the surface than in the core of the liquid jet, leading to the formation of a dry polymer skin around the still liquid core. When the solvent in the core evaporates, the core shrinks to cause the dry polymer skin to collapse to wrap the core, and wrinkles the surface. Figure 2.3 also shows that the diameter of electrospun fibers decreases with an increase of DMF content, which is similar to the electrospinning of poly(ε-caprolactone) using chloroform/DMF mixtures as solvents.[33] It is believed that the reduction in the fiber diameter is due to the increase of the solution conductivity (dielectric constants of chloroform and DMF are 4.8 and 36.7, respectively.)[34]

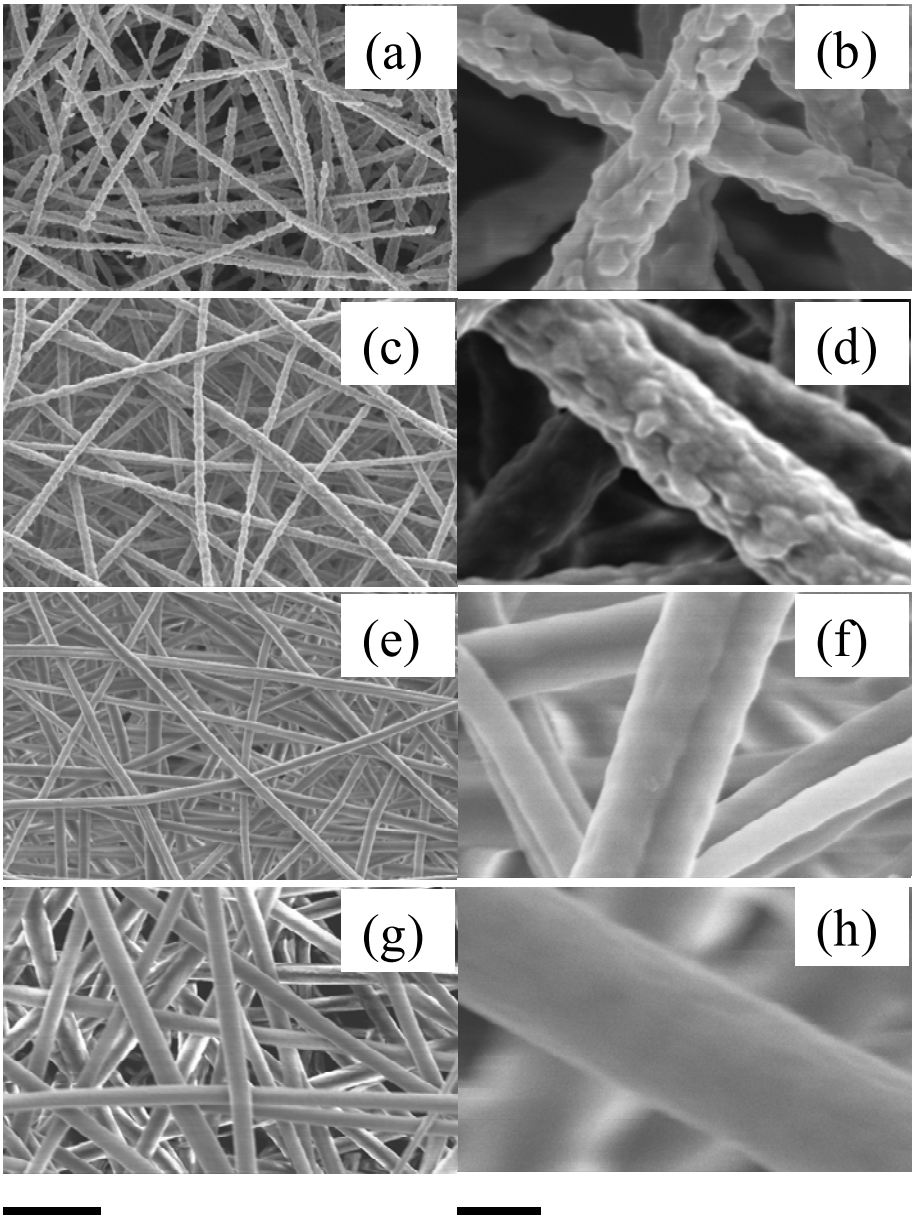

Figure 2.3 Scanning electron microscopy images of electrospun polysilazane fibers from mixtures of chloroform and N,N-dimethylformaide (DMF) at different ratios. (a, b at 1:2; c, d at 1:1; e, f at 2:1; g, h at 5:1. The scale bar for a, c, e, and g is 10 μm, and the scale bar of b, d, f, and g is 1 μm. The fiber surface roughness decreases, while the fiber size increases with the increment of chloroform/DMF ratio.

The chemical composition of electrospun green fibers was examined using a FTIR spectrometer (Figure 2.1) and elemental analysis. The FTIR spectrum (Figure 2.1) and elemental composition (Si:C:N:Al:O = 1:1.7:0.4:0.07:0.01) of electrospun green fibers are very similar to those of aluminum alkoxide modified Ceraset™, suggesting that the chemical composition of the polymer is maintained during the electrospinning process. The obtained non-woven polymer mats were then pyrolyzed at 1000 °C in argon to convert them into SiAlCNO ceramic mats[35] with 80 % yield according to the TGA. The elemental analysis reveals that the molar ratio of Si:C:N:Al:O is 1:0.5:0.41:0.07:0.01. The ratio between silicon and nitrogen was smaller than that in the bulky SiAlCN ceramics (Si:N = 1:0.9) in which smaller amount of aluminum alkoxide was used.[36] It is believed that the low concentration of nitrogen is due to the loss of nitrogen when Ceraset™ VL20 was modified with aluminum tri-sec-butoxide. The FTIR spectrum of the ceramic fibers has two major absorption peaks at 1014 cm^{-1} and 783 cm^{-1}, suggesting the presence of oxygen in the ceramic fibers. The peak at 1014 cm^{-1} is the overlap of Si-O stretching band (1080 cm^{-1})[37] and Si-N stretching band (900-1000 cm^{-1}),[38] while the peak at 783 cm^{-1} is assigned to Si-C stretching band. The SEM images of the resultant ceramic fibers reveal that the nanostructures that formed on polymer fiber surfaces are retained even though ~ 28 % linear shrinkage occurs during the pyrolysis (Figure 2.4).[35]

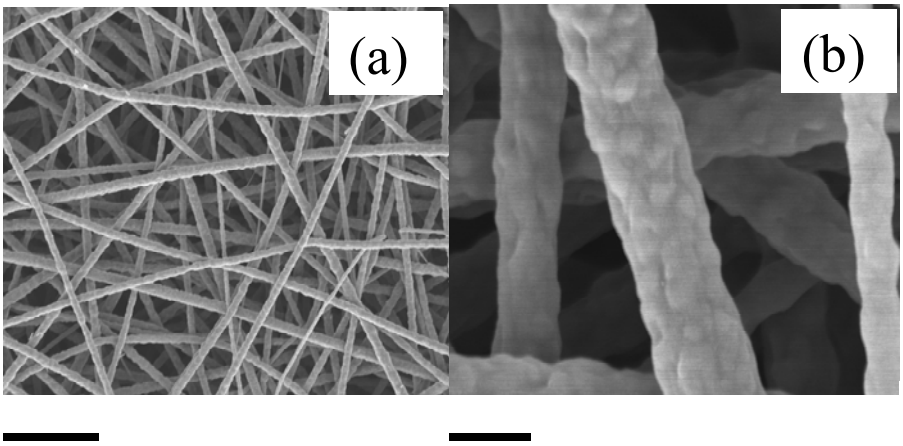

Figure 2.4 SEM images of polysilazane-derived ceramic fibers electrospun from a 1:1 chloroform/DMF mixture. (The scale bar for a and b is 10 μm and 1 μm, respectively.)

Non-woven mats of ceramic fibers with nanostructured surfaces (from the 1:1 chloroform/DMF solution) and smooth ceramic fibers (from the 5:1 chloroform/DMF solution) were produced to investigate the effect of surface nanostructures on the superhydrophobicity. The ceramic fibers were very hydrophilic after the pyrolysis. To lower the surface energy of the dual-feature-scale ceramic fiber mats, trichloro (1H, 1H, 2H, 2H-perfluorooctyl) silane (perfluorosilane) was deposited onto the fiber surfaces using a CVD.[39] The coated mats were then heated at 180 °C for 2 h to form a fluorosiloxane network on the surfaces. After the heat treatment, the ceramic fibers with a nanostructured surface became Superhydrophobic, with an advancing contact angle of 159° and a receding contact angle of 156° (Figure 2.5b, inset), while the smooth fibers were not superhydrophobic (advancing contact angle = 146° and receding contact angle = 115°). It is obvious that surface nanostructures are necessary for constructing superhydrophobic surfaces. The surface of the bare ceramic fibers and perfluorosilane-coated fibers were examined using XPS. The XPS survey of the fiber surface revealed that the composition of the polysilazane-

derived ceramic fibers consisted of silicone, carbon, oxygen and nitrogen (Figure 2.5a). The oxygen in the ceramic is attributed to the sec-butoxide groups that were introduced during the modification. After the deposition of perfluorosilane, the fiber surface was coated with a low surface energy fluorosilane network, which is indicated by the fluorine peak in Figure 2.5b, leading to a superhydrophobic surface.

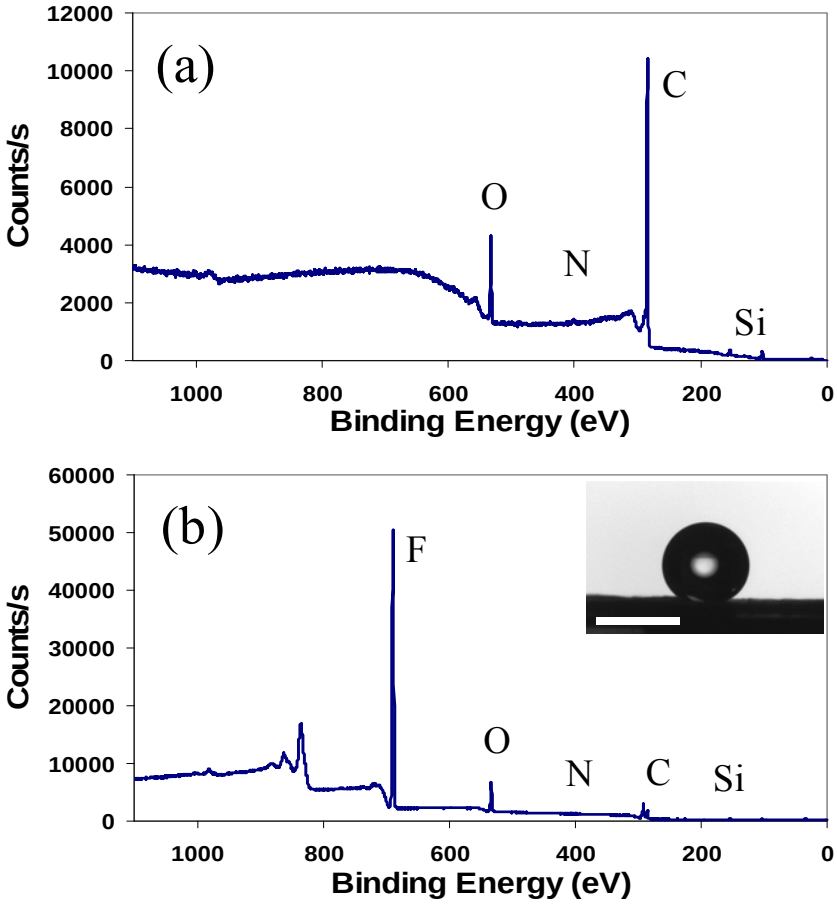

Figure 2.5 (a) X-ray photoelectron spectrometer of the bare ceramic fibers, and (b) perfluorosilane coated ceramic fibers. The inset shows a water droplet sitting on the ceramic superhydrophobic surface. (The scale bar is 4 mm.)

Because the SiAlCNO ceramics possess excellent thermal stability and resistance to oxidation/corrosion, [37, 40] the thermal stability of our superhydrophobic mats is determined only by the fluorosilane coating, which is stable up to 350 °C. The thermal stability of the superhydrophobic mats was tested by heating them at 350 °C for overnight, and it was found that the surfaces retained their superhydrophobicity. The fluorosilane coatings started degrading when heat-treated at 450 °C, and the mats lost their superhydrophobicity after 2 h at this temperature. However, because the ceramic structures were still intact, a superhydrophobic mat could be rebuilt via another deposition of perfluorosilane. Such thermal stability of the ceramic superhydrophobic fibers is important for their applications since various surface contaminations, which degrade superhydrophobicity, can be removed from the surface by a heat treatment to regain the superhydrophobicity. The ceramic superhydrophobic surfaces also showed excellent resistant to organic solvents, strong acids and bases by retaining their superhydrophobicity after overnight immersion in chloroform, DMF, THF, a 1*M* HCl aqueous solution, and a 1*M* NaOH aqueous solution. Consequently, these ceramic superhydrophobic fibers with great chemical and thermal stability have potential applications as fabric materials in the military's toxicological agents protective suit.[41] Additionally, the ceramic mats have applications in fire retardant materials due to the intrinsic inflammable properties of SiAlCNO ceramics.

2.5 Conclusion

In summary, a simple technique for the fabrication of superhydrophobic mats of PDC fibers is demonstrated by electrospinning preceramic polyaluminasilazane followed by a pyrolysis and the deposition of perfluorosilane. The key of the technique is to combine PDC processing and

electrospinning to generate dual-feature-scaled surface structures, which is difficult to form with the conventional ceramic processing. These ceramic fibers are thermal and chemical stable, and have multifunctions, including self-cleaning, resistance to corrosive aqueous solutions and fire. They can be used in such extreme conditions as hot gas or liquid filters, and protective clothing for fire fighters and soldiers.

2.6 List of References

1. L. Feng, S. Li, Y. Li, H. Li, L. Zhang, J. Zhai, Y. Song, B. Liu, L. Jiang, and D. Zhu, "Super-Hydrophobic Surfaces: From Natural to Artificial," *Adv. Mater.* **14** [24] 1857-60 (2002).

2. R. Blossey, "Self-Cleaning Surfaces-Virtual Realities," *Nature Mater*. **2** [5] 301-6 (2003).

3. M. Callies and D. Quéré, "On Water Repellency," *Soft Matter*, **1** [1] 55-61 (2005).

4. Z. –Z. Gu, H. Uetsuka, K. Takahashi, R. Nakajima, H. Onishi, A. Fujishima, and O. Sato, "Structural Color and the Lotus Effect," *Angew. Chem. Int. Ed*., **42** [8] 894-7 (2003).

5. W. Barthlott and C. Neinhuis, "Purity of the Sacred lotus, or Escape from Contamination in Biological Surfaces," *Planta*, **202** [1] 1-8 (1997).

6. N. J. Shirtcliffe, G. Mchale, M. I. Newton, G. Chabrol, and C. C. Perry, "Dual-Scale Roughness Produces Unusually Water-Repellent Surfaces," *Adv. Mater.*, **16** [21] 1929-32 (2004).

7. T. Sun, L. Feng, X. Gao, and L. Jiang, "Bioinspired Surfaces with Special Wettability," *Acc. Chem. Res.*, **38** [8] 644-52 (2005).

8. W. Ming, D. Wu, R. van Benthem, and G. de With, "Superhydrophobic Films from Raspberry-like Particles," *Nano Lett.*, **5** [11] 2298-301 (2005).

9. L. Gao and T. J. McCarthy, "The "Lotus Effect" Explained: Two Reasons Why Two Length Scales of Topography Are Important," *Langmuir*, **22** [7] 2966-7(2006).

10. R. Riedel, G. Passing, H. Schonfelder, and R.J. Brook, "Synthesis of Dense Silicon-Based Ceramics at Low Temperature," *Nature*, **355** [6362] 714-7 (1992).

11. E. Kroke, Y.L. Li, C. Konetschny, E. Lecomte, D. Fasel, and R. Riedel, "Silazane-Derived Ceramics and Related Materials," *Mater. Sci. Eng. R*, **26** [4-6] 97-199 (2000).

12. S. Yajima, Y. Hasegawa, K. Okamura, and T. Matsuzawa, "Development of High Tensile Strength Silicon Carbide Fiber Using an Organosilicon Polymer Precursor," *Nature*, **273** [5663] 525-7 (1978).

13. L. An, W. Xu, S. Rajagopalan, C. Wang, H. Wang, J. Kapat, L. Chow, Y. Fan, L. Zhang, D. Jiang, B. Guo, J. Liang, and R. Vaidyanathan, "Carbon-Nanotube-Reinforced Polymer-Derived Ceramic Composites," *Adv. Mater*., **16** [22] 2036-40 (2004).

14. L. Liew, W. Zhang, L. An, S. Shah, R. Lou, Y. Liu, T. Cross, K. Anseth, V. Bright, and R. Raj, "Ceramic MEMS: New Materials, Innovative Processing and Future Applications," *Am. Ceram. Soc. Bull.*, **80** [5] 25-30 (2001).

15. W. Yang, H. Miao, Z. Xie, L. Zhang, and L. An, "Synthesis of Silicon Carbide Nanorods by Catalyst-Assisted Pyrolysis of Polymeric Precursor," *Chem. Phys. Lett*., **383** [5,6] 441-4 (2004).

16. L. Jiang, Y. Zhao, and J. Zhai, "A Lotus-Leaf-like Superhydrophobic Surface: A Porous Microsphere/Nanofiber Composite Film Prepared by Electrohydrodynamics," *Angew. Chem. Int. Ed.*, **43** [33] 4338-41 (2004).

17. K. Acatay, E. Simsek, C. Ow-Yang, and Y. Z. Menceloglu, "Tunable, Superhydrophobically Stable Polymeric Surfaces by Electrospinning," *Angew. Chem. Int. Ed.*, **43** [39] 5210-3 (2004).

18. M. Ma, R. M. Hill, J. L. Lowery, S. V. Fridrikh, and G. C. Rutledge, "Electrospun Poly(Styrene-block-dimethysiloxane) Block Copolymer Fibers Exhibiting Superhydrophobicity," *Langmuir*, **21** [12] 5549-54 (2005).

19. M. Ma, Y. Mao, M. Gupta, K. K. Gleason, and G. C. Rutledge, "Superhydrophobic Fabrics Produced by Electrospinning and Chemical Vapor Deposition," *Macromolecules*, **38** [23] 9742-8 (2005).

20. A. Singh, L. Steely, and H. R. Allcock, "Poly[bis(2,2,2-trifluoroethoxy)phosphazene] Superhydrophobic Nanofibers," *Langmuir*, **21** [25] 11604-07 (2005).

21. Z. Gu, H. Wei, R. Zhang, G. Han, C. Pan, H. Zhang, X. Tian, and Z. Chen, "Artifical Silver Ragwort Surface," *Appl. Phys. Lett.*, **86** [20] 201915/1-3 (2005).

22. H. M. Shang, Y. Wang, K. Takahashi, G. Cao, D. Li, and Y. Xia, "Nanostructured Superhydrophobic Surfaces," *J. Mater. Sci*., **40** [13] 3587-91 (2005).

23. Y. Zhu, J. Zhang, Y. Zheng, Z. Huang, L. Feng, and L. Jiang, "Stable, Superhydrophobic, and Condutive Polyaniline/Polystryrene Films for Corrosive environments," *Adv. Funct. Mater.*, **16** [4] 568-74 (2006).

24. M. Ma, M. Gupta, L. Zhi, L. Zhai, K. K. Gleason, R. E. Cohen, M. F. Rubner, and G. C. Rutledge, "Decorated Electrospun Fibers Exhibiting Superhydrophobicity," *Adv. Mater.*, **19** [2] 255-9 (2007).

25. Y. Li, E. Kroke, R. Riedel, C. Fasel, C. Gervais, and F. Babonneau, "Thermal Cross-linking and Pyrolytic Conversion of Poly(ureamethylvinyl)silazanes to Silicon-Based Ceramics," *Appl. Organomet. Chem.*, **15** [10] 820-32 (2001).

26. T. A. Pham, D. P. Kim, T. W. Lim, S. H. Park, D. Y. Yang, and K. S. Lee, "Three-Dimensional SiCN Ceramic Microstructures via Nano-Stereolithography of Inorganic Polymer Photoresists," *Adv. Funct. Mater.*, **16** [9] 1235-41 (2006).

27. P. Gupta, C. Elkins, T. E. Long, and G. L. Wilkes, "Electrospinning of Linear Homopolymers of Poly(methyl methacrylate): Exploring Relationships between Fiber Formation, Viscosity, Molecular Weight and Concentration in a Good Solvent," *Polymer*, **46** [13], 4799-481,0(2005).

28. G. Winter, W. Verbeek, and M. Mansmann, "Production of Shaped Articles of Silicon Carbide and Silicon Nitride," U.S. Patent 3892583, 1975.

29. S. Megelski, J.S. Stephens, D.B. Chase, and J.F. Rabolt, "Micro- and Nanostructure Surface Morphology on Electrospun Polymer Fibers," *Macromolecules*, **35** [22] 8456-66 (2002).

30. K. H. Lee, H. Y. Kim, M. S. Khil, Y. M. Ra, and D. R. Lee, "Characterization of Nano-Structured Poly(ε-caprolactone) Nonwoven Mats via Electrospinning," *Polymer*, **44** [4] 1287-94 (2003).

31. R. V. N. Krishnappa, C. Sung, and H. Schreuder-Gibson, "Electrospinning of Polycarbonates and Their Surface Characterization Using the SEM and TEM," *Mat. Res. Soc. Symp. Proc.*, **702**, 235-40 (2002).

32. P. Dayal and T. Kyu, "Porous Fiber Formation in Polymer Solvent System Undergoing Solvent Evaporation," *J. Appl. Phys.*, **100** [4] 043512/1-6 (2006).

33. C. –M. Hsu and S. Shivkumar, "N, N-dimethyformamide Additions to the Solution for the Electrospinning of Poly(ε-caprolactone)," *Macromol. Mater. Eng.*, **289** [4] 334-40 (2004).

34. D. R. Lide (ed) *Handbook of Chemistry and Physics*, 73rd edition, CRC Press, Boca Raton, FL 1993.

35. A. Dhamne, W. Xu, B. Fookes, Y. Fan, L. Zhang, S. Burton, J. Hu, J. Ford, and L. An, "Polymer-Ceramic Conversion of Liquid Polyaluminasilazane for SiAlCN Ceramics," *J. Am. Ceram. Soc.*, **88** [9] 2415-9 (2005).

36. L. An, Y. Wang, L. Bharadwaj, Y. Fan, L. Zhang, D. Jiang, Y. Sohn, V. Desai, J. Kapat, and L. Chow, "Silicalumium Carbonitride with Anomalously High Resistance to Oxidation and Hot Corrosion," *Adv. Eng. Mater*., **6** [5] 337-40 (2004).

37. C. Charles, G. G. Mallakowski, R. W. Boswell, A. Goult, G. Turban, and C. Cardinaud, "Characterization of Silicon Dioxide Films Deposited at Low Pressure and Temperature in a Helicon Diffusion Reactor," *J. Vac. Sci. & Technol. A*, **11** [6] 2954-63 (1993).

38. N. Wada, S. A. Solin, J. Wong, and S. Prochazka, "Raman and IR Absorption Spectroscopic Studies on α, β, and Amorphous Silicon Mitride," *J. Non-Cryst. Solids*, **43** [1] 7-15 (1981).

39. L. Zhai, F. C. Cebeci, R. E. Cohen, and M. F. Rubner, "Stable Superhydrophobic Coatings from Polyelectrolyte Multilayers," *Nano Lett.*, **4** [7] 1349-53 (2004).

40. Y. Wang, W. Fei, Y. Fan, L. Zhang, W. Zhang, and L. An, "Silicoaluminum Carbonitride Ceramic Resist to Oxidation/Corrosion in Water Vapor," *J. Mater. Res.*, **21** [7] 1625-8 (2006).

41. H. L. Schreuder – Gibson, Q. Truong, J. E. Walker, J. R. Owens, J. D. Wander, and W. E. Jones Jr., "Chemical and Biological Protection and Detection in Fabrics for Protective Clothing," *MRS Bulletin*, **28** [8] 574-8 (2003).

CHAPTER 3 POLYMER-DERIVED CERAMIC COMPOSITE FIBERS WITH ALIGNED PRISTINE MULTIWALLED CARBON NANOTUBES

3.1 Abstract

Polymer-derived ceramic fibers with aligned multiwalled carbon nanotubes (MWCNTs) were fabricated through the electrospinning of polyaluminasilazane solutions with well-dispersed MWCNTs followed by pyrolysis. Poly(3-hexylthiophene)-*b*-poly (poly (ethylene glycol) methyl ether acrylate) (P3HT-*b*-PPEGA), a conjugated block copolymer compatible with polyaluminasilazane, was used to functionalize MWCNT surfaces with PPEGA, providing a non-invasive approach to disperse carbon nanotubes in polyaluminasilazane chloroform solutions. The electrospinning of the MWCNT/polyaluminasilazane solutions generated polymer fibers with aligned MWCNTs where MWCNTs are oriented along the electrospun jet by a sink flow. The subsequent pyrolysis of the obtained composite fibers produces ceramic fibers with aligned MWCNTs. The study of the effect of polymer and CNT concentration on the fiber structures showed that the fiber size increases with the increment of polymer concentration; while higher CNT content in the polymer solutions leads to thinner fibers owning to the increased conductivity. Both the SEM and TEM characterization of the polymer and ceramic fibers demonstrated the uniform orientation of CNTs along the fibers, suggesting the excellent dispersion of CNTs and efficient CNT alignment via the electrospinning. The electrical conductivity of a ceramic fibers with 1.2 % aligned MWCNTs is measured to be 1.58×10^{-6} S/cm that is more than 500 times higher than that of bulk ceramic (3.43×10^{-9} S/cm). Such approach

provides a versatile method to disperse CNTs in preceramic polymer solutions and offers a new approach to integrate aligned CNTs in ceramics.

3.2 Introduction

Incorporating carbon nanotubes (CNTs) in polymeric,[1-3] metallic,[4] metal-ceramic[5,6] and ceramic[7-13] matrices can significantly improve their mechanical, electrical, or thermal properties. Furthermore, various interesting anisotropic properties can be obtained by aligning CNTs in matrices since CNTs have extremely high aspect ratios (length/diameter), with diameters of one to tens of nanometers and lengths up to micrometers, or even centimeters.[14,15] For example, CNTs have been aligned in various polymer matrices to achieve anisotropic electrical conductance,[16,17] anisotropic thermal diffusivity[18] and unidirectional reinforcement.[19] Integrating aligned CNTs in ceramic materials is important for applications including rocket nozzles and hot gas filters where requirements such as strength, stiffness and resistance to corrosion prevent the use of polymer or metals. However, the utilization of CNT anisotropic properties in ceramics is limited by the availability of appropriate ceramic materials, effective dispersion and alignment of CNTs in matrices. It is a formidable challenge to achieve proper dispersion and alignment of CNTs in ceramics by conventional powder based processing techniques. In order to disperse and align CNTs in ceramic matrices, a solution processible ceramic precursor and a suitable CNT dispersant that is compatible with the ceramic precursor are necessary. Polymer-derived ceramics (PDCs), unlike conventional ceramics obtained by sintering method, are synthesized by direct thermal decomposition of polymeric precursors.[20,21] This unique direct polymer to ceramics route makes PDCs suitable for fabrication of different unconventionally shaped ceramic components

and devices.[22,23] For example, one-dimensional PDC nanostructures, such as nanowires, nanotubes and nanorods, have been fabricated by the use of off-gases from PDC preparation and also via template approach.[24,25] Previous studies demonstrated the development of a unique simple technique to synthesize ceramic fibers via the electrospinning of aluminum functionalized oligosilazane. Preceramic polymer (polyaluminasilazane) fibers were fabricated via the electrospinning of polymer solutions. The following pyrolysis of the polymer fibers at 1000 °C in Ar produced SiCNAl ceramic fibers.[26] In order to disperse CNTs in various solvents and polymer matrices, Zou and coworkers have developed a novel approach to disperse CNTs into various solvents and polymer matrices using conjugated block copolymers.[27,28] This approach does not require any invasive chemical functionalization of CNT surfaces which deteriorates the electrical and mechanical properties of CNTs. With a simple ultrasonication, the conjugated polymer block such as poly(3-hexyltiophene) (P3HT) can form strong π-π interactions with nanotube walls, whereas non-conjugated polymer block with tunable composition will provide the de-bundled CNTs with good solubility and stability in a wide range of organic solvents and host polymer matrices. These research results provide suitable ceramic matrices and CNT dispersants to incorporate aligned CNTs in ceramics.

Among various existing approaches to align dispersed CNTs including mechanical stretching,[29] assembling under magnetic[30,31] and electric fields,[32] electrospinning has been widely used owning to its ease and flexibility in operation. In a typical electrospinning process, a high electrostatic force is applied to a solution held in a syringe with a needle. A jet is emitted from the cone-like meniscus (Taylor cone) formed on the needle tip when the field strength exceeds a

critical value to overcome the polymer solution surface tension. As the jet moves toward the collecting electrode, its diameter decreases due to lateral excursions, and the solvent evaporates, leading to a non-woven fabric mat on the collecting electrode.[33-35] Various polymer fibers containing aligned CNTs have been fabricated by electrospinning polymer solutions containing dispersed CNTs,[36-45] where CNTs lined up during the electrospinning process due to the sink flow and high extension of the electrospun jet.[46]

Based on the achievement in the material development and well-established electrospinning technology, it is rationalized that ceramic fibers with aligned CNTs could be fabricated by pyrolyzing CNT/preceramic polymer electrospun fibers produced from preceramic polymer solutions with CNTs dispersed by conjugated block copolymers. In this chapter, the fabrication of ceramic fibers with aligned CNTs from preceramic polymer solutions containing dispersed multi-walled carbon nanotubes (MWCNT) is reported. MWCNTs were dispersed uniformly by a conjugated block copolymer-poly(3-hexylthiophene)-*b*-poly (poly (ethylene glycol) methyl ether acrylate) (P3HT-*b*-PPEGA) in chloroform solutions of polyaluminasilazane, a synthesized solution-processible preceramic polymer. SiCNAl ceramic fibers with aligned MWCNTs were fabricated through the electrospinning of CNT/ polyaluminasilazane solutions followed by a pyrolysis of the obtained fibers. The effect of polymer solution concentration and MWCNT/polymer ratio on fiber structures is discussed. The alignment of CNT in ceramic fibers and the improvement of the electrical conductivity by the aligned CNTs is demonstrated. Such approach provides a versatile method to disperse CNTs in preceramic polymer solutions and offers a new approach to integrate aligned CNTs in ceramics.

3.3 Experimental

3.3.1 Materials

All reactions were performed in oven-dried glassware under purified argon. All glassware were assembled while hot and cooled under argon. Before use, tetrahydrofuran (THF) was distilled from sodium /benzophenone under nitrogen. Ceraset™ VL20 was purchased from Kion Corporation, USA. Aluminum tri-sec-butoxide, vinyl magnesium bromide, t-butyl magnesium chloride (t-BuMgCl), 9-bora-bicyclo [3.3.1] nonane (9-BBN), triethylamine (TEA), 2-bromopropionyl bromide, [1,3-bis[(diphenylphosphino)propane]dichloronickel(II)] ($Ni(dppp)Cl_2$), sodium hydroxide, hydrogen peroxide, copper (I) bromide, pentamethyldiethylenetriamine (PMDETA), poly(ethylene glycol)methyl ether acrylate (PEGA) were purchased from Sigma-Aldrich Chemical Co., USA and were used as-received without any further purifications.

3.3.2 Synthesis of Polyaluminasilazane

Solid preceramic polyaluminasilazane was synthesized from Ceraset™ VL20 similar to the procedure reported earlier. 40.100 g of Ceraset™ VL20 was mixed with 8.010 g of aluminum tri-sec-butoxide in a 100 mL conical flask under magnetic stirring and heated at 160 $^{\circ}$C for 36 h under Argon atmosphere under magnetic stirring. The mixture was cooled and a solid polymer was obtained.

3.3.3 Synthesis of vinyl terminated Poly(3-hexylthiophene)(P3HT)

A dry 100 mL three-neck round-bottomed flak was purged with argon and was charged with 2,5-dibromo-3-hexylthiophene (2.016 g, 6.2 mmol) and anhydrous THF (50 mL). A 2*M* solution of t-butyl magnesium chloride (3.2 mL, 6.4 mmol) in diethyl ether (Et_2O) was added via a syringe, and the reaction was refluxed for 90 min. The reaction mixture was then cooled to room temperature, when Ni(dppp)Cl_2 (0.060 g, 0.1 mmol) was added to the reaction mixture. The polymerization was allowed to proceed for 15 min at room temperature followed by the addition of a 1*M* solution of vinyl magnesium bromide (2.2 mL, 2.2 mmol). The reaction solution was continued form 3 min followed by quenching in methanol. The polymer was then purified by alternate Soxhlet extractions with methanol and chloroform. The polymer was finally extracted with chloroform, isolated by solvent evaporation and then dried for overnight under vacuum.

3.3.4 Hydroboration/oxidation of vinyl terminated P3HT

Vinyl terminated P3HT (0.264 g, 0.044 mmol, M_n (NMR) = 6,000) was dissolved in a 100 mL anhydrous THF under argon atmosphere. To this reaction mixture, a 0.5*M* solution of 9-BBN (1.76 mL, 0.88 mmol) in anhydrous THF was added via a syringe. The reaction mixture was magnetically stirred for 24 h at 40 $^{\circ}$C, at which point a 6*M* solution of NaOH (0.9 mL) was added to the reaction flask. The reaction mixture was stirred for another 15 min, at which time the oil bath was removed. The reaction mixture was allowed to cool down to RT followed by addition of 33 % aqueous hydrogen peroxide (0.9 mL), and the reaction was allowed to proceed for additional 24 h at 40 $^{\circ}$C. The hydroxyl terminated P3HT was isolated by precipitation in methanol. The polymer was filtered off and purified by sequential Soxhlet extractions with

methanol and chloroform. The polymer was finally isolated from chloroform by solvent evaporation and dried for overnight.

3.3.5 Synthesis of P3HT macroinitiator

Hydroxy terminated P3HT (0.225 g, 0.04 mmol) was dissolved in 100 mL anhydrous THF under argon. The reaction mixture was stirred for 15 min at 40 °C to completely dissolve the polymer in THF to obtain a homogeneous solution. This is followed by the addition of triethylamine (3.6 mL, 26.4 mmol) and drop-wise addition of 2-bromopropionyl bromide (3.0 mL, 24 mmol). The reaction mixture was allowed to proceed for 24 h at 40 °C. The resulting P3HT macroinitiator was precipitated in methanol and purified by the same procedure as described before by Soxhlet extractions with methanol and chloroform.

3.3.6 Synthesis of the Block Copolymer Poly(3-hexylthiophene)-b-poly (poly (ethylene glycol) methyl ether acrylate) (P3HT-b-PPEGA)

P3HT macroinitiator (180 mg, 0.028 mmol), CuBr (8.0 mg, 0.056 mmol), PMDETA (10.0 mg, 0.056 mmol) and PEGA (2.514 g, 5.537 mmol) were dissolved in 4 mL toluene in a dry Schlenk flask. After degassed by three freeze-pump-thaw cycles, the polymerization was carried out at 100 °C for 20 h. After getting rid of copper by passing through a short column and extracting by chloroform, the block copolymer was precipitated in cold diethyl ether for 3 times and dried under vacuum at 60 °C.

3.3.7 Dispersion of MWCNTs in Polyaluminasilazane Solutions

MWCNTs were purchased from Nanolab (Newton, MA) with a diameter of 10-20 nm and a length of 5-20 μm (The purity is above 95 %). The as-received CNTs were used without any further purification or chemical modification. 1mg/mLCNT dispersion in $CHCl_3$ with P3HT-*b*-PPEGA was prepared by adding 10 mg CNT and 20 mg P3HT-*b*-PPEGA in 10 mL chloroform followed by ultrasonication for 1 h with the water bath temperature maintained at 0-10 °C. Twenty-percent polyaluminasilazane solution containing 0.2 % CNT with respect to polyaluminasilazane was prepared by mixing 1.5 g above prepared CNT/$CHCl_3$ dispersion with 0.5 g polyaluminasilazane and 0.5 g 1 % polyethylene oxide (PEO, M_n = 1,000,000, purchased from Sigma-Aldrich, St. Louise, MO). The ratio of polyaluminasilazane to PEO was maintained at 100. The mixture was sonicated for 5 min.

3.3.8 Electrospinning MWCNT/Polyaluminasilazane Composite Solutions and Pyrolysis

In a typical electrospinning procedure, the CNT/Polyaluminasilazane/PEO solution was loaded in a 5 mL disposable syringe equipped with a stainless steel needle connected to high voltage supply (Glassman High Voltage Inc, High Bridge, NJ). The solution was electrospun at 10 kV with a feed rate of 0.3 mL/h using a syringe pump (New Era Pump Systems Inc., Wantagh, NY). The electrospun fibers were collected on a silicon (Si) wafer at a collector distance of 24.0 cm. The obtained fibers were pyrolyzed at 1000 °C for 1 h in a tube furnace under Ar atmosphere at a heating rate of 5 °C/min to produce ceramic fibers.

3.3.9 Fabrication of Platinum (Pt) Electrodes

Single ceramic fibers were drop-cast on a gold (Au) electrode patterned Si/SiO_2 substrate from their ethanol dispersion. Two platinum (Pt) electrodes were deposited on a fiber with a distance of approximately 100 μm and connected to the adjacent Au electrodes by focused ion beam (FIB) technique.

3.3.10 Characterization

^1H NMR of the block copolymer P3HT-*b*-PPEGA and polyaluminasilazanes were acquired on a Varian Mercury Gemini Spectrometer at 500 MHz using $CDCl_3$ as the solvent. The molecular weight of the block copolymer was determined using JASCO Gel Permeation Chromatography system (JASCO Inc., Easton, MD) with ultraviolet, refractive index and static light scattering detectors. The surface morphology of the electrospun fibers and the surface composition of the Pt deposited fibers were examined by Zeiss Ultra-55 FEG scanning electron microscope (SEM) equipped with Noran System 7 EDS with silicon drift X-ray detector. The orientation of the MWCNTs in the fibers was characterized by FEI Technai F30 transmission electron microscope (TEM). Thin specimens for TEM were prepared by FIB etching of the fibers using FEI 200 TEM FIB using gallium as the liquid metal ion source followed by ex-situ deposition of the specimen on carbon coated copper TEM grids. Raman spectra of the composite fibers were obtained using Renishaw Raman Microscope (Renishaw Inc., Gloucestershire, UK) at 785 nm silicon-solid laser excitation source. Room temperature *I-V* characteristics of the fiber were measured using a two-probe Keithley-238 source-measure unit.

3.4 Results and Discussion

3.4.1 Synthesis of P3HT-b-PPEGA

The conjugated block copolymer, P3HT-*b*-PPEGA, was synthesized using vinyl terminated P3HT as the precursor is shown in the reaction scheme (Figure 3.1). The vinyl terminated P3HT was synthesized by Grignard Metathesis method (GRIM) developed by McCullough et.al.[47] Furthermore, addition of various Grignard reagents (RMgX, R= alkyl group) at the end of the polymerization reaction results in end-capping of regioregular poly(3-alkylthiophenes) with R end groups, which leads to the synthesis of wide variety of end-functionalized poly(3-alkylthiophenes).[48] The vinyl group was easily converted to hydroxyethyl end group with 9BBN/H_2O_2, which then reacts with 2-bromopropionyl bromide to give bromoester terminated P3HT. The later was used as macroinitiator for the synthesis of the block copolymer, P3HT-*b*-PPEGA, by a novel atom transfer radical polymerization, popularly known as ATRP.[27]

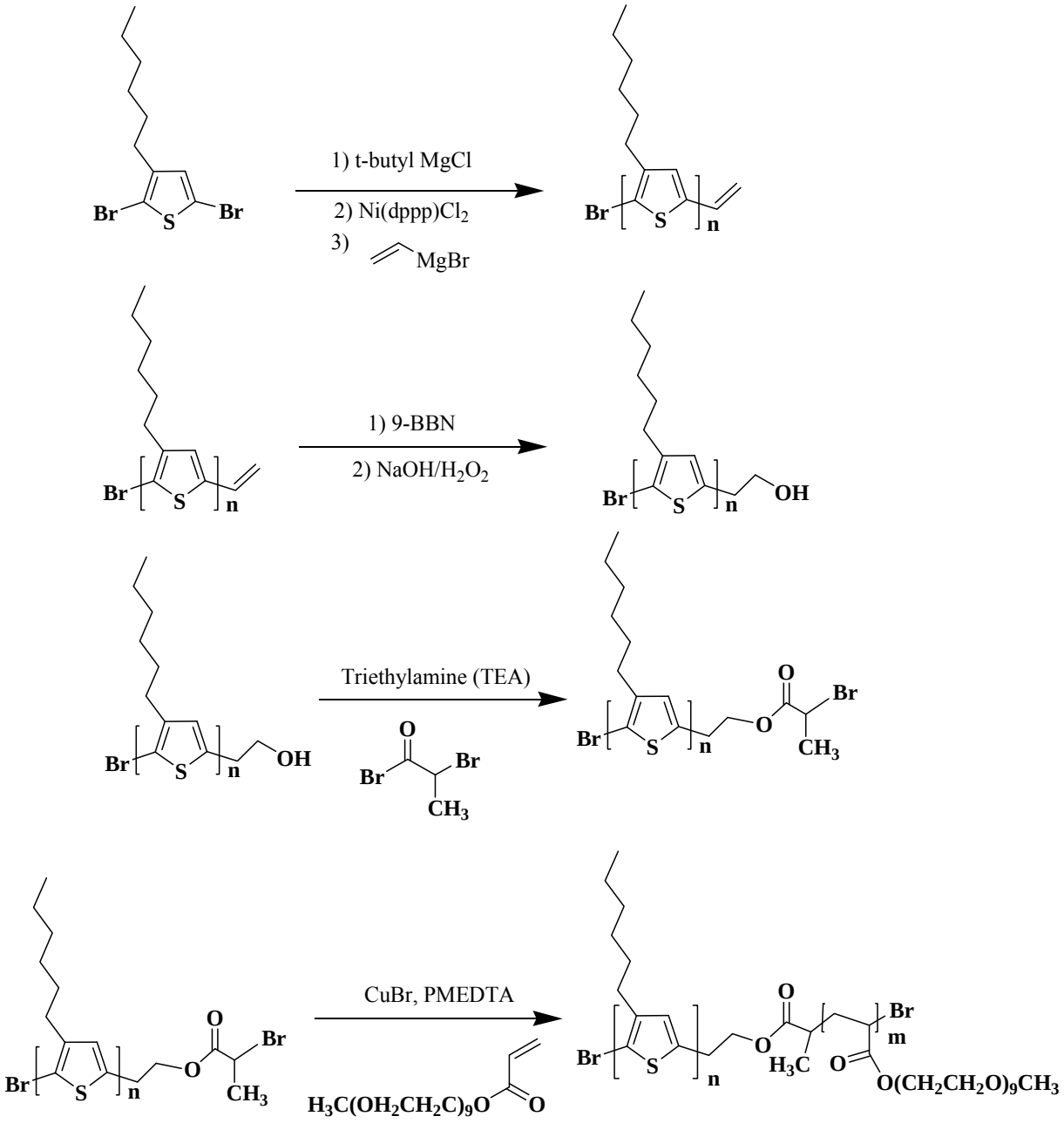

Figure 3.1 Synthesis scheme of conjugated block polymer, P3HT-b-PPEGA.

^{1}H NMR spectrum of vinyl terminated P3HT (Figure 3.2) indicated the presence of vinyl protons at 5.1 ppm (dd) and 5.5 ppm (dd) and 6.8 ppm (m). The degree of polymerization (DP_n) of vinyl

terminated P3HT was estimated from the ^{1}H NMR spectrum comparing the integrated intensities of the vinyl protons (i) and the proton at 4 positions (g). The DP_n was estimated to be 36. The conversion of vinyl to hydroxyethyl terminated P3HT was indicated by the complete disappearance of vinyl protons and the appearance of new signals at 3.0 ppm (t) and 3.9 ppm (t) in the ^{1}H NMR spectrum (Figure 3.3). Also the bromoester terminated P3HT was confirmed by the ^{1}H NMR spectrum (Figure 3.4).

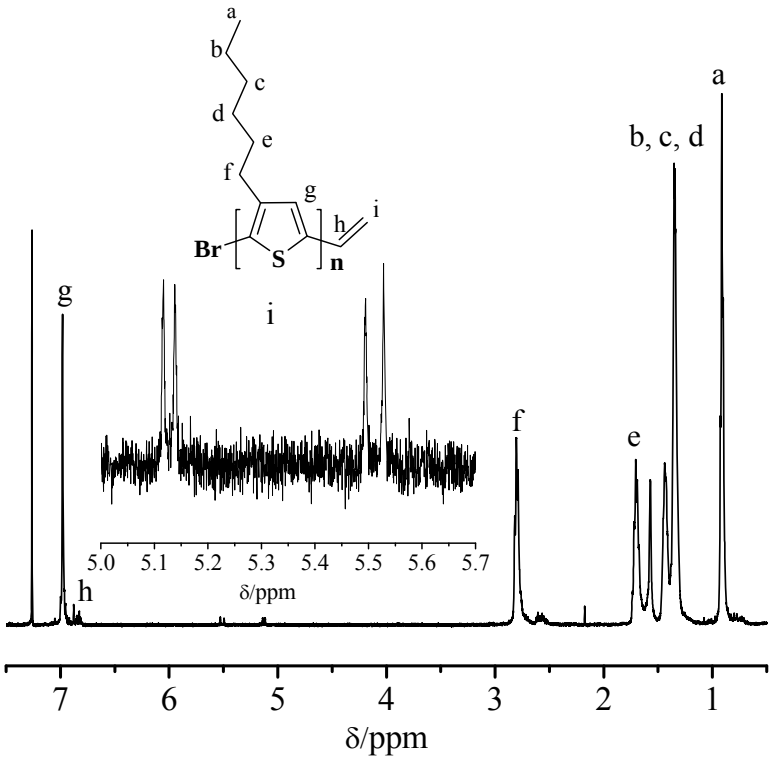

Figure 3.2 ^{1}H NMR of vinyl terminated P3HT.

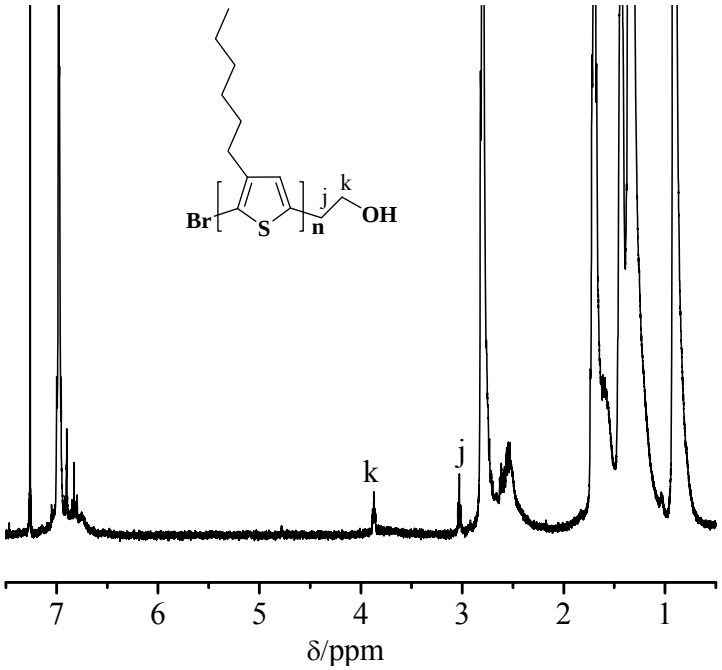

Figure 3.3 [1]H NMR of hydroxyethyl terminated P3HT.

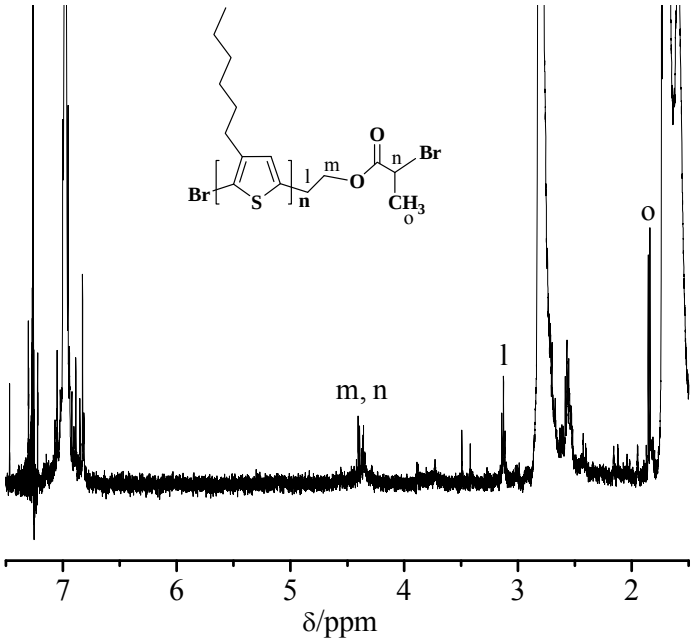

Figure 3.4 [1]H NMR of P3HT macroinitiator.

ATRP of poly(ethylene glycol) methyl ether acrylate was performed using CuBr as a catalyst as a ligand and bromoester terminated poly (3-hexylthiophene) as macroinitiator. Polymerization of the acrylate was performed at molar ratio $[PEGA]_0$: $[Macroinitiator]_0$ $[CuBr]_0$: $[PMDETA]_0$: = 200:1:2:2 in toluene at 100 °C. ^{1}H NMR spectrum of the block copolymer, P3HT-*b*-PPEGA, is shown in Figure 3.5. the molar ratio of 3-hexylthiophene unit to PEGA unit of P3HT-*b*-PPEGA was determined to be 1: 2.8 comparing the protons of a and b as shown in Figure 3.5. The molecular weight (M_n) of P3HT-*b*-PPEGA was determined by GPC to be 16,900 with a polydispersity index (M_w/M_n) of 1.5 (Figure 3.5, inset). ^{1}H NMR ($CDCl_3$): 6.98 (s, 4' proton of 3-hexylthiophene), 4.17 (br, s, CH-COO-C**H$_2$**), 3.64 (t, -O-**CH$_2$-CH$_2$**-O), 3.55 (t, -CH_2-**CH$_2$**-O-CH_3), 3.39 (s, -CH_2-O-**CH$_3$**), 2.79 (t, α-**CH$_2$**).

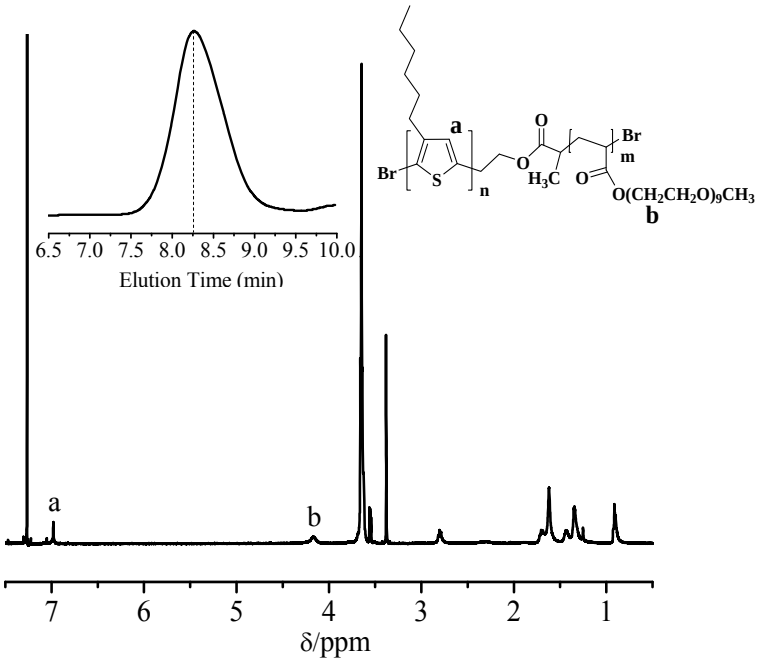

Figure 3.5 ^{1}H NMR of the block copolymer, P3HT-b-PPEGA. (Inset) GPC of P3HT-b-PPEGA.

3.4.2 Synthesis of Polyaluminasilazane and Mechanism

The preceramic polymer used in this study is produced from a commercially available cyclosilazane known as Ceraset™ VL 20. Ceraset™ VL 20 is a low molecular weight (average molecular weight around 300) liquid oligosilazane, and can not be directly used for electrospinning.[49] In previous studies, a solid polyaluminasilazane was synthesized by a treatment of Ceraset™ VL 20 with aluminum tri-sec-butoxide. It was hypothesized that the coupling reaction between aluminum and nitrogen could be the reason for the transformation from liquid oligosilazane to solid polyaluminasilazane. To corroborate the hypothesis, the reaction mechanism was investigated using ^{1}H NMR spectroscopy. ^{1}H NMR spectra of Ceraset™ VL20 (Figure 3.6a) shows four characteristics peaks, which can be assigned to Si-CH=CH_2 (5.73-6.17 ppm), Si-H (4.42-5.02 ppm), N-H (0.82-0.89 ppm) and Si-CH_3 (0.09-0.33 ppm). It is believed that Ceraset™ VL20 became partially crosslinked due to the hydrosilation between Si-H and Si-CH=CH_2 groups at lower temperatures. Therefore, the estimated conversion of Si-H groups by the treatment of Ceraset™ VL20 with varying amounts of aluminum sec-butoxide at the same reaction conditions could be an efficient route to predict the reaction pathway. Expectedly, the conversion of Si-H was calculated to be 18 % and 5 % for 15 % and 30 % Al sec-butoxide treated Ceraset™ VL20, respectively (Figure 3.6b and 3.7c). The decrease in Si-H conversion with increasing aluminum content suggests that the Lewis acid-base complexation reaction between aluminum and nitrogen and the presence of bulky tri- sec-butoxide groups prevents the crosslinking of Ceraset™ VL20 via hydrosilation, and favors the formation of a solvent-soluble solid complex.

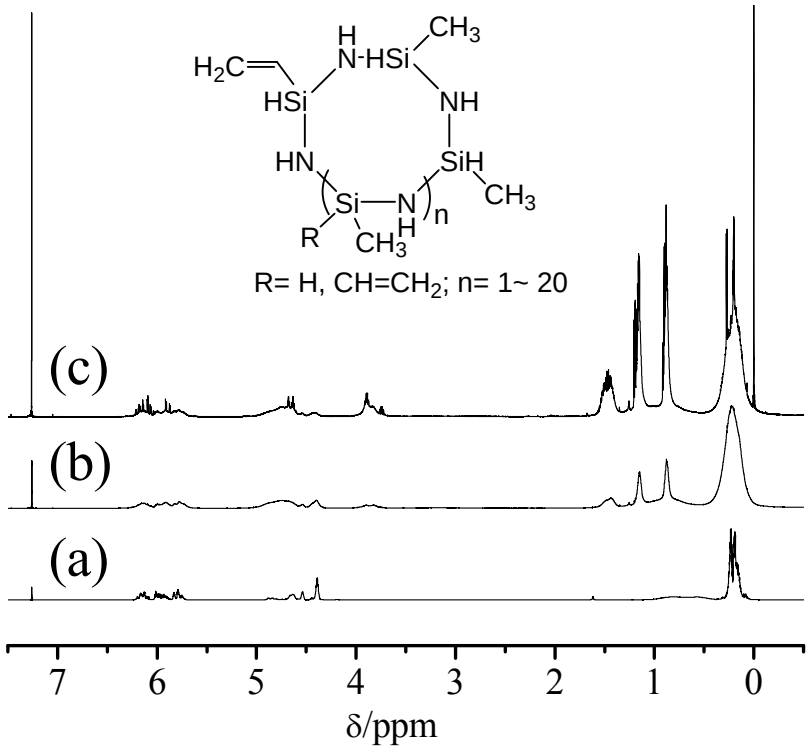

Figure 3.6 ^{1}H NMR of (a) Ceraset™ VL 20, (b) 15 % Al sec-butoxide treated Ceraset™ VL 20 , and (c) 30 % Al sec-butoxide treated Ceraset™ VL 20.

3.4.3 Fabrication of Electrospun Polyaluminasilazane/CNT Fiber and Characterization

The obtained polyaluminasilazane is soluble in common solvents such as chloroform ($CHCl_3$), tetrahydrofuran (THF) and *N,N*-dimethylformamide (DMF) and was electrospun into smooth fibers. SiCNAl with a composition of $Si_{1.0}C_{0.5}N_{0.4}Al_{0.07}O_{0.01}$ was obtained after pyrolyzing the polyaluminasilazane fibers.[26] Incorporating CNTs into polyaluminasilazane requires a stable dispersion of the nanotubes in polyaluminasilazane solutions before electrospinning. However, pristine nanotubes form agglomerates in solvents like $CHCl_3$ without proper dispersion due to strong van der Waals interactions between the nanotubes (Fig 3.7a-A). To create stable CNT

dispersion in polyaluminasilazane chloroform solutions, an amphiphilic conjugated block copolymer, poly(3-hexylthiophene)-*b*-poly (poly (ethylene glycol) methyl ether acrylate) (P3HT-*b*-PPEGA) was synthesized to produce stable CNT dispersion in polyaluminasilazane chloroform solutions.[27] The PPEGA block in P3HT-b-PPEGA has a structure similar to poly(ethylene oxide) (PEO).[50] Such block copolymer is readily soluble in both polar and non-polar solvents, and expected to be compatible with polyaluminasilazane. Indeed, P3HT-*b*-PPEGA is a sufficient dispersant to produce stable CNT dispersion in polyaluminasilazane chloroform solutions. The CNTs were uniformly dispersed in chloroform by P3HT-*b*-PPEGA (The ratio of CNT to P3HT-*b*-PPEGAA was 1:2; Figure 3.7a-B), generating a CNT dispersion (1 mg/mL) stable for several months. The addition of as-synthesized polyaluminasilazane did not disrupt the dispersion (Figure 3.7a-C). The transmission electron microscopy (TEM) characterization of the CNT dispersion in polyaluminasilazane chloroform solutions (Figure 3.7b) indicated that majority of the nanotubes are de-bundled and dispersed into individual tubes.

Electrospinning of the CNT/polyaluminasilazane solutions generated droplets due to insufficient chain entanglement among short polyaluminasilazanes and block copolymer P3HT-*b*-PPEGA polymer chains.[51] To introduce sufficient chain entanglement and facilitate the fiber formation, small amount of high molecular PEO (M_n = 1,000,000) (the ratio of polyaluminasilazane to PEO was 100:1) was added to the polyaluminasilazane solution.[52] Figure 3.8 shows the eletrospun cotton-like fibers formed from pure polyaluminasilazane and CNT/polyaluminasilazane chloroform solutions. The color of the CNT/polyaluminasilazane electrospun fibers is gray because CNTs are embedded in the fibers

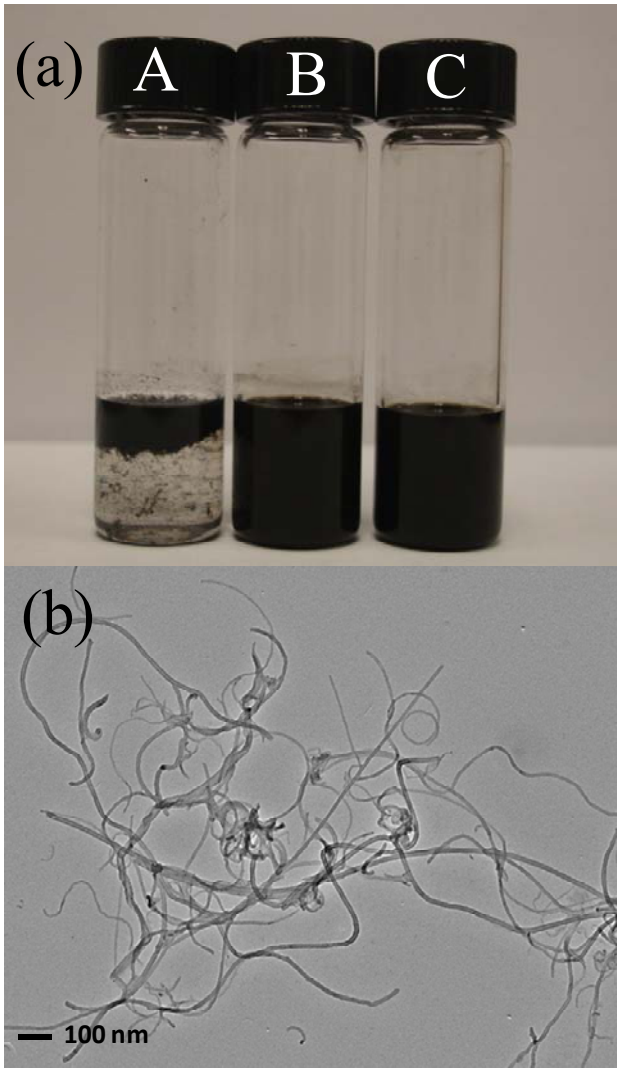

Figure 3.7 (a) The photographs of (A) MWCNT agglomeration in polyaluminasilazane/$CHCl_3$ solution, (B) P3HT-b-PPEGA dispersed MWCNTs in $CHCl_3$, and (C) P3HT-b-PPEGA dispersed MWCNTs in polyaluminasilazane/PEO chloroform solutions, and (b) TEM image of MWCNT dispersed in a polysilazane/P3HT-b-PPEGA/PEO chloroform solution.

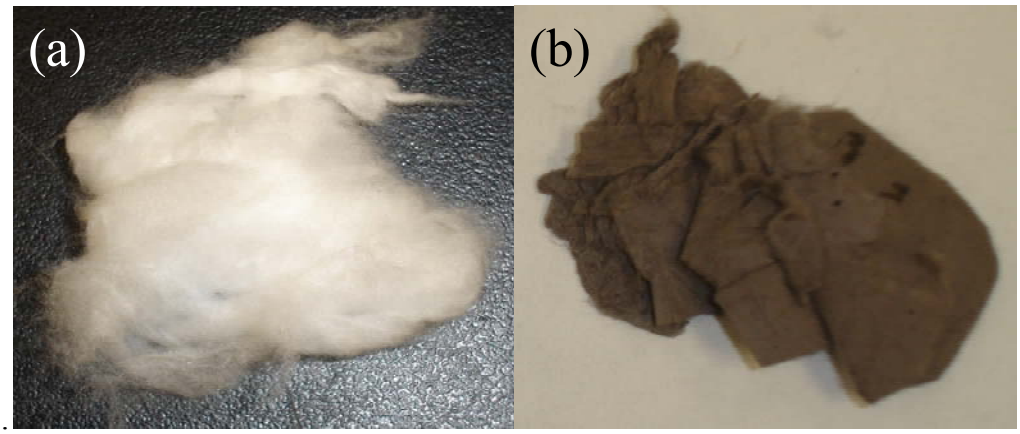

Figure 3.8 Non-woven electrospun fiber mat of (a) pure polyaluminasilazane, and (b) polyaluminasilazane/MWCNT (0.3 wt%).

The effect of MWCNT concentration on the electrospun fiber morphology was investigated using 20 % polyaluminasilazane solutions with different CNT content (0.025 % to 0.2 % related to solid polymer). The scanning electron microscopy (SEM) images (Figure 3.9) show that the fibers become smoother and more regular as the CNT concentration increases possibly due to the increasing of chain entanglement induced by CNTs. The PPEGA blocks of P3HT-*b*-PPEGA attaching to CNT surfaces have similar structures to PEO, and interact with PEO and polyaluminasilazane through hydrogen bonding,[50-52] introducing higher degree of chain entanglement with more P3HT-*b*-PPEGA dispersed CNTs. Such higher degree of chain entanglement increases the viscoelasticity of the solution,[53,54] resulting in smooth and uniform fibers. The fiber diameter change with CNT concentrations (0.025 % to 0.2 %) is not obvious in Figure 3.9. Such observation is unlike the reported effect of CNT concentration on electrospun fiber diameter where the solution conductivity increased with an increment of CNT concentration, generating higher charge density on the solution and producing thinner fibers.[36]

Such trivial effect of CNT concentration on electrospun fiber diameter is probably due to the low CNT concentration that is unable to introduce large conductivity change in solutions. When the CNTs concentration is high enough to increase the solution conductivity, the effect of the CNTs concentration on spun fiber diameter is observable. For example, the CNT/polyaluminasilazane fibers (4 μm) spun from 20 % CNT/polyaluminasilazane (0.2 % CNT related to solid polymer) solutions (Figure 3.10-a) is thinner than the pure polyaluminasilazane fibers (5 μm) spun from 20 % polyaluminasilazane solutions (Figure 3.11). Figure 3.10 shows the SEM images of the CNT/polyaluminasilazane electrospun fibers from the composite solutions of polyaluminasilazane and CNT at different concentrations. The fiber diameter decreases from about 4 μm to 1 μm as the polyaluminasilazane concentration reduces from 20 % to 5 % and the nanotube concentration increases from 0.2 % to 1.2 %. This observation is in good agreement with my previous studies of the effect of polyaluminasilazane concentration on the size of electrospun fibers showing that the fiber diameter increases with the increasing of polymer concentration. The fibers become rough, porous and irregular in shape as the polymer content decreases. The formation of the pores is possibly caused by the condensation of moistures during the electrospinning process as explained by a "breath figure" model.[55] During the electrospinning, the temperature of spinning jet drops with the evaporation of solvents, which causes the ambient moisture to condense onto the fiber surface. The condensed water droplets form pores when the solvent and water evaporates completely to generate solid fibers. The roughening of the fibers at high CNT concentration is possibly due to the increased electric field caused by the high electrical conductivity of CNT in the polymer solution.[42]

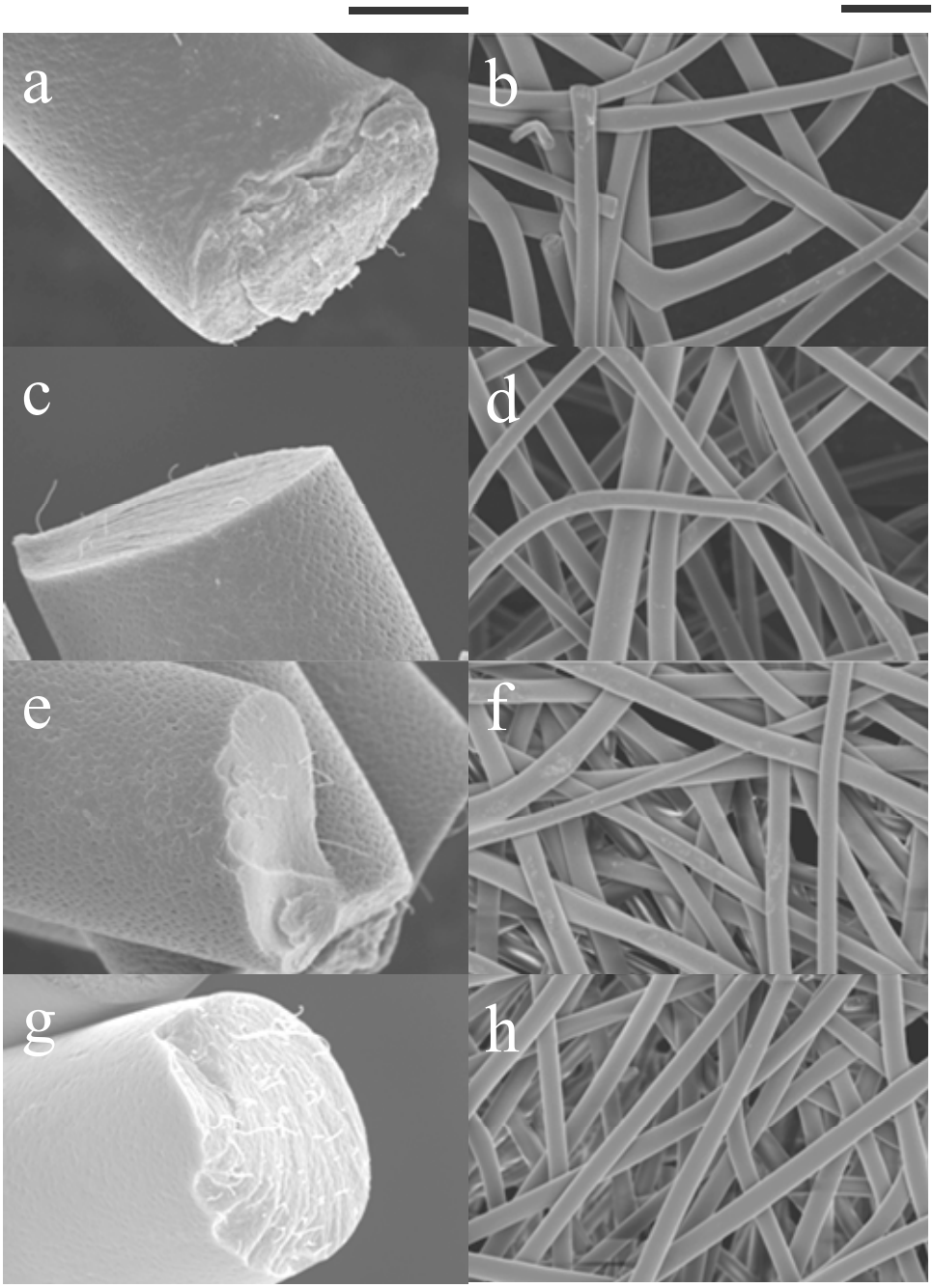

Figure 3.9 SEM images of electrospun fibers at different concentrations of MWCNT in 20 % polyaluminasilazane solutions: (a,b) 0.025 % MWCNT; (c,d) 0.05 % MWCNT; (e,f) 0.1 % MWCNT; (g,h) 0.2 % MWCNT). The scale bar for a, c, e, g is 2 μm and for b, d, f, h is 10 μm. Fibers become regular in shape as the MWCNT concentration increases.

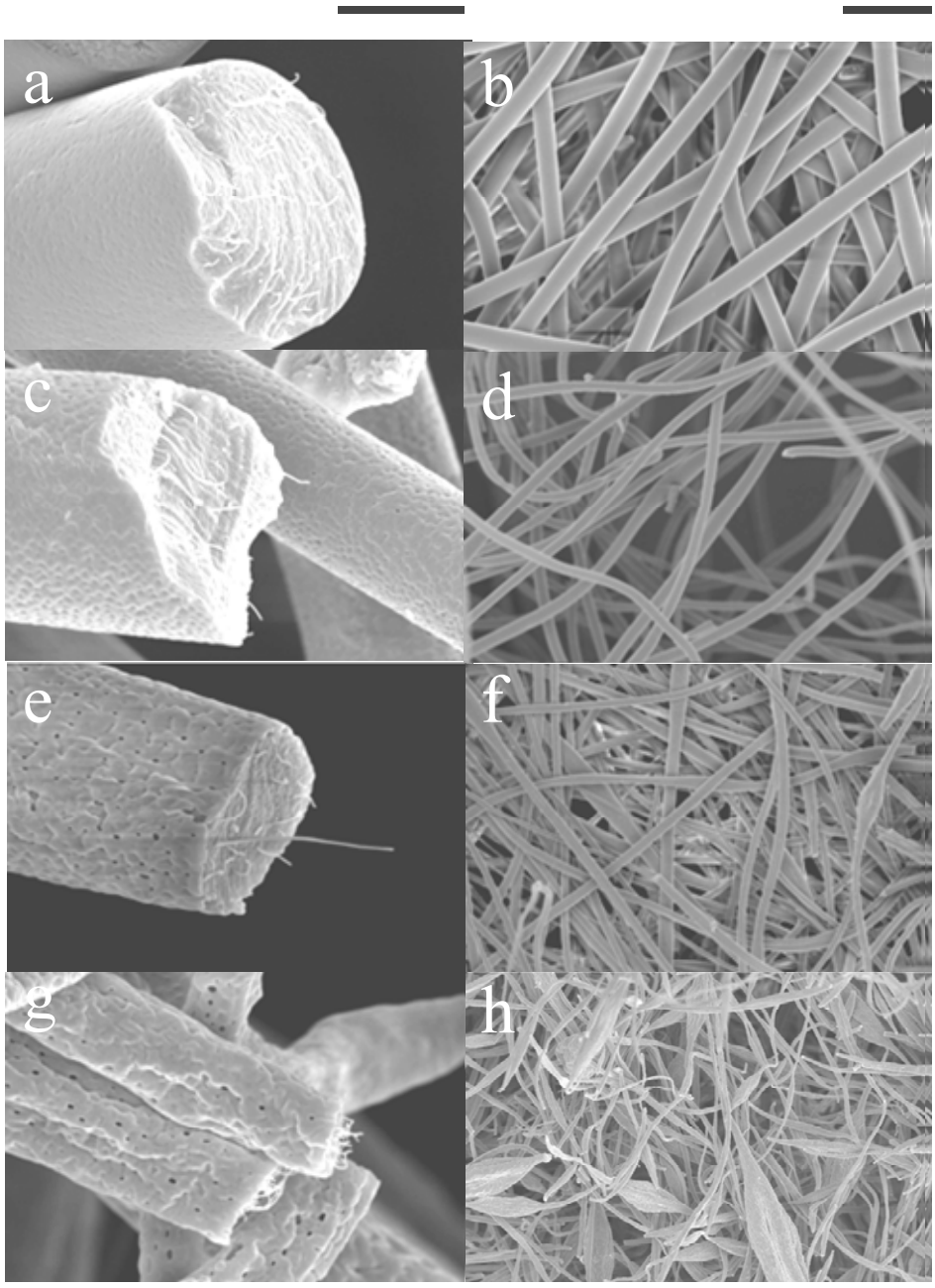

Figure 3.10 SEM images electrospun of electrospun fibers from different composition of polyaluminasilazane and MWCNT: (a,b) 20 % polyaluminasilazane/0.2 % MWCNT; (c,d) 15 % polyaluminasilazane/0.3% MWCNT; (e,f) 10 % polyaluminasilazane/0.5 % MWCNT; (g,h) 5 % polyaluminasilazane/1.2 % MWCNT). The scale bar for a, c, e, g is 2 μm and for b, d, f, h is 10 μm.

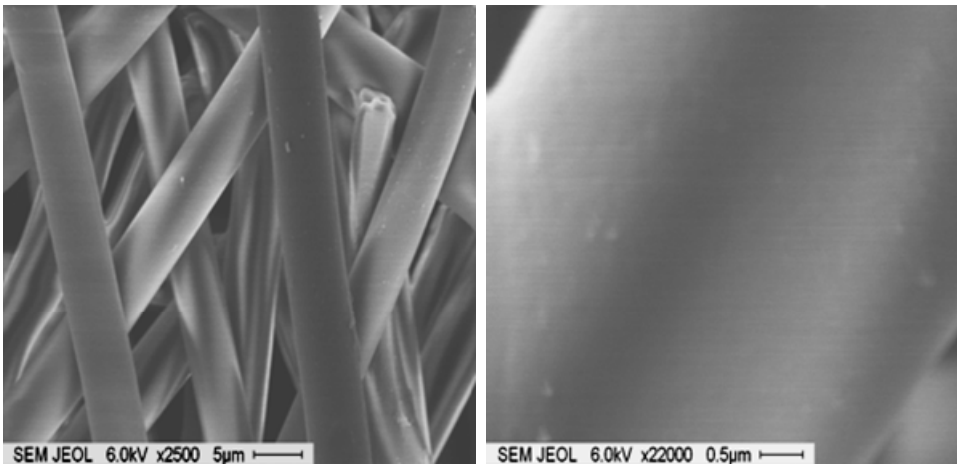

Figure 3.11 SEM images of polyaluminasilazane fibers electrospun from 20 % polyaluminasilazane in chloroform solutions.

The microscopic distribution of the CNTs in the composite fibers was investigated by examining the fractured surface of the electrospun fibers by SEM. Individual CNTs are protruding out of the fractured surface with a density increased with CNT concentration. This suggests excellent dispersion of CNTs by P3HT-*b*-PPEGA and good orientation of nanotubes along the fiber axis. The CNT/polyaluminasilazane fibers were then pyrolyzed at 1000 $^{\circ}$C for an hour under Ar atmosphere. SEM images (Figure 3.12) of the SiCNAl ceramic fibers show that the fiber structure and the aligned CNTs remain unchanged despite 28 % shrinkage of the fiber during the pyrolysis.[56]

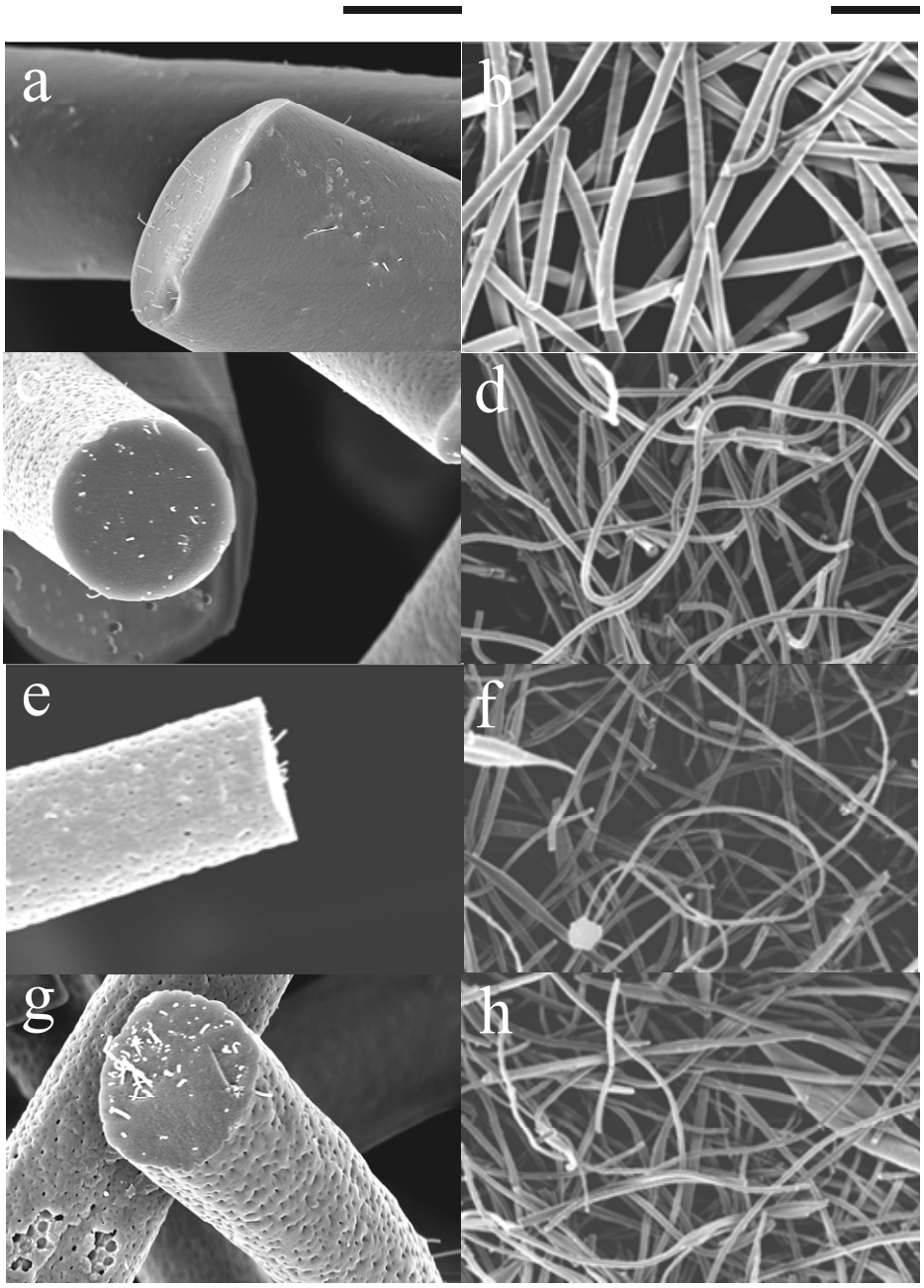

Figure 3.12 SEM images of pyrolyzed ceramic fibers from different composition of polyaluminasilazane and MWCNT (a,b) 20 % polyaluminasilazane/0.2 % MWCNT;(c,d) 15 % polyaluminsilazane/0.3 % MWCNT; (e,f) 10 % polyaluminasilazane/0.5 % MWCNT; (g,h) 5 % polyaluminsilazane/1.2 % MWCNT). The scale bar for a, c, e, g is 2 μm and for b, d, f, h is 10 μm.

In order to study the orientation of the CNTs inside the ceramic fibers, thin specimen of the fibers were characterized by high resolution transmission electron microscopy (HRTEM). Although TEM is an effective tool to observe the orientation of nanotubes in electrospun nanofibers,[41,44,57] micrometer-size ceramic fiber is not suitable for direct TEM imaging. Therefore, portions of the ceramic fibers were removed by a focused ion beam (FIB) using liquid gallium (Ga) ion source. The schematic representation of the thin ceramic fiber preparation by FIB is shown in Figure 3.13a-d, where a thin slice of ceramic fiber was cut from an electrospun ceramic fiber and drop-cast ex-situ onto a TEM grid. The obtained thin ceramic fiber specimen (about 150 nm) was examined by HRTEM (Figure 3.14a-d). Figure 3.14a-c are the TEM images of different parts on a CNT/SiCNAl (0.3 % CNT) ceramic fiber while Figure 3.14d is a high resolution TEM image of a single MWCNT inside the fiber. MWCNTs (15-20 nm in diameter) have a darker concentric tubular structure in the ceramic matrix compared to the uniform matrix. It is evident that MWCNTs align in a considerable length along the fiber axis. The dark spots are the contaminants (Ga) deposited while the thin specimens were prepared for TEM by the FIB.

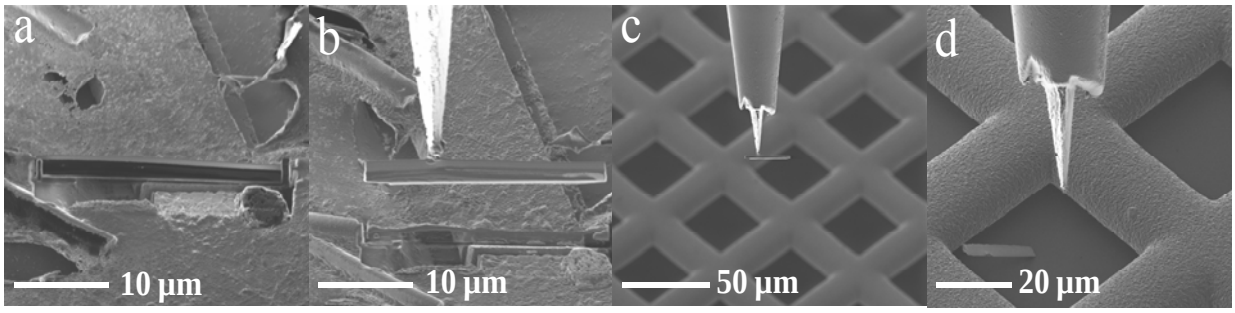

Figure 3.13 Preparation of the thin ceramic fiber specimen for HRTEM characterization.

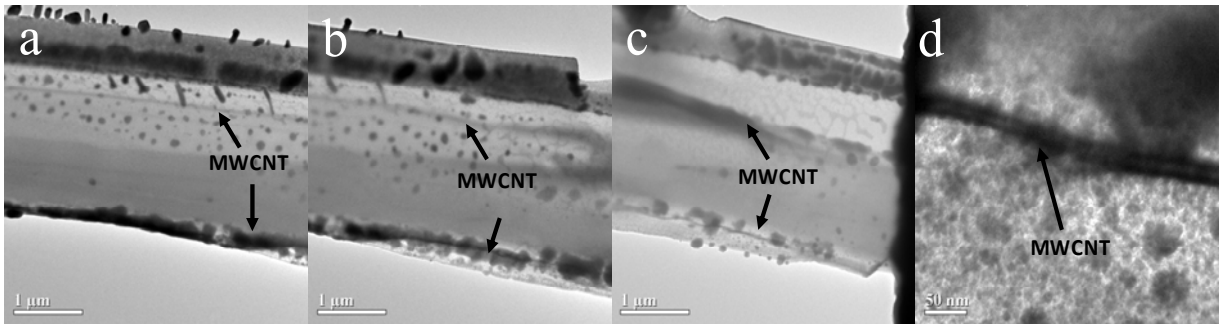

Figure 3.14 HRTEM images of (a,b,c) a FIB-cut 0.3 % MWCNT/SiCNAl ceramic fiber, and (d) MWCNT inside the ceramic fiber.

These observations clearly suggest that CNTs are well dispersed in the solution and align parallel to the fiber axis due to sink flow and high extension forces exerted on the electrospun jet.[46] Before an electric field is applied to the droplet of a CNT/polyaluminasilazane solution, the CNTs behave like rod-like particles that orient randomly in the droplet. During the electrospinning, when an electrical field is applied to the droplet and generates a Taylor cone, the sink flow, also known as Hamel flow[58] causes CNTs to gradually orient along the electrospun jet (Figure 3.15). The alignment of the CNTs embedded in the electrospun fiber is strongly dependent on the quality of CNT dispersion.[45] Electrospinning of the polymer solutions with poorly dispersed CNTs usually generate fibers with humps containing CNT aggregates.[39] Aligned CNTs without any noticeable entanglement inside the ceramic fibers clearly illustrates the excellent dispersion of CNTs by P3HT-*b*-PPEGA and efficient alignment of CNT through electrospinning.

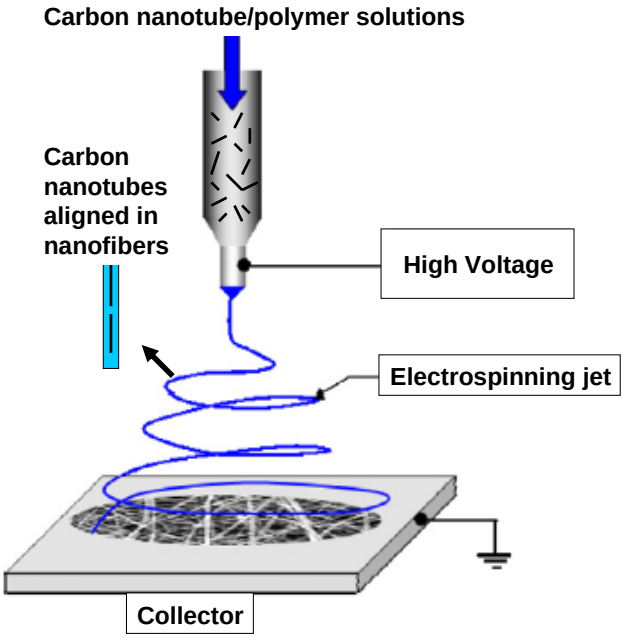

Figure 3.15 Schematic diagram of the electrospinning of polymer/CNT solution.

Raman spectroscopy was used to confirm the presence of aligned MWCNTs in polyaluminasilazane fibers (Figure 3.16). The MWCNTs embedded in polyaluminasilazane matrices show two strong characteristics peaks. The strong peak at 1302 cm^{-1}, D band, could be assigned as the disorder induced features due to finite particle size effect or lattice distortion of graphitic crystals.[41] The other strong peak at 1588 cm^{-1}, called G band, was due to the vibration of the sp^2 hybridized carbon atoms on the MWCNTs. The intensity of both peaks increases with increased MWCNT concentration, while the intensity ratio between the two peaks, I_D/I_G, remains constant. Also the peaks show a little shift (6 to 9 cm^{-1}) towards the lower wave numbers as the MWCNT concentration increases from 0.2 % to 1.2 %.[59]

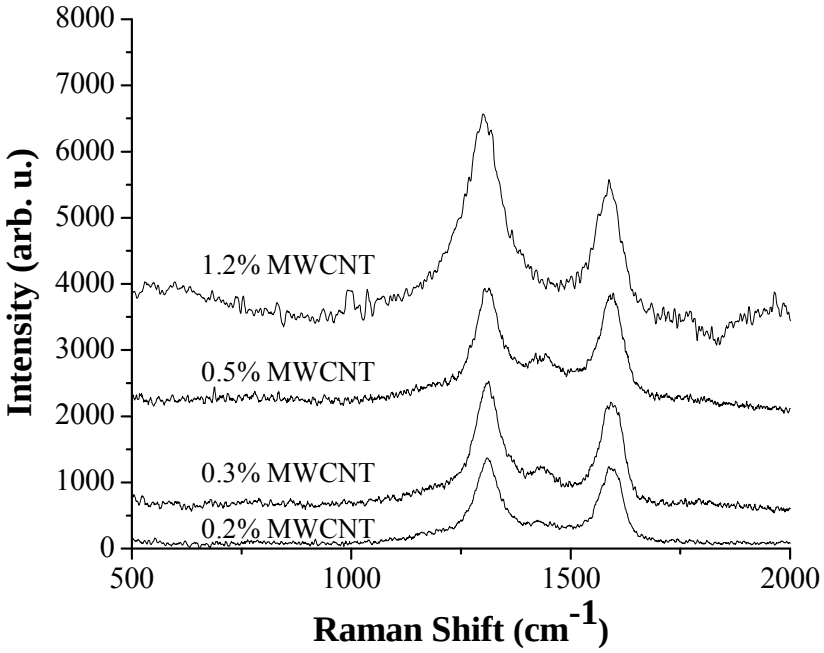

Figure 3.16 Raman spectra of the electrospun fibers with different weight percentages of MWCNTs. The intensity of the peaks decreases and shows a blue shift with the decrease of MWCNT concentrations.

In order to study the electrical properties of the MWCNT/SiCNAl ceramic fibers, the fibers were dispersed in ethanol by ultrasonication to obtain single fibers. The obtained single ceramic fibers were drop-cast onto an Au patterned SiO_2/Si substrate. The single fiber chosen for *I-V* measurement was close to the two adjacent Au electrodes. The fiber was then connected to these electrodes by the deposition of Pt using FIB. Since Ga metal is used in FIB as the ion source for imaging and Pt might be deposited along the fiber to make the fiber conductive, the elemental composition of the fiber surface were investigated by energy dispersive spectroscopy (EDS) analysis. No trace of Ga and Pt contamination was found on the surface of the fiber after successful deposition of Pt electrodes, indicating that the electrical conductivity is solely from

composite fibers. The *I-V* characteristic of a single MWCNT (1.2 %)/ceramic fiber (Figure 3.17) shows non-linear behavior similar to that of MWCNT/poly(vinyl acetate) fibers.[39]

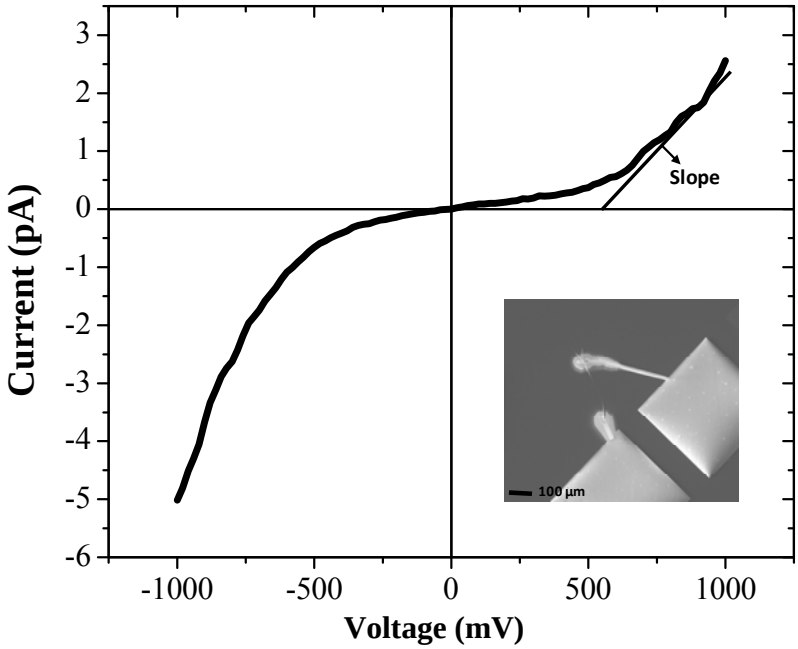

Figure 3.17 I-V characteristics curve of a single MWCNT (1.2 %)/SiCNAl ceramic fiber showing non-linear behavior. The inset shows an image of a single fiber between two platinum (Pt) electrodes.

It is believed that the non-linear characteristics of the *I-V* curve of the MWCNT/ceramic composite fiber could arise from the intrinsic semi-metallic nature of the MWCNT/ceramic composite as well as could possibly be due to the contact resistance between the semiconductor-metal contact, typically known as Schottky contact. The dc conductivity of the MWCNT (1.2 %)/ceramic fiber was measured from the slope of the linear region of the *I-V* characteristics as indicated in Figure 3.17. The obtained conductivity (1.58×10^{-6} S/cm) is more than 500 times higher than that of bulk SiCNAl ceramic (3.43×10^{-9} S/cm). This result suggests that the aligned

nanotubes in ceramic fibers contribute to the increased electrical conductivity.[60] The effects of CNT concentration on the electrical and mechanical properties of CNT/ceramic fibers is currently under investigation.

3.5 Conclusions

In summary, MWCNT/SiCNAl ceramic fibers from polyaluminasilazane electrospun fibers with aligned CNTs were prepared. The effective dispersion of MWCNTs in polyaluminasilazane was achieved by using a conjugated block copolymer, P3HT-*b*-PPEGA. PPEGA groups on P3HT-*b*-PPEGA functionalized CNTs are compatible with polyaluminasilazane through hydrogen bonding and generate a stable dispersion of MWCNT in polyaluminasilazane solutions. Electrospinning of the MWCNT/polyaluminasilazane solutions produced polyaluminasilazane fibers with well-aligned CNTs. The pyrolysis of the obtained composite fibers generated SiCNAl ceramic fibers with aligned MWCNT. SiCNAl ceramic fibers with 1.2 % MWCNTs have electrical conductivity 500 times higher than that of SiCNAl bulk samples, demonstrating the large improvement of electrical conductivity attributed to align CNTs. The reported method provides a versatile approach to disperse CNT in ceramics and paves a new path to align CNTs in ceramic fibers, which may find applications in ceramic matrix composites (CMC) with excellent electrical and mechanical properties.

3.6 List of References

1. J. N. Coleman, U. Khan, and Y. K. Gun' Ko, "Mechanical Reinforcements of Polymers Using Carbon Nanotubes," *Adv. Mater.*, **18** [6] 689-706 (2006).

2. M. Moniruzzaman, and K. I. Winey, "Polymer Nanocomposites Containing Carbon Nanotubes," *Macromolecules*, **39** [16] 5194-205 (2006).

3. S. S. Ojha, M. Afshari, R. Kotek, and R. E. Gorga, "Morphology of Electrospun Nylon-6 Nanofibers as a function of Molecular Weight and Processing Parameters," *J. Appl. Polym. Sci.*, **108** [1] 308-19 (2008).

4. W. X. Chen, J. P. Tu, L. Y. Wang, H. Y. Gan, Z. D. Xu, and X. B. Zhang, " Tribiological Application of Carbon Nanotubes in a Metal-Based Composite Coating and Composites," *Carbon*, 41 [2] 215-22 (2003).

5. Ch. Laurent, A. Peigney, O. Dumoortier, and A. Rousset, "Carbon Nanotubes-Fe-Alumina Composites. Part II: Microstructure and Mechanical Properties of the Hot-Pressed Composites," *J. Eur. Ceram. Soc.*, **18** [14] 2005-13 (1998).

6. A. Peigney, Ch. Laurent, O. Dumoortier, and A. Rousset, "Carbon Nanotubes-Fe-Alumina Composites. Part I: influence of Fe Content on the Synthesis of Powders," *J. Eur. Ceram. Soc.*, **18** [14] 1995-2004 (1998).

7. N. P. Padture, "Multifunctional Composites of Ceramics and Carbon Nanotubes," *Adv. Mater.*, **21** [17] 1767-70 (2009).

8. E. Solvas-Z, R. Poyato, D. Garcia-G, A. Rodriguez-D, V. Radmilovic, and N. P. Padture, "Creep Resistant Composites of Alumina and Single-Wall Carbon Nanotubes," *Appl. Phys. Lett.*, **92** [11] 111912-1- 111912-3 (2008).

9. K. Woan, G. Pyrgiotakis, and W. Sigmund, "Photocatalytic Carbon-Nanotube-TiO_2 Composites," *Adv. Mater.*, **21** [21] 2233-9 (2009).

10. L. Gao, L. Jiang, and J Sun, "Carbon Nanotube-Ceramic Composites," *J. Electroceram.*, **17** [1] 51-5 (2006).

11. J. Tatami, T. Katashima, K. Komeya, T. Meguro, and T. Wakihara, "Electrically Conductive CNT-Dispersed Silicon Nitride Ceramics," *J. Am. Ceram. Soc.*, **88** [10] 2889-93 (2005).

12. G-D. Zhan, J. D. Kunitz, J. Wan, and A. K. Mukherjee, "Single-Wall Carbon Nanotubes as Attractive Toughening Agents in Alumina Based Nanocomposites," *Nat. Mater.*, **2** [1] 38-42 (2003).

13. G-D. Zhan, J. D. Kunitz, J. E. Garay, and A. K. Mukherjee, "Electrical Properties of Nanoceramics Reinforced with Ropes of Single-Walled Carbon Nanotubes," *Appl. Phys. Lett.*, **83** [6] 1228-30 (2003).

14. S. Li, Z. Yu, C. Rutherglen, and P. J. Burke, "Electrical Properties of 0.4 cm Long Single-Walled Carbon Nanotubes," *Nano Lett.*, **4** [10] 2003–7 (2004).

15. L. X. Zheng, M. J. O'Connell, S. K. Doorn, X. Z. Liao, Y. H. Zhao, E. A. Akhadov, M. A. Hoffbauer, B. J. Roop, Q. X. Jia, R. C. Dye, D. E. Peterson, S. M. Huang, J. Liu, and Y. T. Zhu, *Nat. Mater.*, **3** [10] 673–6 (2004).

16. Y. Yao, C. Liu, and S. Fan, "Anisotropic Conductance of the Multiwall Carbon Nanotube Array/Silicone Elastomer Composite Film," *Nanotechnology*, **17** [17] 4374-8 (2006).

17. N. Adachi, T. Fukawa, Y. Tatewaki, H. Shirai, and M. Kimura, "Anisotropic Electrical Conductivity in Layer-By-Layer Composite Film Composed of Water Soluble Conjugated Polymers and SWNTs," *Macromol. Rapid Commun.*, **29** [23] 1877–81 (2008).

18. T. Borca-Tasciuc, M. Mazumder,Y. Son, S. K. Pal, L. S. Schadler, and P. M. Ajayan, "Anisotropic Thermal Diffusivity Characterization of Aligned Carbon Nanotube-Polymer Composites," *J. Nanosci. Nanotechnol.*, **7** [4-5] 1581-8 (2007).

19. J. Che, W. Yuan, G. Jiang, J. Dai, S. U. Lim, and M. B. Chan-Park, "Epoxy Composite Fibers Reinforced with Aligned Single-Walled Carbon Nanotubes Functionalized with Generation 0-2 Dendritic Poly(amidoamine)," *Chem. Mater.*, **21**[8] 1471-9 (2009).

20. R. Riedel, G. Passing, H. Schonfelder, and R. J. Brook, "Synthesis of Dense Silicon-Based Ceramics at Low Temperatures," *Nature*, **355** [6362] 714-7 (1992).

21. E. Kroke, Y.L. Li, C. Konetschny, E. Lecomte, D. Fasel, and R. Riedel, "Silazane-Derived Ceramics and Related Materials," *Mater. Sci. Eng. R*, **26** [4-6] 97-199 (2000).

22. L. Liew, W. Zhang, L. An, S. Shah, R. Lou, Y. Liu, T. Cross, K. Anseth, V. Bright, and R. Raj, "Ceramic MEMS: New Materials, Innovative Processing and Future Applications," *Am. Ceram. Soc. Bull*., **80** [5] 25-30 (2001).

23. L. An, W. Xu, S. Rajagopalan, C. Wang, H. Wang, J. Kapat, L. Chow, Y. Fan, L. Zhang, D. Jiang, B. Guo, J. Liang, and R. Vaidyanathan, "Carbon-Nanotube-Reinforced Polymer-Derived Ceramic Composites," *Adv. Mater*., **16** [22] 2036-40 (2004).

24. M. Pashchanka, J. Engstler, J. J. Schneider, V. Siozios, C. Fasel, R. Hauser, I. Kinski, R. Riedel, S. Lauterbach, H-J. Kleebe, S. Flege, and W. Ensinger, "Polymer-Derived SiOC Nanotubes and Nanorods via a Templated Appraoch," *Eur. J. Inorg. Chem.*, **2009** [23] 3496-506 (2009).

25. Y-G. Li, D-X. Li, H. Wang, and L. Liu, "Long SiC Nanowires Synthesized from Off-Gases of the Polycarbosilane-Derived SiC preparation," *Appl. Phys. A*, **98** [2] 293-8 (2010).

26. S. Sarkar, A. Chunder, W. Fei, L. An, and L. Zhai, "Superhydrophobic Mats of Polymer-Derived Ceramic Fibers," *J. Am. Ceram. Soc.*, **91** [8] 2751-5 (2008).

27. J. Zou, S. I. Khondalker, Q. Huo, and L. Zhai, "General Strategy to Disperse and Functionalize Carbon Nanotubes with Conjugated Block Copolymers," *Adv. Func. Mater.*, **19** [3] 479-83 (2009).

28. J. Zou, L. Liu, H. Chen, S. I. Khondaker, R. McCullough, Q. Huo, and L. Zhai, "Dispersion of Pristine Carbon Nanotubes with Conjugated Block Copolymers," *Adv. Mater.*, **20** [11] 2055-60 (2008).

29. L. Jin, C. Bower, and O. Zhou, "Alignment of Carbon Nanotubes in a Polymer Matrix by Mechanical Stretching," *Appl. Phys. Lett.*, **73** [9] 1197-99 (1998).

30. E. Camponeschi, R. Vance, A-H. Marwan, H. Garmestani, and R. Tannenbaum, "Properties of Carbon Nanotueb-Polymer Composites in a Aligned Magnetic Field," *Carbon*, **45** [10] 2037-46 (2007).

31. B. W. Smith, Z. Benes, D. E. Luzzi, J. E. Fishcer, D. A. Walters, M. J. Casavant, J. Schimdt, and R. E. Smalley, "Structural Anisotropy of Magnetically Aligned Single Wall Carbon Nanotube Films," *Appl. Phys. Lett.*, **77** [5] 663-5 (2000).

32. C. Park, J. Wilkinson, S. Banda, Z. Ounaies, K. E. Wise, G. Sauti, P. T. Lillehel, and J. S. Harrison, "Aligned Single-Wall Carbon Nanotube Polymer Composite Films Using an Electric Field," *J. Polym. Sci., Part B: Polym. Phys*., **44** [12] 1751-62 (2006).

33. A. L. Yarin, S. Koombhongse, and D. H. Reneker, "Bending Instability in Electrospining of Nanofibers," *J. Appl. Phys.*, **89** [5] 3018-26 (2001).

34. Y. M. Shin, M. M. Hohman, M. P. Brenner, and G. C. Rutledge, "Electrospinning: A Whipping Fluid Jet Generates Submicron Polymer Fibers," *Appl. Phys. Lett.*, **78** [8] 1149-51 (2001).

35. Y. M. Shin, M. M. Hohman, M. P. Brenner, and G. C. Rutledge, "Experimental Characterization of Electrospinning: The Electrically Forced Jet and Instabilites," *Polymer*, **42** [25] 9955-67 (2001).

36. S. Mazinani, A. Ajji, and C. Dubois, "Morphology, Structure and Properties of Conductive PS/CNT Nanocompsite Electrospun Mat," *Polymer*, **50** [14] 3329-42 (2009).

37. S. D. McCullen, D. R. Stevens, W. A. Roberts, S. S. Ojha, L. I. Clarke, and R. E. Gorga, "Morphological, Electrical and Mechanical Characterization of Electrospun Nanofiber Mats Containing Multiwalled Carbon Nanotubes," *Macromolecules*, **40** [4] 997-1003 (2007).

38. J. S. Jeong, J. S. Moon, J. H. Park, P. S. Alegaonkar, and J. B. Yoo, "Mechanical Properties of Electrospun PVA/MWNTs Compsoite Nanofibers," *Thin Solid Films*, **515** [12] 5136-41 (2007).

39. G. Wang, Z. Tan, X. Liu, S. Chawda, J-S. Koo, V. Samuilov, and M. Dudley, "Conducting MWNT/Poly(vinyl acetate) Composite Nanofibers by Electrospinning," *Nanotechnology*, **17** [23] 5829-35 (2006).

40. B. Sundaray, V. Subhramanian, T. S. Natarajan, and K. Krishnamurthy, "Electrical Conductivity of a Single Electrospun Fiber of Poly(methyl methacrylate) and Multiwalled Carbon Nanotube Composites," *Appl. Phys. Lett*., **88** [14] 143114-1 – 143114-3 (2006).

41. H. Hou, J. J. Ge, J. Zeng, Q. Li, D. H. Reneker, A. Greiner, and S. Z. D. Cheng, "Electrospun Polyacrylonitrile Nanofibers Containing a High Concentration of Well-Aligned MultiWall Carbon Nanotubes," *Chem. Mater.*, **17** [5] 967-73 (2005).

42. G. Mathew, J. P. Hong, J. M. Rhee, H. S. Lee, and C. Nah, "Preparation and Characterization of Properties of Electrospun Poly(butylene terepthalate) Nanofibers Filled with Carbon Nanotubes," *Polymer Testing*, **24** [6] 712-7 (2005).

43. W. Zhou, Y. Wu, F. Wei, G. Luo, and W. Qian, "Elastic Deformation of Multiwalled Carbon Nanotubes in Electrospun MWCNTs-PEO and MWCNTs-PVA Nanofibers," *Polymer*, **46** [26] 12689-95 (2005).

44. J. H. Sung, H. S. Kim, H-J. Jin, H. J. Choi, and I-J. Chin, "Nanofibrous Membranes Prepared by Multiwalled Carbon Nanotube/Poly(methyl methacrylate) Composites," *Macromolecules*, **37** [26] 9899-902 (2004).

45. W. Salaha, Y. Dror, R. L. Khalfin, Y. Cohen, A. L. Yarin, and E. Zussman, "Single-Walled Carbon Nanotubes Embedded in Oriented Polymeric Nanofibers by Electrospinning," *Langmuir*, **20** [22] 9852-55 (2004).

46. Y. Dror, W. Salalha, R. L. Khalfin, Y. Cohen, A. L. Yarin, and E. Zussman, "Carbon Nanotubes Embedded in Oriented Polymer Nanofibers by Electrospinning," *Langmuir*, **19** [17] 7012-20 (2003).

47. R. S. Lowe, S. M. Khersonsky, and R. D. Mccullough, "A Simple Method to Prepare Head-to-Tail Coupled, Regioregular Poly(3-alkylthiophenes) Using Grignard Metathesis," *Adv. Mater.*, **11** [3] 250-253 (1999).

48. Jeffries-EL, M.; Sauvé, G., and McCullough, R. D. "In-Situ End-Group Functionalization of Regioregular Poly (3-alkylthiophene) Using the Grignard Metathesis Polymerization Method," *Adv. Mater.*, **16** [12] 1017-1019 (2004).

49. T. A. Pham, D. P. Kim, T. W. Lim, S. H. Park, D. Y. Yang, and K. S. Lee, "Three – dimensional SiCN Microstructures via Nano-Stereolithography of Inorganic Polymer Photoresists," *Adv. Func. Mater.*, **16** [9] 91235-41 (2006).

50. J. Wan, A. Alizadeh, S. T. Taylor, P. R. L. Malenfant, M. Manoharan, and S. M. Loureiro, "Nanostructured Non-Oxide Ceramics Templated via Block Copolymer Self-Assembly," *Chem. Mater.*, **17** [23] 5613-7 (2005).

51. P. Gupta, C. Elkins, T. E. Long, and G. L. Wilkes, "Electrospinning of Linear Homopolymers of Poly(methyl methacrylate): Exploring Relationships Between Fiber Formation, Viscosity, Molecular Weight and Concentration in a Good Solvent," *Polymer*, **46** [13] 4799-810 (2005).

52. G. Winter, W. Verbeek, and M. Mansmann, "Production of Shaped Articles of Silicon Carbide and Silicon Nitride," U.S. Patent No. 3892583, 1975.

53. E. R. Kenway, J. M. Layman, J. R. Watkins, G. L. Bowlin, J. A. Matthews, D. G. Simpson, "Electrospinning of Poly(ethylene-co-vinyl alcohol) Fibers," *Biomaterials*, **24** [6] 907-13 (2003).

54. S. L. Shenoy, W. D. Bates, H. L. Frisch, and G. E. Wnek, "Role of Chain Entanglements on Fiber Formation During Electrospinning of Polymer Solutions: Good Solvent, Non-specific Polymer-Polymer Interaction Limit," *Polymer*, **46** [10] 3372-84 (2005).

55. B. Francois, O. Pitois, and J. Francois, "Polymer Films with a Self-organized Honeycomb Morphology," *Adv. Mater.*, **7** [12] 1041-4 (1995).

56. Y-L, Li, E. Kroke, R. Riedel, C. Fasel, C. Gervais, and F. Babonneau, "Thermal Cross-Linking and Pyrolytic Conversion of Poly(ureamethylvinyl)silazanes to Silicon-Based Ceramics," *Appl. Organomet. Chem.*, **15** [10] 820-32 (2001).

57. M. T. Hunley, P. Pötschke, and T. E. Long, "Melt Dispersion and Electrospinning of Non-Functionalized Multiwalled Carbon Nanotubes in Thermoplastic Polyurethanes" *Macromol. Rapid Commun.*, **30** [24] 2102- 6 (2009).

58. L. Rosenhead, *Laminar Boundary Layers*: Clarendon Press: Oxford, 1963, 144-50.

59. C. Stephan, T. P. Nguyen, M. Chapelle, S. Lefrant, C. Journet, and P. Bernier, "Characterization of Singlewalled Carbon Nanotubes-PPMA Composites," *Synth. Met.*, **108** [2] 139-49 (2000).

60. F. Du, J. E. Fischer, and K. I. Winey, "Effect of Nanotube Alignment on Percolation Conductivity in Carbon Nanotube/Polymer Composites," *Phys. Rev. B: Condens. Matter Mater. Phys.* **72** [12] 121404-1 - 121404-4 (2005).

CHAPTER 4 STRUCTURAL EVOLUTION OF POLYMER-DERIVED AMORPHOUS SILICONBOROCARBONITIRDE CERAMICS AT HIGH TEMPERATURE

4.1 Abstract

Polymer-derived amorphous siliconborocarbonitride (SiBCN) ceramics with Si/B-ratios 2/1 ($Si_{2.0}B_{1.0}$) and 4/1 ($Si_{4.0}B_{1.0}$) are synthesized by simple dehydrocoupling and hydroboration reaction of an oligosilazane, containing amine and vinyl groups, with $BH_3 \bullet Me_2S$ followed by pyrolysis. The structural evolution of these ceramics with pyrolysis temperature and boron doping level by spectroscopic techniques, such as Solid-state NMR, Raman and EPR spectroscopy was primarily investigated. Solid-state NMR suggested the presence of three major components: (i) hexagonal boron nitride (*h*-BN), (ii) turbostratic boron nitride (*t*-BN), and (iii) BN_2C groups. Increasing pyrolysis temperature shows the appearance of boron nitride (BN_3) and "free" carbon with the disappearance of BN_2C groups. A well-defined thermodynamic model could well explain such transformation of BN_2C groups into BN_3 and "free" carbon. Raman spectroscopy measurements followed Solid-state NMR results. It is believed that the metastable BN_2C groups decomposes completely to generate the BN_3 groups and most importantly, the "free" carbon which initiates the crystallization of $Si_{4.0}B_{1.0}$ ceramics at 1500 $^{\circ}$C, whereas $Si_{2.0}B_{1.0}$ ceramics is stable upto 1600 $^{\circ}$C.

4.2 Introduction

Polymer-derived ceramics (PDCs), unlike conventional ceramics obtained by sintering method, are synthesized by direct thermal decomposition of polymer precursors.[1,2] Such unique direct

polymer to ceramic route makes PDCs suitable for the fabrication of unconventionally shaped ceramic components and devices.[3,4] Polymer-derived non-oxide amorphous siliconborocarbonitride (SiBCN) ceramics have demonstrated exceptional high-temperature stability,[5-9] oxidation resistance,[10] and creep resistance[11] at elevated temperatures with superior mechanical[12] and electrical properties,[13,14] granting them potential applications in coatings,[15,16] membranes,[17] microelectronics,[14,16] and high temperature stable ceramic fibers for composites.[18,19] Understanding the structural evolution of SiBCN ceramics at high temperature is essential to realize these applications. It is well known that polymer to ceramic conversion is accompanied by the formation of several amorphous intermediates. This phenomenon makes the conventional characterization techniques such as X-ray diffraction (XRD), transmission electron microscopy (TEM) unsuitable to determine the structural evolution of SiBCN ceramics. Techniques such as solid-state NMR spectroscopy, electron paramagnetic resonance (EPR) spectroscopy are vital tools in analyzing the structural transformation from polymer precursor to amorphous SiBCN ceramics.[20,21] Solid-state NMR probes the molecular environment around selected nuclei (up to few angstroms), whose magnetic properties are determined by the local electronic environment and its interaction with the surrounding neighbor nuclei. Reported studies suggested that the continuous transformation from pre-ceramic polymer to amorphous ceramic takes place above 600 $^{\circ}$C. At 1400 $^{\circ}$C the amorphous ceramic contains three major structural components: (i) amorphous (graphite-like) carbon clusters in nanoscale, also called "free" carbon, (ii) boron nitride (BN) domains in the form of hexagonal boron nitride; and (iii) a Si-C-N matrix (SiC_xN_{4-x} units with x=0, 1, 2 or 4). [20,21] Further annealing of the as-thermolyzed SiBCN

PDCs at higher temperatures leads to the formation of silicon carbide (SiC) nanocrystallites within the amorphous microstructure as the primary crystalline phase.[22,23] Studies have also revealed that boron atoms are embedded in turbostratic B-C-N layers at the grain boundaries in amorphous SiBCN ceramics, resulting in the decrease in the grain boundary mobilities and suppressing crystallization.[24] The turbostratic stacked B-C-N layers is supposed to act as an encapsulation that retards the decomposition of silicon nitride (Si_3N_4) to form SiC nanocrystallites, firstly because the activity of carbon in these integrated B-C-N layers is reduced compared to "free" carbon, and secondly, the nitrogen gas formed by the decomposition reaction of Si_3N_4 cannot escape and leads to the internal pressure stabilization.[10] However, whether the amorphous carbon and BN remain as separate domains or a B-C-N phase homogeneously distributed in the ceramic matrix still remains an open question. Recent results demonstrated that the development of covalent B-N bonds form a rigid SiBCN network that causes the depression in crystallization at higher temperatures, and the increased boron content decelerates the crystallization of SiBCN ceramics.[25] Recently a number theoretical models were proposed to explain the crystallization behavior of SiBCN ceramics and the impact of addition of boron on the crystallization behavior. Although the thermodynamic models which include Gibbs free energies of the amorphous SiCN domains and the completely crystallized state cannot completely enunciate the crystallization of SiBCN ceramics, it proves that the addition of boron increases the driving energy required for the crystallization process.[26,27] These models of metastable phase equilibria including the Gibbs energies of the amorphous SiCN phase and the nanocrystalline phases,[28] can satisfactorily describe the crystallization behavior in accordance

with the experimental results obtained with polymer-derived SiBCN ceramics.[29] However these models describe the promoting role of boron on the formation of nanocrystalline SiC, whereas fewer attempts have been made to model the evolution of boron nitride (BN) and possible "free" carbon formation during the amorphous to crystalline transformation of SiBCN ceramics. "Free" carbon formed during the pyrolysis of PDCs contributes as an important structural feature that has significant influence on the thermal stability of PDCs.[30,31] Nevertheless, previous extensive investigations on the structures of SiBCN ceramics has not shed much light into the amorphous intermediates of these ceramics due to the limited information of the amorphous microstructures.

In this chapter, the structural evolution study of SiBCN ceramics upon the pyrolysis at different temperatures using ceramic precursors with different Si/B ratios is reported. Two ceramic precursors with Si/B ratios of 4/1 and 2/1 were synthesized according to the previously reported synthetic procedure.[32] SiBCN ceramics were obtained through the pyrolysis of these precursors and their structures were examined using various approaches. Solid-state NMR was employed as an important tool for the in-depth analysis of the structural changes of SiBCN ceramics when pyrolyzed and to model the structural evolution of boron nitride during the amorphous to crystalline transformation. Raman spectroscopy was utilized to measure the "free" carbon semi-quantitatively and showed the dependence of "free" carbon concentration on the doping level of boron. The structural evolution was completed by EPR studies on the specimens after heat treatment at different elevated temperatures. Such systematic investigation provides a new perspective on the amorphous microstructures of SiBCN ceramics.

4.3 Experimental

4.3.1 Synthesis of SiBCN preceramic polymer precursors

In a typical procedure, 3.0 g Ceraset™ VL20 (42 mmol, purchased from Kion Corporation, Charlotte, NC) was dissolved in 20 mL toluene (purchased from Alfa Aesar, USA) in a 100 mL two-necked round bottomed flask equipped with rubber septa, a magnetic stirrer and a reflux condenser. The flask was then purged with N_2 gas for 20 min. Then stoichiometric amount of borane dimethyl sulfide (BH_3•Me_2S, BH_3 concentration 10.2*M*, purchased from Aldrich, USA; 1.0 mL (10.2 mmol) and 2.0 mL (20.4 mmol) for Si/B ratios of 4/1 and 2/1 respectively) was added dropwise at room temperature. The stirring was continued for 3 h. The solution was then slowly heated to reflux and heated at reflux for 3 h. Then the solvent and Me_2S was removed under vacuum. A white odorless solid was obtained and dried for overnight under vacuum.

4.3.2 Pyrolysis

The ceramic samples were prepared by the pyrolysis of the obtained polymer powders in a quartz tube under a steady flow of argon (Ar) in a tube furnace. The following heating cycle was used: (i) an initial 3 $^{\circ}$C/min ramp upto 900 $^{\circ}$C, (ii) 1 $^{\circ}$C/min ramp to the desired pyrolysis temperature, (iii) a 4 h dwell time at the desired pyrolysis temperature, and (iv) sample cooling rate at 5 $^{\circ}$C/min, during the time the sample was cooled to room temperature.

4.3.3 Characterization

Solid polyborosilazane precursors were characterized by PerkinElmer Fourier transform infrared (FTIR) spectrometer (PerkinElmer Inc., Waltham, MA). The thermogravimetric analysis (TGA) was performed on a Q5000 Thermogravimetric Analyzer (Texas Instruments, Dallas, TX), at a heating rate of 3 $^{\circ}$C/min to 1000 $^{\circ}$C in an inert atmosphere of N_2. The crystallization behavior was characterized by X-ray diffraction (XRD) analysis (XRD Rigaku, Tokyo, Japan) using a monochromatic Cu-K_α radiation with a wavelength of $\lambda/2$ = 154.06 pm. The solid-state NMR experiments were carried out on Bruker Avance 600 spectrometer at a static magnetic field of 14.1 T (^{1}H frequency: 600 MHz) using 4 mm magic angle spinning (MAS) probe. ^{11}B NMR experiments were performed at 192.6 MHz. ^{11}B NMR spinecho were recorded at 96.2 kHz at a pulse length of 1.30 and 2.60 μs with a recycle delay of 15 s and a sample rotation frequency of 12.5 kHz. The spectra were calibrated relative to an aqueous solution of H_3BO_3 (δ = 19.6 ppm) as an external standard and are given relative to BF_3•OEt_2 (δ = 0 ppm). High-field, high-frequency EPR spectra were recorded at room temperatures on a home-built spectrometer at the EMR facility of National High Magnetic Field Laboratory (NHMFL), Tallahassee, Florida. The instrument is a transmission-type device in which microwaves are propagated in cylindrical lightpipes. The microwaves are generated by a phase-locked Virginia Diodes source generating frequency of 13 ± 1 GHz and producing its harmonics of which the 2nd, 4th, 6th, 8th, 16th, 24th and 32nd are available. A superconducting magnet (Oxford Instruments) capable of reaching a field of 17 T was employed. In order to characterize the samples for Raman spectroscopic measurements, the ceramic materials were ground into fine powders using high energy ball

milling (8000M-115, Spex Certiprep Group, Metuchen, NJ) for 30 minutes. The obtained powders were then pressed into disks of 12.5 mm in diameter and 3 mm in thickness. The Raman spectra are obtained for the disks using Renishaw inVia Raman microscopy (Renishaw Inc., Gloucestershire, UK). The excitation source used is the 532 nm line of a silicon-solid laser, and the size of the focused laser beam is about 10 μm.

4.4 Results and Discussion

The preceramic polymers used in this study were synthesized from a readily available commercial cyclosilazane precursor, Ceraset™ VL20 (Si: C: N=1:1.4:1), to produce SiBCN ceramics upon pyrolysis. Previous studies demonstrated that the reaction of cyclic oligosilazane, $(CH_3SiHNH)_n$, with $BH_3 \bullet Me_2S$ results in the evolution of hydrogen on amine groups, called dehydrocoupling reaction, and the formation of the crosslinked products that contain borazine rings with boron atoms attaching to three nitrogen atoms.[32] These polymer precursors produced SiBCN ceramics through a pyrolysis under an inert atmosphere. Similar strategy was utilized in our studies to synthesize the SiBCN preceramic polymers. Borane is expected to react with the vinyl groups (hydroboration reaction) and the amine groups (dehydrocoupling reaction) of Ceraset™ VL20, generating colorless, glass-like powders after a complete removal of the solvent. The preceramic SiBCN polymers were then characterized by Fourier-transform infrared (FTIR) spectroscopy (Figure 4.1). In Ceraset™ VL20, the bands related to Si-NH-Si include N-H stretching at 3370 cm^{-1} and deformation vibration at 1171 cm^{-1}. A stretching vibration for Si-N stretching vibration appears at 859 cm^{-1}. The bands ascribed to vinyl groups ($Si-CH=CH_2$) are C=C stretching vibration at 1582 cm^{-1} and C-H stretching vibrations at 3034 cm^{-1}. A strong

absorption band assigned to Si-H vibration appears at 2104 cm^{-1}. Characteristics band of Si-CH_3 groups locates at 1250 cm^{-1}, coupled with C-H stretching and methyl (CH_3) group deformation vibrations at 2950 cm^{-1} and 1398 cm^{-1}, respectively. The FTIR spectra of the SiBCN polymer precursors indicate the formation and disruption of various covalent bonds. The spectra indicate that N-H stretching (3370 cm^{-1}) and deformation vibration (1171 cm^{-1}) decrease with a consequent increase of a broad absorption band in the range of 1330-1450 cm^{-1} (assigned to B-N vibration) overlapping with CH_3 deformation vibration.

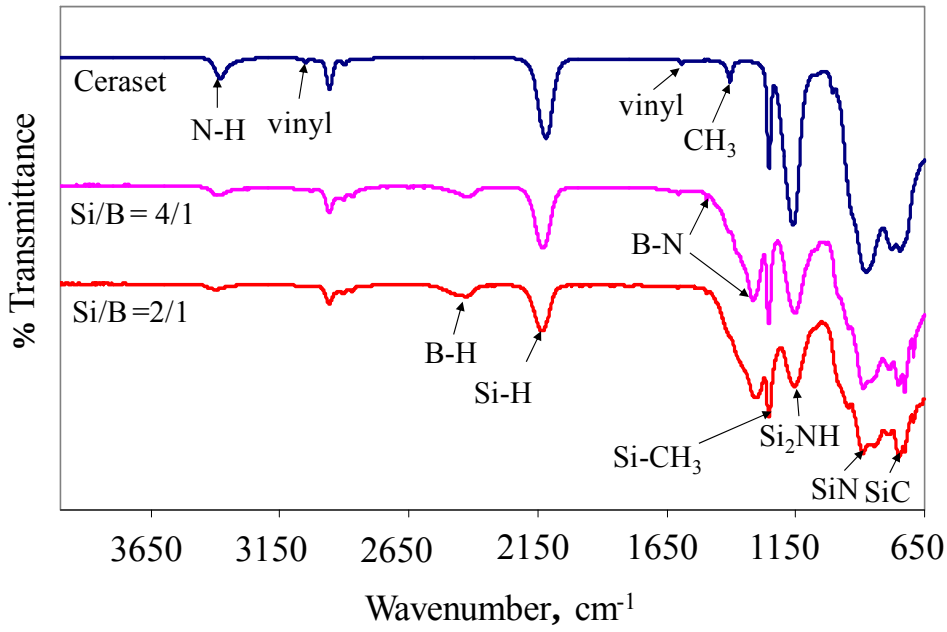

Figure 4.1 FTIR spectra of Ceraset™ VL20 and SiBCN preceramic polymers (Si/B-ratios of 4/1 and 2/1).

This observation is in accordance with the dehydrocoupling reaction between amine (N-H) groups of ceraset and B-H functional groups of borane. The absorption band at 1582 cm^{-1} assigned to vinyl group decreases, suggesting that the hydroboration reaction between B-H and

$CH{=}CH_2$ proceeds simultaneously with the dehydrocoupling reaction. The absorption band at 2415 cm^{-1} clearly confirms the presence of the B-H vibrations. These B-H groups can act as active functional sites for further crosslinking reactions.[17]

The conversion of preceramic polymer precursors into ceramics was investigated by thermogravimetric analysis (TGA) (Figure 4.2). Crosslinked Ceraset™ VL20 shows four distinct stages of mass losses: i) 0.9 % between 25-300 °C, ii) 5.4 % between 300-500 °C iii) 10 % between 500-800 °C and iv) 1.3 % between 800-1000 °C. The final ceramic yield is about 82.4 %. Earlier results suggest[33] that these losses are due to the evolution of methane (CH_4) and hydrogen (H_2) along with the evolution of low-molecular weight oligomers. SiBCN preceramic polymers show thermal behavior similar to ceraset. For example, $Si_{2.0}B_{1.0}$ ceramic precursor shows an initial mass loss of about 2 % due to the evolution of solvent and the oligomers. The subsequent 3 % mass loss from 300-500 °C was probably due to the release of C_2 and C_4 units similar to the report by Hauser and coworkers.[17] The major mass loss took place in the temperature range from 500-800 °C by releasing CH_4 and H_2 as the decomposition products. The final 1 % mass loss was due to the evolution of H_2, giving a high ceramic yield of 87 %. Expectedly, $Si_{2.0}B_{1.0}$ preceramic polymer precursor gives a higher ceramic yield than $Si_{4.0}B_{1.0}$ preceramic polymer precursor (85 %).

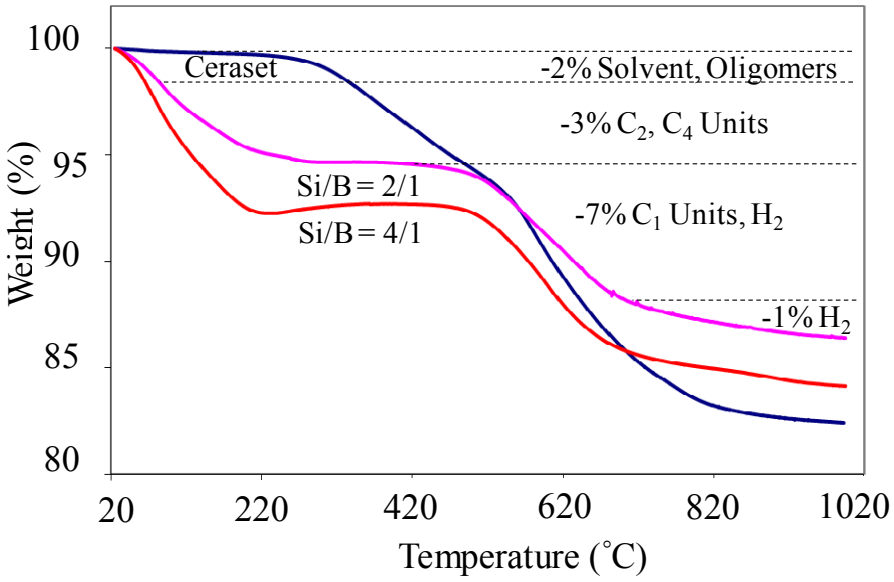

Figure 4.2 Thermogravimetric analysis (TGA) of Ceraset™ VL20 and SiBCN preceramic polymers (Si/B- ratios of 4/1 and 2/1).

In order to investigate the crystallization behavior of the SiBCN ceramics, polymer precursors were pyrolyzed under Ar and were characterized by X-ray Diffraction (XRD) (Figure 4.3). Since SiBCN ceramics are known to be amorphous and stable at higher temperatures compared to SiCN based ceramics, as-synthesized SiBCN preceramic polymers were pyrolyzed at 1500 ˚C. Phase identification is accomplished by locating the characteristics diffraction peaks present in the XRD spectra. XRD spectra indicate that $Si_{4.0}B_{1.0}$ ceramics become crystalline at 1500 ˚C (Figure 4.3a). Sharp peaks of β –SiC were observed at 2θ = 35˚, 60˚ and 72˚ corresponding to the reflections from (111), (220) and (311) β –SiC.[34] However, no graphitic carbon (C) phase were detected by XRD, although the presence of carbon cannot be completely eliminated. On the other hand, $Si_{2.0}B_{1.0}$ ceramics remains amorphous upto 1600 ˚C, with no noticeable crystalline features

(Figure 4.3b). When pyrolyzed at 1650 °C, $Si_{2.0}B_{1.0}$ ceramics indicates the development of β – SiC crystallites, similar to $Si_{4.0}B_{1.0}$ ceramics.

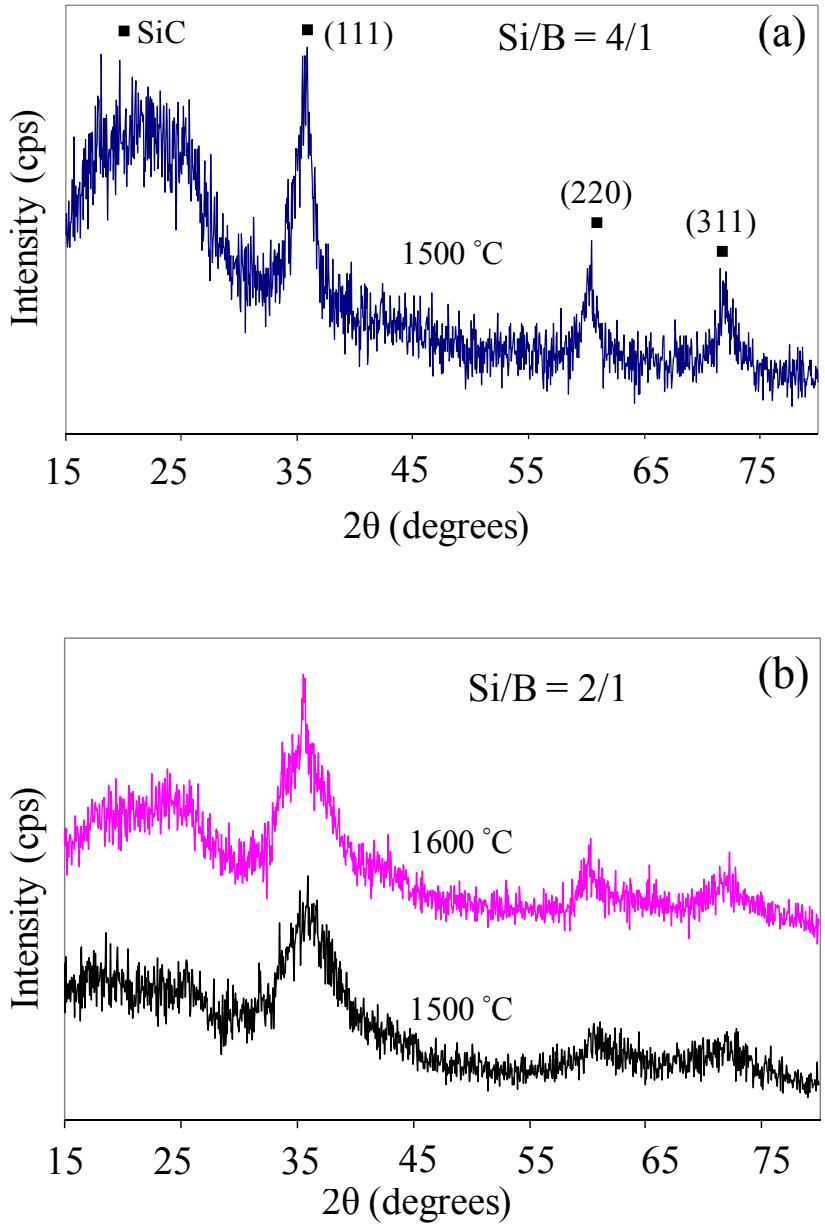

Figure 4.3 X-ray diffraction (XRD) of (a) $Si_{4.0}B_{1.0}$ ceramics pyrolyzed at 1500 °C, and (b) $Si_{2.0}B_{1.0}$ ceramics pyrolyzed at 1500 °C and 1600 °C.

Solid-state NMR spectroscopy is a powerful characterization technique to study the atomic scale structure and the dynamics of solids. It provides the information about the local structure around nuclei in both crystalline and amorphous materials. As mentioned before, the pyrolysis of polymer-derived ceramics contains different amorphous intermediates. Therefore, the structural changes of the SiBCN ceramics pyrolyzed in the temperature ranging from 1000 $^{\circ}$C to 1600 $^{\circ}$C were examined by solid-state NMR spectroscopy to reveal the structural evolution. In my investigation, ^{11}B was chosen as the nucleus of interest because the coordination around boron provides important information about chemical reactions during the pyrolysis. Figure 4.4 shows the ^{11}B NMR spectra of the $Si_{2.0}B_{1.0}$ ceramics obtained at different pyrolysis temperatures. The spectra of the $Si_{2.0}B_{1.0}$ ceramic samples except the sample pyrolyzed at 1600 $^{\circ}$C can be fitted with three lorentzian peaks at δ = 19.6, 24.2 and 30.4 ppm. The peaks at 19.6 and 24.2 ppm fit well with the reported chemical shifts of two BN_3 forms, turbostratic boron nitride (*t*-BN) and hexagonal boron nitride (*h*-BN), respectively.[35] BN_3 groups were generated from the groups obtained through the dehydrocoupling reaction in preceramic polymers during the pyrolysis. The peak at 30.4 ppm can be attributed to the BN_2C groups resulted from the pyrolysis of the groups obtained through both dehydrocoupling reaction and hydroboration reaction in preceramic polymers. The ^{11}B NMR spectra of the $Si_{2.0}B_{1.0}$ ceramics obtained at different pyrolysis temperatures also indicate the structural evolution from BN_2C to BN_3.

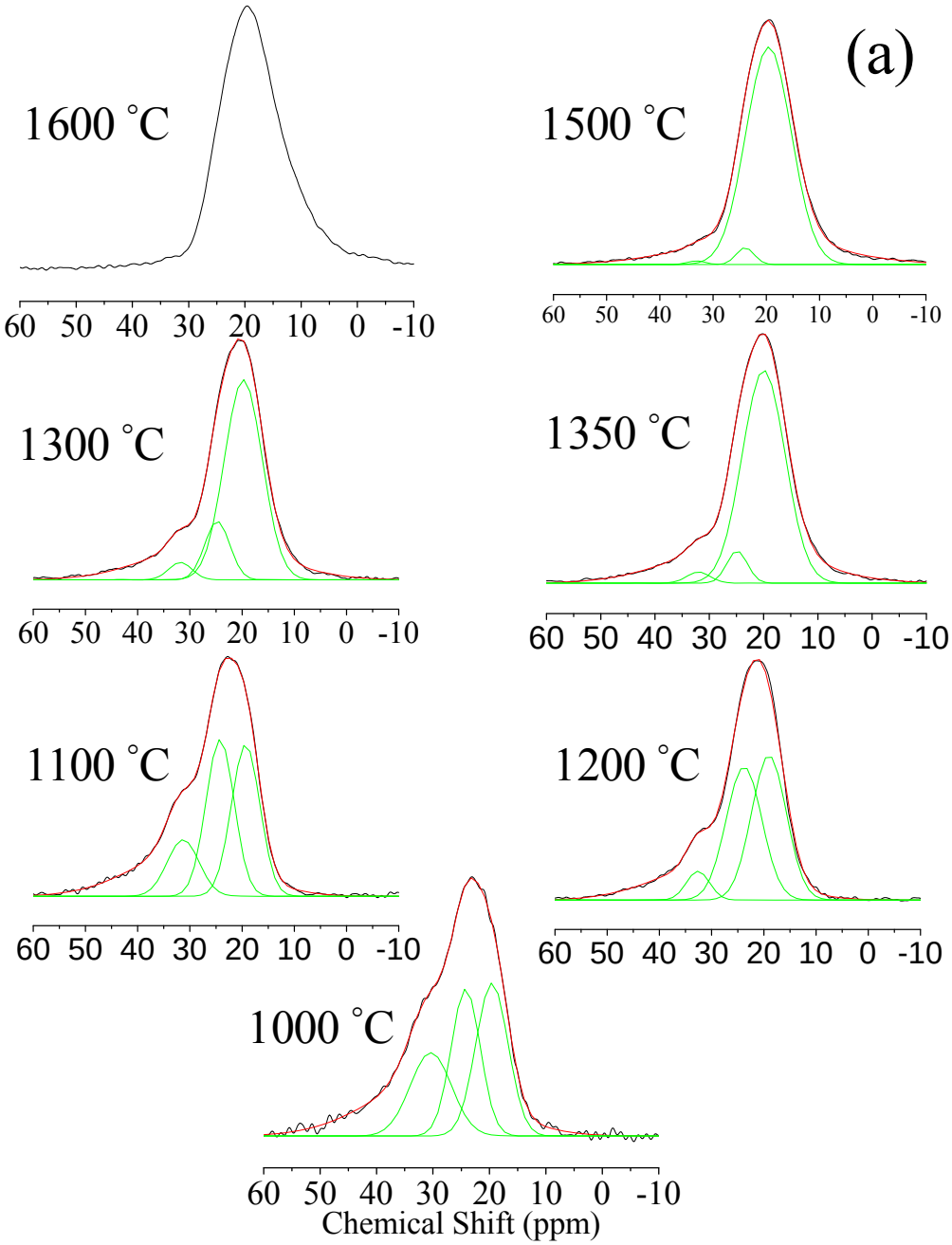
(a)
1600 ˚C
1500 ˚C
1300 ˚C
1350 ˚C
1100 ˚C
1200 ˚C
1000 ˚C
60 50 40 30 20 10 0 -10
Chemical Shift (ppm)

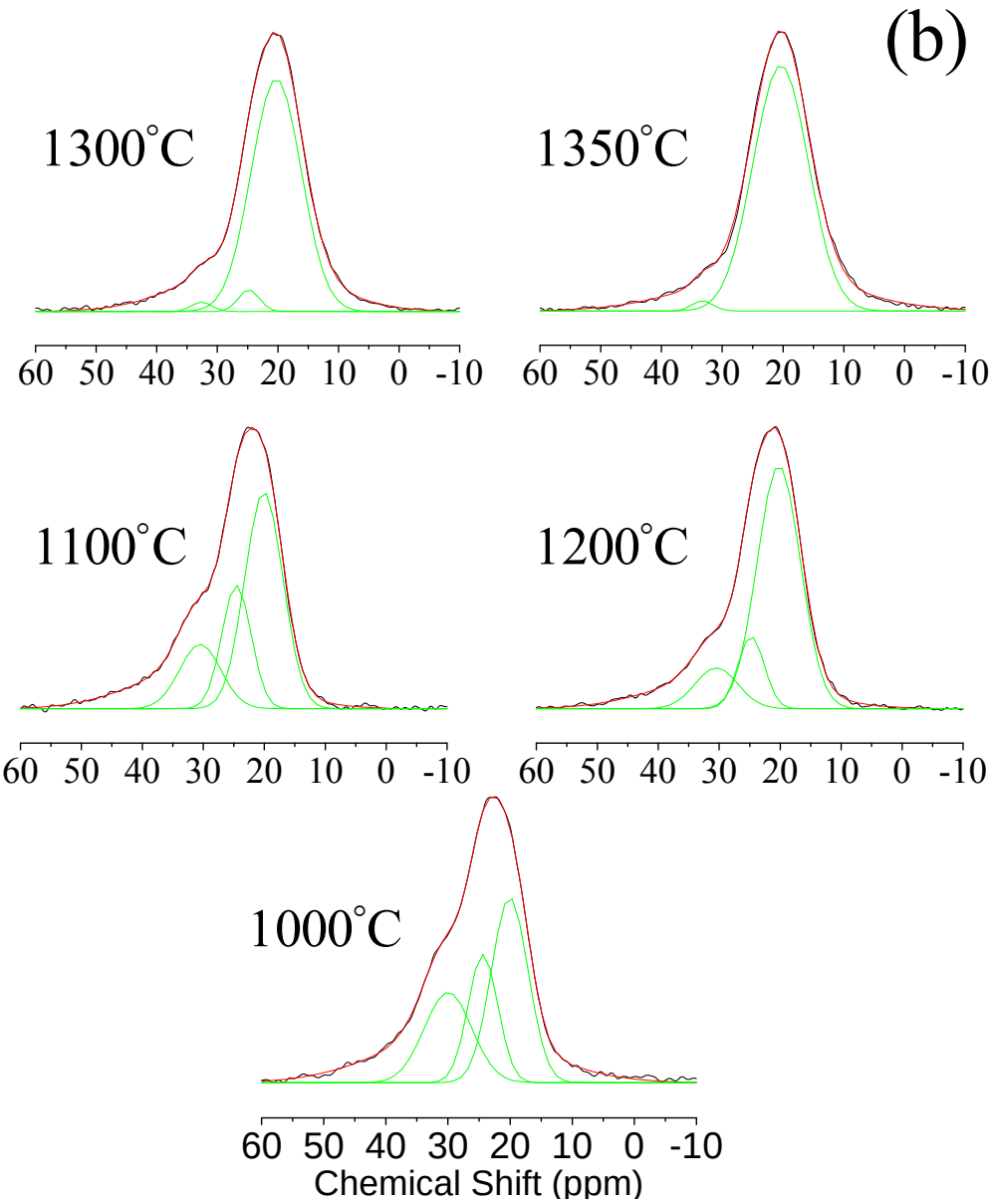

Figure 4.4 ^{11}B magic angle spinning (MAS) NMR spectra recorded for (a) $Si_{2.0}B_{1.0}$ ceramics pyrolyzed in the temperature ranging from 1000 ˚C to 1600 ˚C, and (b) $Si_{4.0}B_{1.0}$ ceramics pyrolyzed in the temperature ranging from 1000 ˚C to 1350 ˚C.

As shown in Figure 4.4, the peak area ratio between BN_3 and BN_2C increases with increased pyrolysis temperature, suggesting that B-C bonds in BN_2C groups are not stable at higher temperatures and decompose into B-N and "free" carbon until all BN_2C groups are converted to BN_3 groups and "free" carbon as shown by the NMR spectrum of SiBCN ceramic obtained at 1600 $^{\circ}$C. Similar results were obtained for $Si_{4.0}B_{1.0}$ ceramic samples except that BN_2C disappears at a lower temperature of 1500 $^{\circ}$C (Figure 4.4b). Such observation possibly is due to a lower concentration of BN_2C groups at a lower boron doping level. It is also observed that the peak area ratio of *t*-BN to *h*-BN increases with increased pyrolysis temperature. However, the reason is still not yet clear. The conversion of BN_2C to BN_3 demonstrated in ^{11}B MAS NMR spectra leads to propose the possible reaction forming BN_3, SiC, and "free" carbon (C).

$$BN_2C + SiCN \rightarrow BN_3 + SiC + C\text{……..} \qquad \textit{Equation 4.1}$$

The equilibrium constant, K, for this reaction can be expressed as

$$K = [BN_3]*[SiC]*[C] / [BN_2C]*[SiCN]\text{……..} \qquad \textit{Equation 4.2}$$

where $[BN_3]$, [SiC], [C], $[BN_2C]$ and [SiCN] are the respective concentrations. Based on an assumption that [SiCN] is equal to unity and $[BN_3]$ = [SiC] = [C], Equation 4.2 can be rearranged as

$$K = [BN_3]^3 / [BN_2C]\text{……..} \qquad \textit{Equation 4.3}$$

From van't Hoff equation on the temperature dependence of the equilibrium constant

$$\ln K = -\Delta G^0 /RT = -\Delta H^0/RT + \Delta S^0/R\text{……} \qquad \textit{Equation 4.4}$$

where, ΔH^0 and ΔS^0 are the standard enthalpy and entropy of formation respectively, R is the universal gas constant and T is the reaction temperature in Kelvin.

Combining Equation 4.3 and Equation 4.4,

$$\ln ([BN_3]^3 / [BN_2C]) = -\Delta H^0/RT + \Delta S^0/R\ldots\ldots.. \qquad \textit{Equation 4.5}$$

Equation 4.5 suggests that the ln $[BN_3]^3$ / $[BN_2C]$ should exhibit a linear relationship with 1/T. From the slope and intercept of the straight line, ΔH^0 and ΔS^0 can be obtained as

$$\Delta H^0 = - \text{ slope } * R\ldots\ldots.. \qquad \textit{Equation 4.6}$$

$$\Delta S^0 = \text{intercept } * R\ldots\ldots.. \qquad \textit{Equation 4.7}$$

Figure 4.5a and 4.5b plot ln ($[BN_3]^3$ / $[BN_2C]$) with (1/T) for both $Si_{2.0}B_{1.0}$ and $Si_{4.0}B_{1.0}$ respectively. A well-defined linear plot with a negative slope is obtained from both the ceramics as predicted by Equation (4.5). Such well-defined linear relationship supports the proposed reaction pathway. The straight line with negative slope means that the reaction is endothermic. Endothermic reactions are favored by the increase in temperature and hence the conversion of BN_2C to BN_3 proceeds to completion with the increasing of the temperature. BN_3 contributes significantly to the high temperature stability of SiBCN ceramics as it act as a barrier inhibiting the diffusion of the "free" carbon to Si_3N_4 that cause the formation of crystalline SiC at higher temperatures.[36]

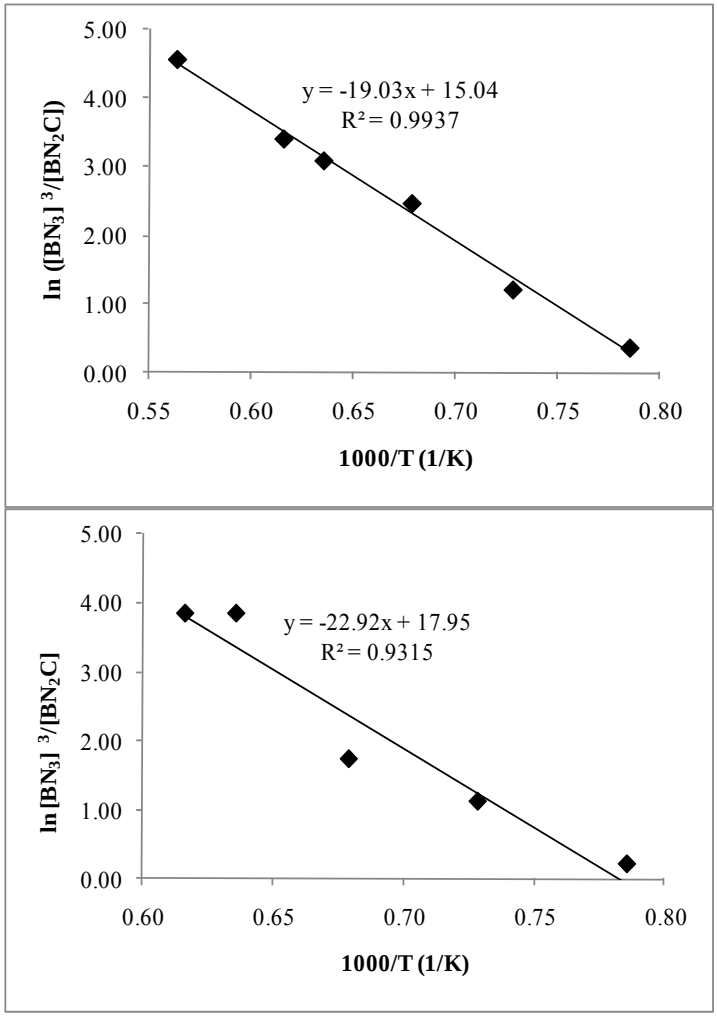

Figure 4.5 Plot of ln ($[BN_3]^3$/ $[BN_2C]$) versus (1000/T) for SiBCN ceramic samples with Si/B-ratios (a) 2/1, and (b) 4/1.

Slope and intercept of the straight lines were used to calculate ΔH^0 and ΔS^0 for both $Si_{2.0}B_{1.0}$ and $Si_{4.0}B_{1.0}$ ceramics. The values of ΔH^0 and ΔS^0 for $Si_{2.0}B_{1.0}$ ceramics were found to be 38.06 kcal/mol and 30.08 cal/mol, respectively. Similarly, the ΔH^0 and ΔS^0 values for $Si_{4.0}B_{1.0}$ ceramics were calculated to be 45.84 kcal/mol and 35.90 cal/mol, respectively. From thermodynamics, Gibbs free energy (ΔG^0) can be written as

$$\Delta G^0 = \Delta H^0 - T\Delta S^0 \ldots\ldots\ldots \quad \textit{Equation 4.8}$$

Substituting the values of ΔH^0 and ΔS^0 in Equation 4.8, the Gibbs free energy of two ceramics can be expressed as

$$\Delta G^0_{2/1} = 38060 - 30.08T \text{ and } \Delta G^0_{4/1} = 45840 - 35.90T \ldots\ldots \quad \textit{Equation 4.9}$$

When the pyrolysis temperature is above 1000 $^{\circ}$C, ΔG^0 values are negative, suggesting a spontaneous conversion of BN_2C to BN_3. In addition, $\Delta G^0_{4/1}$ is less than $\Delta G^0_{2/1}$, which suggests that the equilibrium constant ($K = [BN_3]^3 / [BN_2C]$) of such conversion reaction in $Si_{4.0}B_{1.0}$ ceramics is larger than that of $Si_{2.0}B_{1.0}$. The larger equilibrium constant suggests higher concentration of "free" carbon in ceramics. These free carbon subsequently reacts with silicon nitride (Si_3N_4) to form crystalline silicon carbide (SiC) and N_2 according to the following reaction.[10,36]

$$Si_3N_4 + 3C \rightarrow 3SiC + 2\ N_2\uparrow \ldots\ldots\ldots \quad \textit{Equation 4.10}$$

The reason why $Si_{2.0}B_{1.0}$ contains higher "free" carbon compared to $Si_{4.0}B_{1.0}$ ceramics is not yet clear; however, the proposed thermodynamic model could well explain the structural evolution of BN and a possible "free" carbon phase during the thermal annealing leading to crystallization. Furthermore, complete dissociation of BN_2C groups into BN_3 and C at lower temperatures in case of $Si_{4.0}B_{1.0}$ could well explain the early crystallization of these ceramics. Such temperature dependent "free" carbon concentration is believed to be one of the causes of higher thermal stability of the SiBCN ceramics with higher boron doping level. Therefore, it would be interesting to investigate the dependence of "free" carbon concentration on boron doping level.

Raman spectroscopy, a standard nondestructive and one of the most sensitive tools for the characterization of different forms of carbon,[37-39] was used to study the structural change of carbon in SiBCN ceramics including the dependence of "free" carbon concentration on boron doping level. Figure 4.6a and 4.6b shows the Raman spectra recorded from the $Si_{2.0}B_{1.0}$ and $Si_{4.0}B_{1.0}$ ceramic samples pyrolyzed at different temperatures, after the subtraction of the background. The Raman spectra of these two SiBCN ceramic samples have similar structural features. Two Raman bands were observed at around 1350 cm^{-1} and 1600 cm^{-1}, which are assigned to the D and G band, respectively. These two bands are the most striking features of disordered graphitic-like carbon. Also, the presence of these two peaks suggests the formation of significant fraction of carbon atoms bonded as ring-like configurations.[40] The G band has E_{2g} symmetry and is generated by the in-plane bond stretching of sp^2 hybridized carbon atoms.[41,42] This band is active at all sites and not necessarily limited to those arranged in six-fold symmetry. The D-band has A_{1g} symmetry and is assigned to the breathing mode of aromatic rings.[41,42] This band is forbidden in perfect graphitic structures and becomes actively only in presence of local disorder. Apparently, the overall relative intensity of the spectra (both Figure 4.6a and 4.6b) progressively decreased with increasing pyrolysis temperature.[43] Such observation suggests that the "free" carbon composition decreases with increasing thermolysis temperature which is opposite to our thermodynamic assumption that more free carbon will be generated at elevated temperature. It is possible that the generated "free" carbon dissolves into Si-C-N matrix as reported by Yive and coworkers[44] and is undetectable by Raman. The Raman spectra were fitted using two Gaussian curves to extract information about the relative intensities of the D and G

bands (I_D/I_G) and the total integrated intensities ($I_D + I_G$) of both of these two bands. Figure 4.6c and 4.6d plots the change of I_D/I_G and ($I_D + I_G$) with both pyrolysis temperature and Si/B ratio. The intensity ratio of these two bands, I_D/I_G, was found to decrease with an increase in the pyrolysis temperature from 1100 $^{\circ}$C to 1350 $^{\circ}$C. This result indicates that the bonding character of the carbon changes from sp^3 to sp^2 and ordered graphitic structures have formed. Interestingly, $Si_{2.0}B_{1.0}$ ceramics have smaller I_D/I_G value than $Si_{4.0}B_{1.0}$. In other words, increasing boron content enhances the formation of ordered graphite structures. The reason of such phenomenon is currently under investigation. In addition, we assume that the total integrated intensity, ($I_D + I_G$), could be used as a semi- quantitative measure of the amount of "free" carbon present in the materials provided that the sample scan size remains same. Figure 4.6d shows that ($I_D + I_G$) decreases with an increase in the pyrolysis temperature probably due to the dissolving of generated "free" carbon in Si-C-N matrix as discussed before. It is also evident that $Si_{2.0}B_{1.0}$ ceramics have smaller ($I_D + I_G$) value than $Si_{4.0}B_{1.0}$ ceramics at the same pyrolysis temperature, suggesting that increasing boron content reduces the formation of "free" carbon. Such observation is in good agreement with solid-state NMR studies.

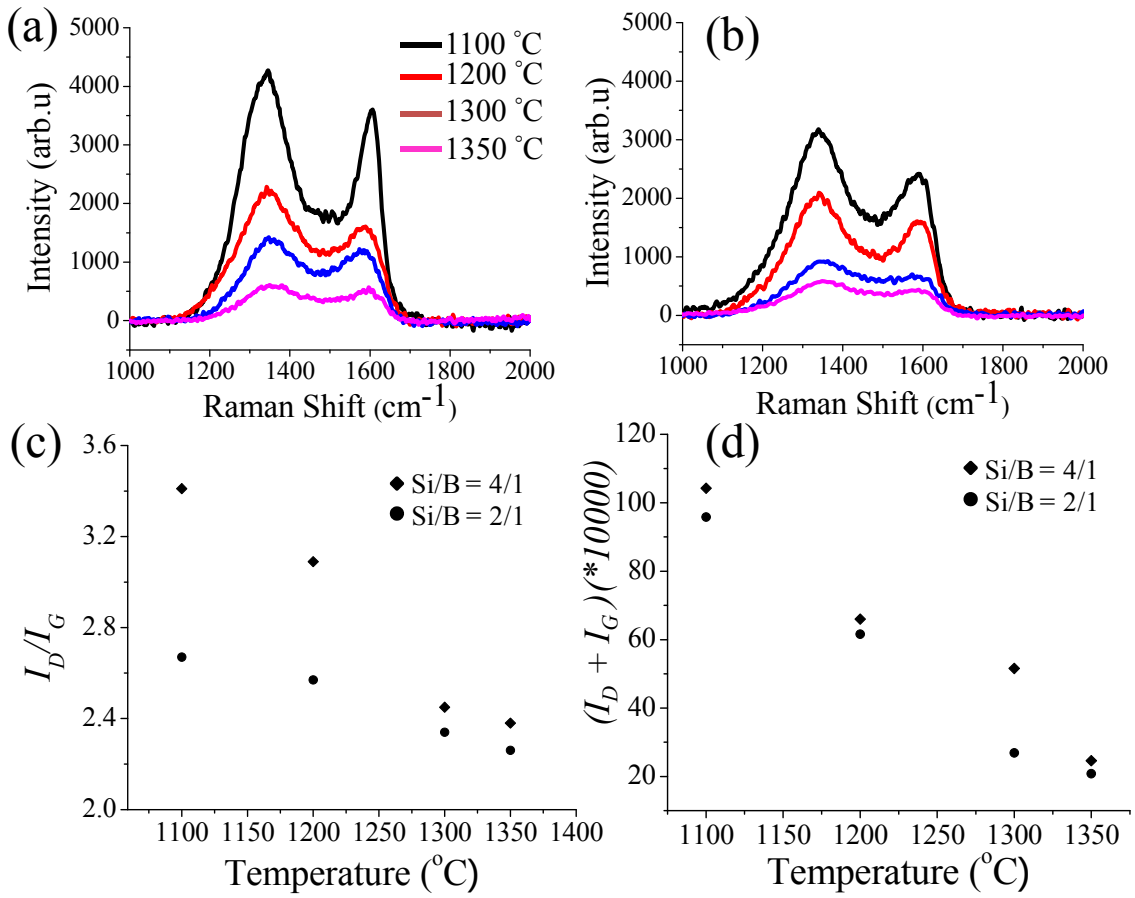

Figure 4.6 Raman Spectra of SiBCN ceramic samples pyrolyzed in the temperature range from 1100 ˚C to 1350 ˚C with Si/B-ratios of (a) 2/1, and (b) 4/1. Signal intensity decreases with increasing temperature and the intensity increases with the increase in Si/B-ratio from 2/1 to 4/1. (c) Intensity ratio of D and G band (I_D/I_G) of SiBCN ceramics pyrolyzed in the temperature range from 1100 ˚C to 1350 ˚C with Si/B-ratios 2/1 and 4/1. I_D/I_G decreases with increase in temperature. (d) Total integrated intensity (I_D+I_G) of the same samples. (I_D+I_G) increases with increase in Si/B-ratio from 2/1 to 4/1.

Free carbon formed in the bulk SiBCN ceramic matrices as nanoparticles with a size about 1 nm during the pyrolysis where CH_3 functional groups of the polymer chains are decomposed and the bonds are formed from unpaired electrons.[45] The appearance of the unpaired electrons should result in a pronounced EPR response, which allows EPR to be used as a useful nondestructive

tool to monitor the structural evolution of the SiBCN ceramics with pyrolysis. Figure 4.7a shows the room- temperature EPR spectra of $Si_{2.0}B_{1.0}$ ceramics pyrolyzed in the temperature ranging from 1000 °C to 1600 °C. The spectra show only one intense line, predominantly lorentzian in shape, regardless of the pyrolysis temperature with a *g*-value equal to 2.0032 ± 0.0001. This *g*-factor suggests that the observed EPR line is due to the carbon dangling bonds (unpaired electrons) presented in the defects in the bulk SiBCN ceramic matrices.[46] The difference of this *g*-value from other *g*-values (2.018, 2.02, and 2.012) that are corresponsive to ordered carbon networks such as planar graphite phase,[47] turbostratic carbon[21] and multiwalled carbon nanotubes[47] indicates that the synthesized SiBCN ceramics do not contain any ordered networks. In addition, the absence of hyperfine lines (boron or nitrogen dangling bonds) and hyperfine satellites (silicon dangling bonds) indicates that no dangling bonds are formed on boron, nitrogen or silicon. Figure 4.7c plots the change in linewidth, i.e., peak-to-peak width, with the pyrolysis temperature and indicates that the linewidth decreases initially upto 1350 °C and then increases with increasing temperature.[45] This phenomenon is probably caused by the unresolved proton hyperfine couplings resulting from the loss of hydrogen.[48] Similar EPR signal features were also observed with $Si_{4.0}B_{1.0}$ ceramic samples (Figure 4.7b and d).

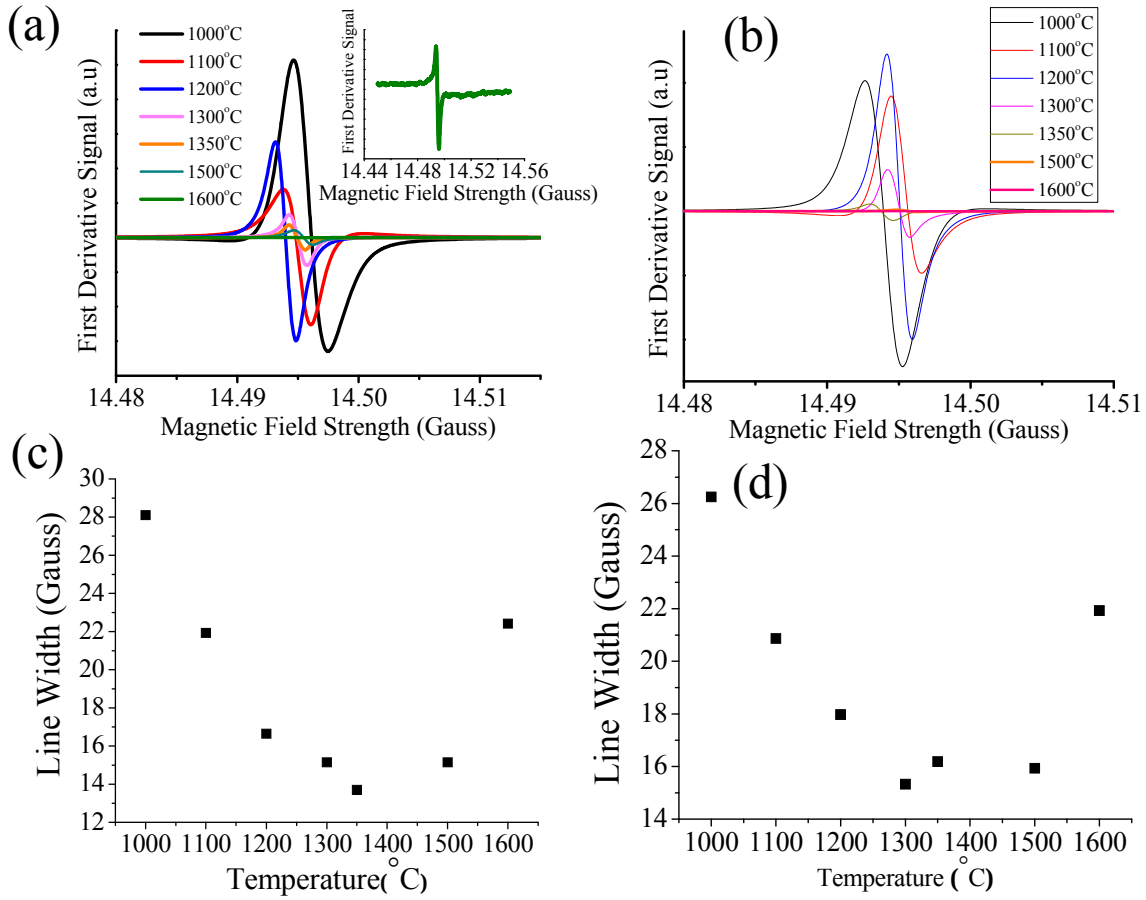

Figure 4.7 (a,b) Experimental EPR spectra of the SiBCN ceramics with Si/B-ratios 2/1 and 4/1 pyrolyzed in the temperature range from 1000 °C to 1600 °C, and (c,d) line width variation of the same samples with pyrolysis temperature.

Apart from the linewidth, integrated intensity is important information to relate the dangling bond concentration with the SiBCN ceramic structural evolution. Figure 4.8 shows the plot of integrated intensity per mg of the sample with the pyrolysis temperature and also with the Si/B-ratio. EPR integrated intensities were calculated from the EPR spectra as the product of (peak-to-peak width)^2 * (peak-to-peak height). In the absence of peak fitting and the spin concentration of the reference sample materials, these values of integrated intensities are only an approximate and

intended to illustrate the relative differences in the paramagnetic concentration of these SiBCN samples pyrolyzed at different temperatures. Figure 4.8 shows that the integrated intensities per mg of the samples decrease with increasing pyrolysis temperature.

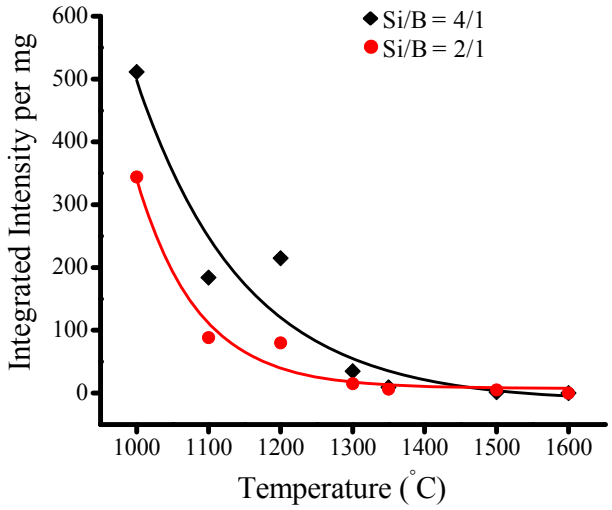

Figure 4.8 Plot of Integrated intensity per mg of ceramic samples with Si/B-ratios 2/1 and 4/1 with increasing pyrolysis temperature.

Such trend is possibly caused by two factors: the decrease in the concentration of carbon related species by the recombination of the paramagnetic centers or the consumption of the carbon paramagnetic centers by the electron deficient boron atom forming metastable B-C bond, which further dissociates to form B-N bond as discussed earlier. The latter factor seems to be more likely since Figure 4.8 shows that decreasing boron content (Si/B-ratio 4/1) increases the integrated intensity by several multiples of magnitude. It can also be observed that at pyrolysis temperatures greater than 1300 °C, the integrated spin intensity becomes independent of the Si/B ratio. This could possibly mean that all the boron atoms are involved in the bond formation

through either B-N and/or B-C at a certain temperature leading to the saturation of carbon dangling bonds.

4.5 Conclusions

In Summary, polymer-derived SiBCN ceramics with Si/B ratios 2/1 and 4/1 were synthesized through dehydrocoupling and hydroboration reaction of Ceraset™ VL20 with BH_3•Me_2S followed by pyrolysis. The structural evolution of the pyrolyzed ceramics was examined by XRD, Solid-state NMR, Raman and EPR spectroscopy. Three major structural components, such as, hexagonal boron nitride (*h*-BN), turbostratic boron nitride (*t*-BN), and BN_2C groups were found to be present in the amorphous matrix. Pyrolysis of the ceramic samples at higher temperatures shows the evolution of boron nitride (BN_3) and 'free' carbon with the disappearance of BN_2C groups. Thermodynamic modeling involving equilibrium constants and Gibbs free energies satisfactorily describe the amorphous phase transitions from BN_2C to BN_3 with a possible evolution of "free" carbon. Gibbs free energy calculations suggested the formation of higher concentration of "free" carbon in $Si_{4.0}B_{1.0}$ ceramic samples compared to $Si_{2.0}B_{1.0}$ ceramics, the reason of which is yet to be understood and needs further investigation. Semiquantitative Raman spectra measurements confirmed the presence of high concentration of "free" carbon in $Si_{4.0}B_{1.0}$ ceramics and hence the early onset of crystallization for $Si_{4.0}B_{1.0}$ ceramics. Detailed investigation into the Raman characterization is required to get more insight into the "free" carbon analysis. Finally, the EPR spectra suggested the presence of carbon centered radical as the source for paramagnetic center, and a possible formation of B-C bond, which further dissociates into stable B-N bond. Such preliminary study on the thermal stability

of SiBCN ceramics and thermodynamic modeling of the structural evolution and characterization of the boron-rich phase could well provide a new direction in the research field of amorphous SiBCN ceramics.

4.6 List of References

1. R. Riedel, G. Passing, H. Schonfelder, and R. J. Brook, "Synthesis of Dense Silicon-Based Ceramics at Low Temperatures," *Nature*, **355** [6362] 714-717 (1992).

2. E. Kroke, Y. L. Li, C. Konetchny, E. Lecomte, D. Fasel, and R. Riedel, "Silazane Derived Ceramics and Related Materials." *Mater. Sci. Eng. R.*, **26** [4-6] 97- 199 (2000).

3. L. Liew, W. Zhang, L. An, S. Shah, R. Lou, Y. Liu, T. Cross, K. Anseth, V. Bright, and R. Raj, "Ceramic MEMS – New Materials, Innovative Processing and Futuristic Applications," *Am. Ceram. Soc. Bull.*, **80** [5] 25-30 (2001).

4. L. An, W. Xu, S. Rajagopalan, C. Wang, H. Wang, J. Kapat, L. Chow, Y. Fan, L. Zhang, D. Jiang, B. Guo, J. Liang, and R. Vaidynathan, "Carbon-Nanotube Reinforced Polymer-Derived Ceramic Composites," *Adv. Mater.*, **16** [22] 2036-2040 (2004).

5. R. Reidel, A. Kienzle, W. Dressler, L. Ruwisch, J. Bill, and F. Aldinger, "A Silicoboron Carbonitride Ceramic Stable to 2,000 °C," *Nature*, **382** [6594] 796-798 (1996).

6. T. Wideman, E. Cortez, E. E. Remsen, G. A. Zank, P. J. Carrol, and L. G. Sneddon, "Reactions of Monofunctional Boranes with Hydridopolysilazane: Synthesis, Characterization, and Conversion Reactions of New Processible Precursors to SiNCB Ceramic Materials," *Chem. Mater.*, **9** [10] 2218-2230 (1997).

7. D. Srivastava, E. N. Duesler, and R. T. Paine, "Synthesis of Silylborazines and Their Utilization as Precursors to Silicon-Containing Boron Nitride," *Eur. J. Inorg. Chem.*, **1998** [6] 855-859 (1998).

8. F. Aldinger, M. Weinmann, and J. Bill, "Precursor-Derived Si-B-C-N Ceramics," *Pure & Appl. Chem.*, **70** [2] 439-448 (1998).

9. Z-C. Wang, F. Aldinger, and R. Riedel, "Novel Silicon-Boron-Carbon-Nitrogen Materials Thermally Stable up to 2200 °C," *J. Am. Ceram. Soc.*, **84** [10] 2179-2183 (2001).

10. M. Weinmann, J. Schumacher, H. Kummer, S. Prinz, J. Peng, H. J. Seifert, M. Christ, K. Muller, J. Bill, and F. Aldinger, "Synthesis and Thermal Behavior of Novel Si-B-C-N Ceramic Precursors," *Chem. Mater.*, **12** [3] 623-632 (2000).

11. R. Riedel, L.M. Ruswisch, L. An, and R. Raj, "Amorphous Silicoboron Carbonitride Ceramic with Very High Viscosity at Temperatures above 1500 °C," *J. Am. Ceram. Soc.* **81** [12] 3341-3344 (1998).

12. J. Vlček, S. Potocký, J. Čížek, J. Houška, M. Kormunda, P. Zeman, V. Peřina, J. Zemek, Y. Setsuhara, and S. Konumaand, " Reactive Magnetron Sputtering of Hard Si-B-C-N Films with a High-Temperature Oxidation Resistance," *J. Vac. Sci. Technol. A,* **23** [6] 1513-1522 (2005).

13. A. M. Hermann, Y-T. Wang, P. A. Ramakrishnan, D. Balzar, L. An, C. Haluschka, and R. Riedel, "Structure and Electronic Transport Properties of Si-(B)-C-N Ceramics," *J. Am. Ceram. Soc.*, **84** [10] 2260-2264 (2001).

14. P. A. Ramakrishnan, Y-T. Wang, D. Balzar, L. An, C. Haluschka, R. Riedel, and A. M. Hermann, "Silicoboron-Carbonitride Ceramics: A Class of High-Temperature Dopable Electronic Materials," *Appl. Phys. Lett.* **78** [20] 3076-3078 (2001).

15. M. A. Rooke, and P. M. A. Sherwood, " Surface Studies of Potentially Oxidation Protective Si-B-C-N Films for Carbon Fibers," *Chem. Mater.*, **9** [1] 285-296 (1997).

16. D. Hegemann, R. Riedel, and C. Oehr, "PACVD –Derived Thin Film in the System Si-B-C-N," *Chem. Vap. Deposition*, **5** [2] 61-65 (1999).

17. R. Hauser, S.N-. Borchard, R. Riedel, Y. H. Ikuhara, and Y. Iwamoto, "Polymer-Derived SiBCN Ceramic and Their Potential Appliaction for High Temperature Membranes," *J. Ceram. Soc. Jpn.*, **114** [1330] 524-528 (2006).

18. L. Lu, Y.C. Song, and C.X. Feng, "Composition and Structure of Boron-Containing Si-N-C Fibers at High-Temperature," *J. Mater. Sci. lett.*, **17** [7] 599-602 (1998).

19. S. Bernard, M. Weinmann, P. Gerstel, P. Miele, and F. Aldinger, "Boron-Modified Polysilazane as a Novel Single-Source Precursor for SiBCN Ceramic Fibers: Synthesis, Melt-Spining, Curing and Ceramic Conversion," *J. Mater. Chem.*, **15** [2] 289-299 (2005).

20. J. Schuhmacher, F. Berger, M. Weinmann, J. Bill, F. Aldinger, and K. Muller, "Solid-State NMR and FTIR Studies of the Preparation of Si-B-C-N Ceramics from Boron Modified Polysilazanes," *Appl. Organomet. Chem.*, **15** [10] 809-819 (2001).

21. F. Berger, A. Muller, F. Aldinger, and K. Muller, "Solid-State NMR Investigations on the Si-B-C-N Ceramics Derived From Boron-Modified Poly(allylmethylsilazane)," *Z. Anorg. Allg. Chem.*, **631** [2-3] 355-363 (2005).

22. A. Müller, A. Zern, P. Gerstel, J. Bill, and F. Aldinger, "Boron-Modifed Poly(propenylsilazane)-Derived Si-B-C-N Ceramics: Preparation and High Temperature Properties," *J. Eur. Ceram. Soc.*, **22** [9-10] 1631-43 (2002).

23. A. Müller, P. Gerstel, M. Weinmann, J. Bill, and F. Aldinger, "Correlation of Boron Content and High Temperature Stability in Si-B-C-N Ceramics," *J. Eur. Ceram. Soc.*, **20** [14-15] 2655-9 (2000).

24. A. Jalowiecki, J. Bill, F. Aldinger, and J. Mayer, "Interface Characterization of B-Doped Si_3N_4/SiC Ceramics," *Composites Part A*, **27** [9] 717-721 (1996).

25. K. Yamamoto, N. Tsuganezawa, S. Makimura, D. Sawa, S. Nakhigashi, K. Kojima, and Y. Hasegawa, "Local Structure and Defects in Ultra-High Temperature Materials of Borosilicon Carbonitride," *J. Mater. Res.*, **23** [6] 1642-1646 (2008).

26. J. A. Golczewski, and F. Aldinger, "Thermodynamic Modeling of Amorphous Si-C-N Ceramics From Polymer Precursors," *J. Non-Cryst. Solids,* **347** [1-3] 204-10 (2004).

27. A. H. Tavakoli, P. Gerstel, J. A. Golczewski, and J. Bill, "Effect of Boron on the Crystallization of Si-(B-)C-N Polymer-Derived Ceramics," *J. Non-Cryst. Solids*, **355** [48-49] 2381-9 (2009).

28. J. A. Golczewski, "Thermodynamic analysis of Isothermal Crystallization of Amorphous Si-C-N Ceramics Derived From Polymer Precursors," *J. Ceram. Soc. Japan,* **114** [11] 950-7 (2006).

29. A. H. Tavakoli, P. Gerstel, J. A. Golczewski, and J. Bill, "Quantitative X-ray Diffraction Analysis and Modeling of the Crystallization Process in Amorphous Si-B-C-N Polymer-Derived Ceramics," *J. Am. Ceram. Soc.*, **93** [5] 1470-8 (2010).

30. R. Raj, R. Riedel, and G. D. Soraru, "Introduction to the Special Topical issue on the Ultra-High Temperature Polymer-Derived Ceramics," *J. Am. Ceram. Soc.*, **84** [10] 2158-2159 (2001).

31. T. Varga, A. Navrotsky, J. L. Moats, R. M. Morcos, F. Poli, K. Muller, A. Saha, and R. Raj, "Thermodynamically Stable $Si_xO_yC_z$ Polymer-Like Amorphous Ceramics," *J. Am. Ceram. Soc.*, **90** [10] 3213-3219 (2007).

32. D. Seyferth, and H. Plenio, "Borasilazane Polymer Precursors for Borosilicon Nitride," *J. Am. Ceram. Soc.*, **73** [7] 2131-2133 (1990).

33. Y-L. Li, E. Kroke, R. Riedel, C. Fasel, C. Gervais, and F. Babonneau, "Thermal Cross-linking and Pyrolytic Conversion of Poly(ureamethylvinyl)silazanes to Silicon-Based Ceramics," *Appl. Organomet. Chem.*, **15** [10] 820-832 (2001).

34. Z-C. Wang, T. W. Kamphowe, S. Katz, J. Peng, H. J Seifert, J. Bill, and F. Aldinger, "Effect of Polymer Thermolysis on Composition, Structure and High Temperature Stability of Amorphous Silicoboron Carbonitride Ceramics," *J. Mater. Sci. Lett.*, **19** [19] 1701-1704 (2000).

35. P.S. Marchetti, D. Kwon, W. R. Schmidt, L. V. Interrante, and G. E. Maciel, "High-Field 11B Magic-Angle Spinning NMR Characterization of Boron Nitrides," *Chem. Mater.*, **3** [3] 482-486 (1991).

36. J. Bill, and F. Aldinger, "Precursor-Derived Covalent Ceramics," *Adv. Mater.*, **7** [9] 775-787 (1995).

37. Y. Wang, D. C. Alsmeyer, and R. L. McCreery, "Raman Spectroscopy of Carbon Materials: Structural Basis of Observed Spectra," *Chem. Mater.*, **2** [5] 557-563 (1990).

38. F. Tunistra, and J. L. Koenig, "Raman Spectrum of Graphite," *J. Chem. Phys.*, **53** [2] 1126-1130 (1970).

39. S. Trassl, G. Motz, E. Rossler, and G. Ziegler, "Characterization of the Free-Carbon Phase in Precursor-Derived SiCN Ceramics," *J. Non-Cryst. Solids*, **293-295**, 261-262 (2001).

40. N. Janakiraman, and F. Aldinger, "Fabrication and Characterization of Fully Dense Si-C-N Ceramics from a poly(ureamethylvinyl)silazane precursor," *J. Eur. Ceram. Soc.*, **29** [1] 163-173 (2009).

41. G. Gregori, H. J. Kleebe, H. Brrequel, S. Enzo, and G. Ziegler, "Microstructure Evolution of Precursor-Derived SiCN Ceramics upon Thermal Treatment between 1000 and 1400 $^{\circ}$C," *J. Non-Cryst. Solids*, **351** [16-17] 1393-1402 (2005).

42. A. C. Ferrari, and J. Robertson, "Interpretation of Raman Spectra of Disordered and Amorphous Carbon," *Phys. Rev. B: Condens. Matter*, **61** [20] 14095-14107 (2000).

43. Y. S. Wang, L. G. Zhang, W. X. Xu, T. Jiang, Y. Fan, and D. P. Jiang, "Effect of Thermal Initiator Concentration on the Electrical Behavior of Polymer-Derived Amorphous Silicon carbonitrides," *J. Am. Ceram. Soc.*, **91** [12] 3971-3975 (2008).

44. N. S. C. K. Yive, R. Corriu, D. Leclercq, P. H. Mutin, and A. Vioux, " Polyvinylsilazane - A Novel Precursor to Silicon Carbonitride," *New J. Chem.*, **15** [1] 85-92 (1991).

45. S. Trassl, H. –J. Kleebe, H. Stormer, G. Motz, E. Rossler, and G. Ziegler, "Characterization of the Free-Carbon Phase in Si-C-N Ceramics: Part II, Comparison of Different Polysilazane Precursors," *J. Am. Ceram. Soc.*, **85** [5] 1268-1274 (2002).

46. S. I. Andrenenko, I. Stiharu, and S. K. Mishra, "Synthesis and Characterization of Polyureasilazane Derived SiCN Ceramics," *J. Appl. Phys.*, **99** [11] 113907-1 – 113907-4 (2006).

47. H. J. Bardeleben, J. L. Cantin, A. Zeinert, B. Racine, K. Zellama, and P. N. Hai, "Spins and Microstructure of Hydrogenated Amorphous Carbon: A Multiple frequency Electron Paramagnetic Resonance Study," *Appl. Phys. Lett.*, **78** [19] 2843-2845 (2001).

48. G. Jeschke, M. Kroschel, and M. Jansen, "A Magnetic Resonance Study on the Structures of Amorphous Networks in the Si-B-N(-C) System," *J. Non-Cryst. Solids*, **260** [3] 216-227 (1999).

CHAPTER 5 CONCLUSION

In summary, the research interest first focuses on the fabrication of PDC fibers from a commercially available liquid oligomer, Ceraset™ VL20. The liquid oligomer is not suitable for electrospinning. Therefore, Ceraset™ VL20 was reacted with aluminum sec-butoxide to form an organic solvent-soluble polyaluminasilazane solid. The formation of solid polymer is believed to be due to the complexation reaction between aluminum (Al) of aluminum sec-butoxide and nitrogen (N) of Ceraset™ VL20 and the presence of bulky sec-butoxide group that prevents the crosslinking of ceraset via hydrosilylation and favors the formation of solvent-soluble complex. Once the preceramic polyaluminasilazane is solvent soluble, a simple electrospinning technique is demonstrated for the fabrication of superhydrophobic mats of PDC fibers from preceramic polyaluminasilazane electrospun fibers followed by a pyrolysis and the deposition of perfluorosilane. The key of this technique is the combination of PDC processing and electrospinning to generate hierarchical surface structures, which is difficult to obtain with the conventional ceramic processing. These ceramic fibers are thermal and chemical stable, and possess multifunctionality which includes self-cleaning, resistance to corrosive aqueous solutions and fire. These fibers have the potential to be useful in such extreme conditions as hot gas or liquid filters, and protective clothing for fire fighters and soldiers.

Secondly, MWCNT/SiCNAl ceramic fibers were fabricated from polyaluminasilazane electrospun fibers with aligned CNTs. MWCNTs were effectively dispersed in polyaluminasilazane by using a conjugated block copolymer, P3HT-*b*-PPEGA. The conjugated polymer, P3HT, disrupts the van der Wall's interaction between the CNTs to prevent it from

agglomeration, while the other polymer, PPEGA, makes the debundled CNTs soluble in variety of solvents and polymers. The PPEGA groups on P3HT-*b*-PPEGA functionalized CNTs are compatible with polyaluminasilazane through hydrogen bonding and generated a stable dispersion of MWCNT in polyaluminasilazane solutions. Electrospinning of the MWCNT/polyaluminasilazane solutions followed by a pyrolysis produced SiCNAl ceramic fibers with aligned MWCNT. SiCNAl ceramic fibers with 1.2 % MWCNTs have electrical conductivity 500 times higher than that of SiCNAl bulk ceramics, demonstrating the large improvement of electrical conductivity attributed to the incorporation of CNTs. This method provides a unique approach to disperse CNT in ceramics and paves a new direction to align CNTs in ceramic fibers. This may find applications in ceramic matrix composites (CMC) with excellent electrical and mechanical properties.

Finally, polymer-derived SiBCN ceramics with Si/B ratios 2/1 and 4/1 were synthesized by reacting Ceraset™ VL20 with BH_3•Me_2S followed by pyrolysis. The structural evolution of the pyrolyzed ceramics was examined by spectroscopic techniques such as solid-state NMR, Raman and EPR spectroscopy. The result suggested the presence of three major structural components: (i) hexagonal boron nitride (*h*-BN), (ii) turbostratic boron nitride (*t*-BN), and (iii) BN_2C groups in the final ceramic. Pyrolysis of the ceramic samples at increasingly higher temperatures showed the evolution of boron nitride (BN_3) with simultaneous decomposition of BN_2C groups. A possible reaction was proposed to explain structural changes from BN_3 to BN_2C and possibly, "free" carbon. The thermodynamic modeling involving equilibrium constants and Gibbs free energies successfully supported this amorphous phase transition from BN_2C to BN_3 and carbon.

Gibbs free energy calculations suggested the formation of higher concentration of "free" carbon in $Si_{4.0}B_{1.0}$ ceramic samples compared to $Si_{2.0}B_{1.0}$ ceramics, the reason of which is yet to be understood and needs further examination. Raman spectra semiquantitatively confirmed the presence of high concentration of "free" carbon in $Si_{4.0}B_{1.0}$ ceramics and hence the early onset of crystallization for $Si_{4.0}B_{1.0}$ ceramics. Much detailed investigation into the Raman characterization is required to get more insight into the "free" carbon analysis. Finally, the EPR spectra suggested the presence of carbon centered radical as the source for paramagnetic center, and a possible formation of B-C bond, which further dissociates into stable B-N bond. Such preliminary study on the thermal stability of SiBCN ceramics relating to structural changes corresponding to boron environment and to correlate the changes from thermodynamic modeling could well provide a new direction in the research field of amorphous SiBCN ceramics.

Current and Future Prospect:

The broader perspective of this research is that solution processibility of preceramic polymers has opened a new opportunity to fabricate PDCs with tunable compositions and structural components from electrospun ceramic fibers to fully dense ceramic films. For example, the current research focus is to fabricate a high temperature stable conductive SiAlCN/carbon (C) ceramic composite for space craft components where requirements such as high temperature stability and dissipation of electrical charges prevent the use of polymers or metals. In order to achieve that, carbon (C) is impregnated *in-situ* as graphite from the decomposition of carbon-forming polymer, polyacrylonitrile (PAN), which can form a homogenous solution with polyaluminasilazane in DMF. PAN is a widely used polymer precursor for the fabrication of

carbon nanofibers (CNFs). During carbonization, the polymer, PAN, loses non-carbon elements such as HCN, NH_3, and H_2, and finally formed graphite like structure. The electrical conductivity results of the SiAlCN/C composite are promising. The conductivity can reach as high as 750 S/m. Preliminary studies on the oxidized composite shows an anisotropic alignment of graphitic crystals in the unoxidized samples. Future work is dedicated to study the morphology of the composite ceramics in their unoxidized state and also, to optimize the graphite composition in the final composites with respect to the percolation threshold, a critical value of graphitic carbon which forms a conductive percolation network for electrical conductivity. In conclusion, the research on the functionalization of ceramics, either chemical or structural, has paved an exciting path for the research in PDCs.